

Climate4you update September 2023



1

Summary of observations until September 2023:

1: Observed average global air temperature change last 40 years is about $+0.157^{\circ}\text{C}$ per decade. If unchanged, additional average global air temperature increase by year 2100 will be about $+1.2^{\circ}\text{C}$. However, part of the apparent temperature increase reported is due to administrative changes, and the real future increase may therefore be smaller.

2: Tide gauges along coasts indicate a typical global sea level increase of about 1-2 mm/yr. Coastal sea level change rate last 100 year has essential been stable, without recent acceleration. If unchanged, global sea level at coasts will typically increase 8-16 cm by year 2100, although many locations in regions affected by glaciation 20,000 years ago, will experience a relative sea level drop.

3: Since 2004 the global oceans above 1900 m depth on average have warmed about 0.07°C . The maximum warming (about 0.2°C , 0-100 m depth) mainly affects oceans near Equator, where the incoming solar radiation is at maximum.

4: Changes in atmospheric CO_2 follow changes in global air temperature.
Changes in global air temperature follow changes in ocean surface temperature.

5: There was no perceptible effect on atmospheric CO_2 due to the 2020-21 COVID-related drop in GHG emissions. Thus, natural sinks and sources for atmospheric CO_2 far outweigh human contributions.

Contents:

Page 3:	September 2023 global surface air temperature overview
Page 4:	September 2023 global surface air temperature overview versus September last 10 years
Page 5:	September 2023 global surface air temperature compared to September 2022
Page 6:	Temperature quality class 1: Lower troposphere temperature from satellites
Page 7:	Temperature quality class 2: HadCRUT global surface air temperature
Page 8:	Temperature quality class 3: GISS and NCDC global surface air temperature
Page 11:	Comparing global surface air temperature and satellite-based temperatures
Page 12:	Global air temperature linear trends
Page 13:	Global temperatures: All in one, Quality Class 1, 2 and 3
Page 15:	Global sea surface temperature
Page 18:	Ocean temperature in uppermost 100 m
Page 20:	Pacific Decadal Oscillation (PDO)
Page 21:	North Atlantic heat content uppermost 700 m
Page 22:	North Atlantic temperatures 0-800 m depth along 59N, 30-0W
Page 23:	Global ocean temperature 0-1900 m depth summary
Page 24:	Global ocean net temperature change since 2004 at different depths
Page 25:	La Niña and El Niño episodes, Oceanic Niño Index
Page 26:	Zonal lower troposphere temperatures from satellites
Page 27:	Arctic and Antarctic lower troposphere temperatures from satellites
Page 28:	Arctic and Antarctic surface air temperatures
Page 31:	Long Arctic annual surface air temperature series
Page 32:	Long Antarctic annual surface air temperature series
Page 33:	Temperature over land versus over oceans
Page 34:	Troposphere and stratosphere temperatures from satellites
Page 35:	Sea ice; Arctic and Antarctic
Page 39:	Sea level in general
Page 40:	Global sea level from satellite altimetry
Page 41:	Global sea level from tide gauges
Page 42:	Snow cover; Northern Hemisphere weekly and seasonal
Page 44:	Greenland Ice Sheet net surface mass balance
Page 45:	Atmospheric specific humidity
Page 46:	Atmospheric CO ₂
Page 47:	Relation between annual change of atm. CO ₂ and La Niña and El Niño episodes
Page 48:	Phase relation between atmospheric CO ₂ and global temperature
Page 49:	Global air temperature and atmospheric CO ₂
Page 53:	Latest 20-year QC1 global monthly air temperature change
Page 54:	Sunspot activity and QC1 average satellite global air temperature
Page 55:	Sunspot activity and average neutron counts
Page 56:	Sunspot activity, ONI, and change rates of atmospheric CO ₂ and specific humidity
Page 57:	Monthly lower troposphere temperature and global cloud cover
Page 58:	Climate and history: <i>Napoleon's Russian 1812 campaign</i>

September 2023 global surface air temperature overview

General: This newsletter contains graphs and diagrams showing a selection of key meteorological variables, updated to the most recent past month, if possible. All temperatures are given in degrees Celsius.

Traditionally, a 30-year reference period is often used by various meteorological institutions for comparison purposes and are supposed to be updated through the end of each decade ending in zero (e.g., 1951-1980, 1961-1990, 1971-2000, etc.). The concept of a normal climate goes back to the first part of the 20th century. At that time, lasting to about 1960, it was generally believed that for all practical purpose's climate could be considered constant, no matter how obvious year-to-year fluctuations might have been. On this basis meteorologist decided to operate with an average or normal climate, defined by a 30-year period, called the normal period, assuming that it was of sufficient length to iron out all intervening variations. In fact, using a 30-yr 'normal' period is genuinely unfortunate, as observations clearly demonstrate that various global climate parameters (see, e.g., page 20) are influenced by periodic changes of 50-70 years. The often used 30-yr reference period is roughly half this time interval and is therefore very unsuited as reference period. In the maps on page 4, showing the geographical pattern of surface air temperature anomalies, the last previous 10 years are therefore used as reference period. This decadal approach corresponds well to the typical memory horizon for many people and is also adopted as reference period by other institutions, e.g., the Danish Meteorological Institute (DMI).

In many diagrams shown in this newsletter the thin line represents the monthly global average value, and the thick line indicate a simple running average, in most cases a simple moving 37-month average, nearly corresponding to a three-year average. The 37-month average is calculated from values covering a range from 18 months before to 18 months after, with equal weight given to all individual months.

The year 1979 has been chosen as starting point in many diagrams, as this approximately corresponds to both the beginning of satellite observations and the onset of the late 20th century warming period. However, several of the data series have a longer

record length, which may be inspected in greater detail on www.climate4you.com.

September 2023 surface air temperature

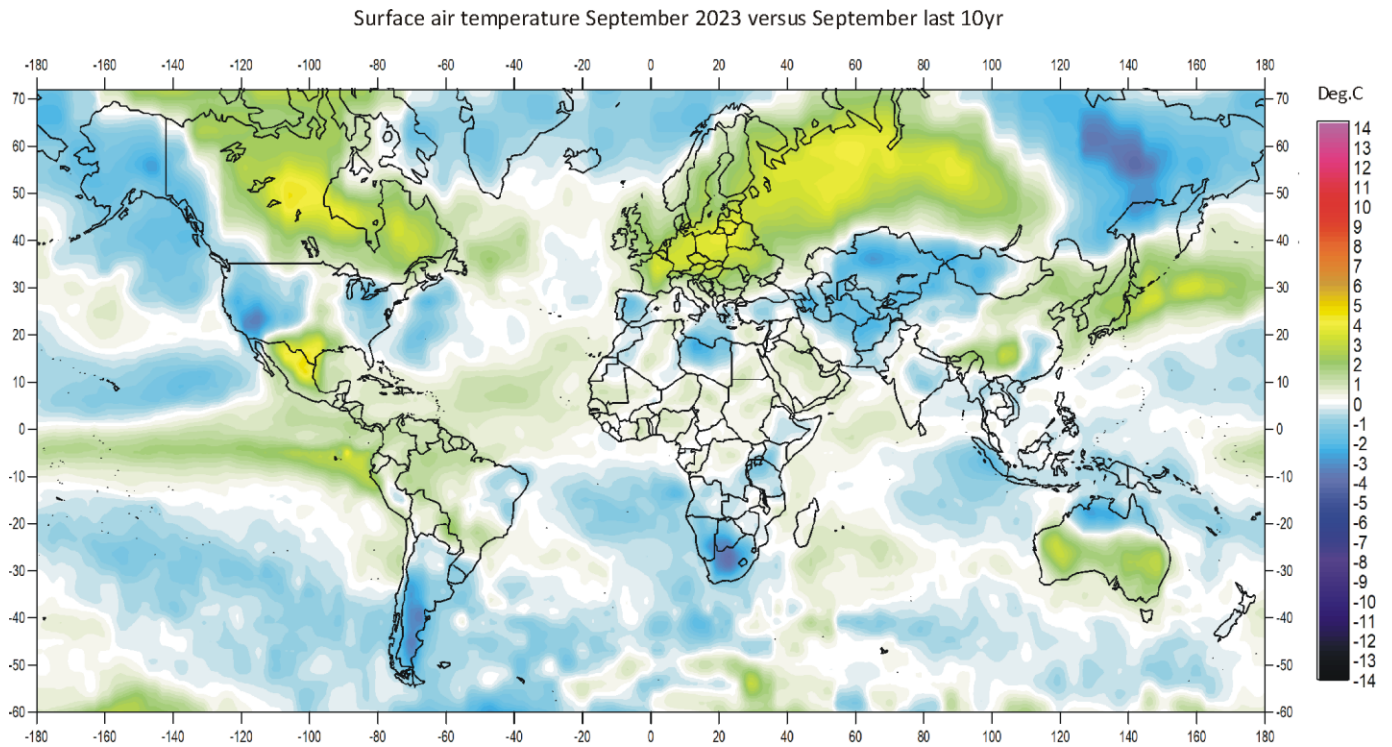
General: For September 2023, the GISS data portal provided AIRS interpolated surface air data, based on satellite observations. According to the GISS and NCDC records, the September global temperature anomaly was record high. The UAH lower troposphere satellite records also show the September 2023 temperature anomaly to be very high (RSS has not yet published data for September). According to AIRS v6 the September global average temperature anomaly was higher (+0.27°C) than the global September average for the last 10 years. Relatively high temperatures in September 2023 did not characterise the entire globe but was primarily restricted to land regions, including Antarctica. The atmosphere up to the tropopause has on average warmed (p.34), and much heat will be lost to space in the coming months.

The Northern Hemisphere surface temperature anomaly pattern (p.4) was characterised by strong regional contrasts, controlled by the dominant jet stream position. Especially Canada, Europe and western Russia were warm relative to the average for the last 10 years. In contrast, much of Siberia, USA and western Asia were relatively cold. Ocean wise, the Norwegian Sea and the Greenland Sea were cold, while most of the remaining part of the North Atlantic was relatively warm. In the northern Pacific, much of the ocean was cold, although the western regions north of 20°N were relatively warm. PDO (p.20) remains at low value. Arctic Ocean surface air temperatures were low in the Europe-Siberian sectors, while the Canada sector was relatively warm.

Near the Equator temperatures were generally above the 10-year average. Especially the part of the Pacific Ocean affected by the ongoing warm El Niño episode display above average surface temperatures, as is also the case for major parts of the Atlantic Ocean north of the Equator.

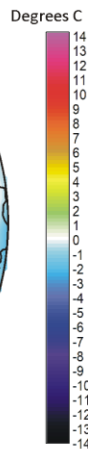
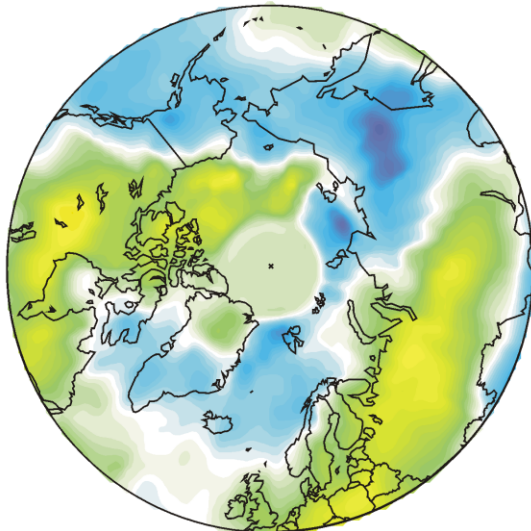
Southern Hemisphere temperatures were near the 10-yr average. Australia was divided between relatively cold in the north and warm in the south. Much of southern Africa and -America were relatively cold. Most of the Antarctic continent was relatively warm.

September 2023 global surface air temperature overview versus average September last 10 years

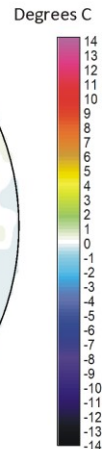
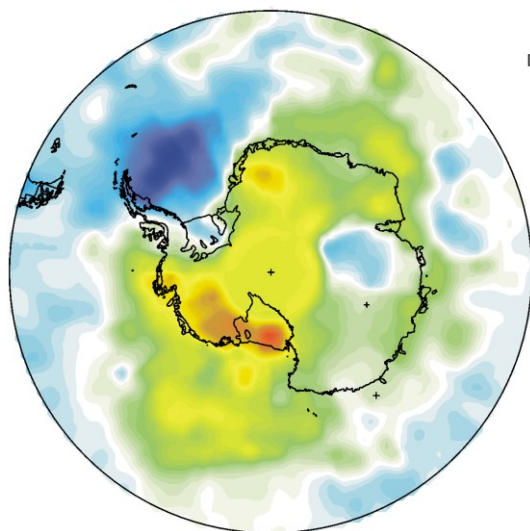


4

Surface air temperature September 2023 versus September last 10 yr

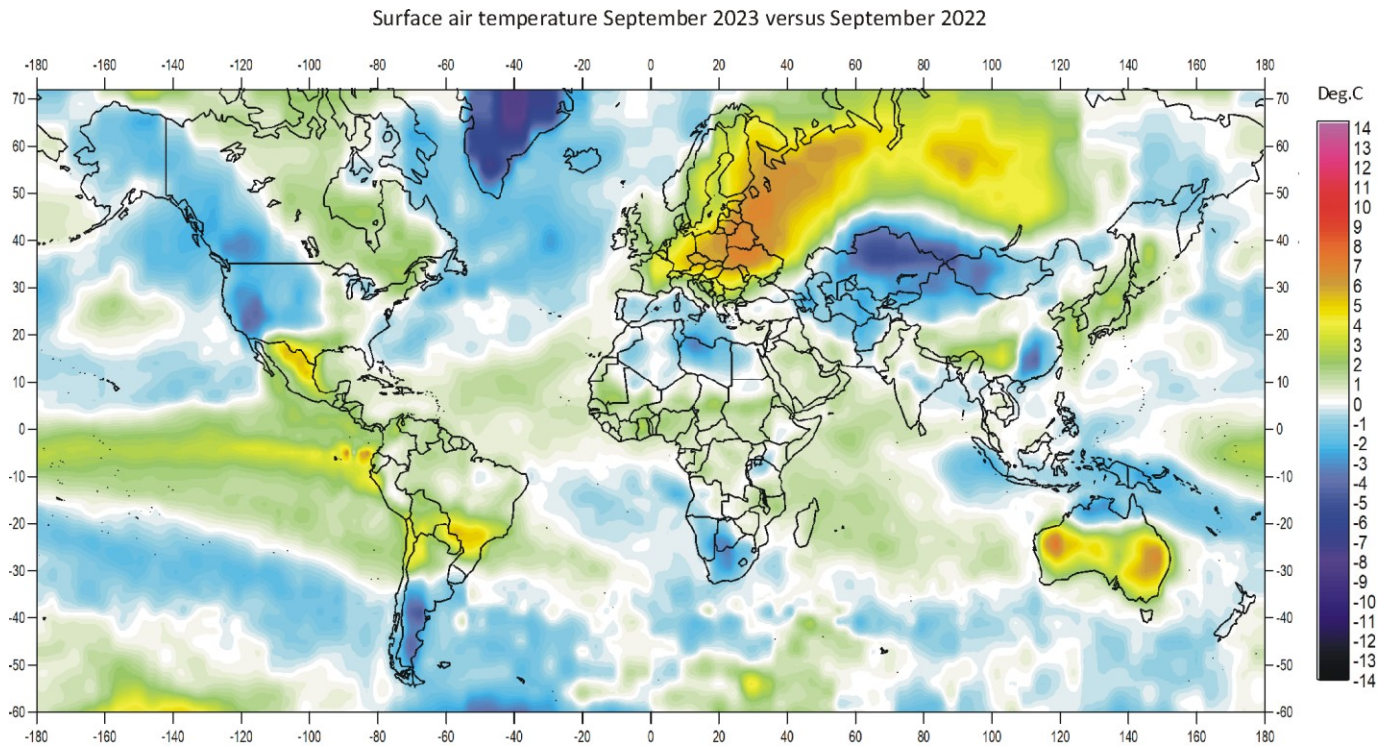


Surface air temperature September 2023 versus September last 10 yr



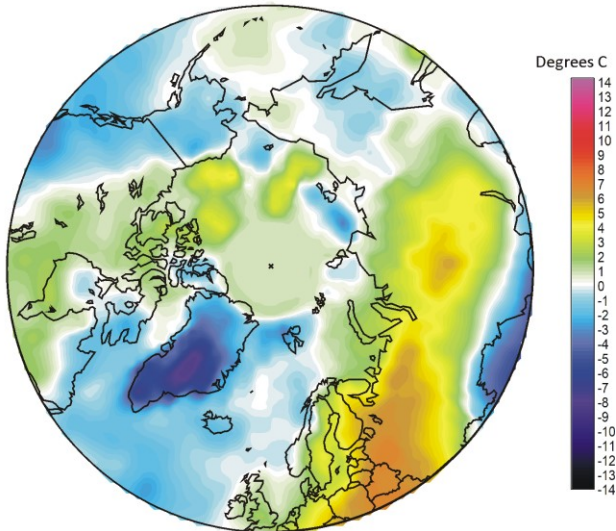
September 2023 surface air temperature compared to the average of September over the last 10 years. Green-yellow-red colours indicate areas with higher temperature than the 10-year average, while blue colours indicate lower than average temperatures. Data source: Remote Sensed Surface Temperature Anomaly, AIRS/Aqua L3 Monthly Standard Physical Retrieval 1-degree x 1-degree V006 (<https://airs.jpl.nasa.gov/>), obtained from the GISS data portal (https://data.giss.nasa.gov/gistemp/maps/index_v4.html).

September 2023 global surface air temperature compared to September 2022

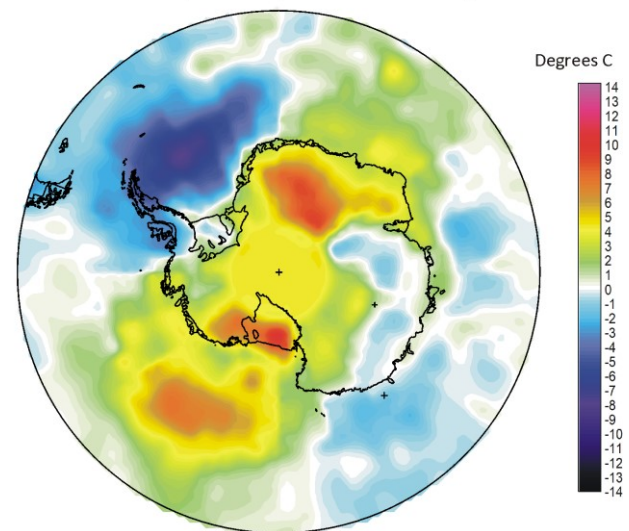


5

Surface air temperature September 2023 versus September 2022

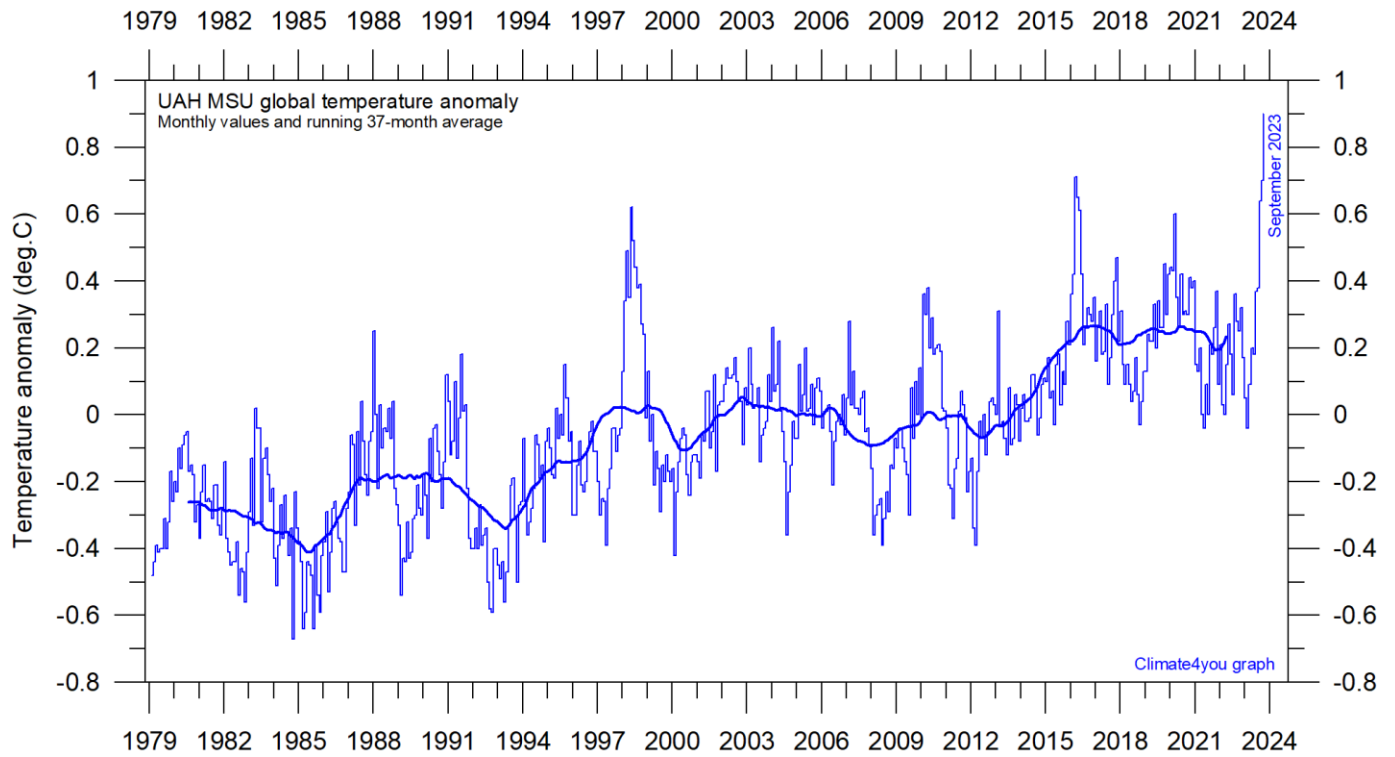


Surface air temperature September 2023 versus September 2022



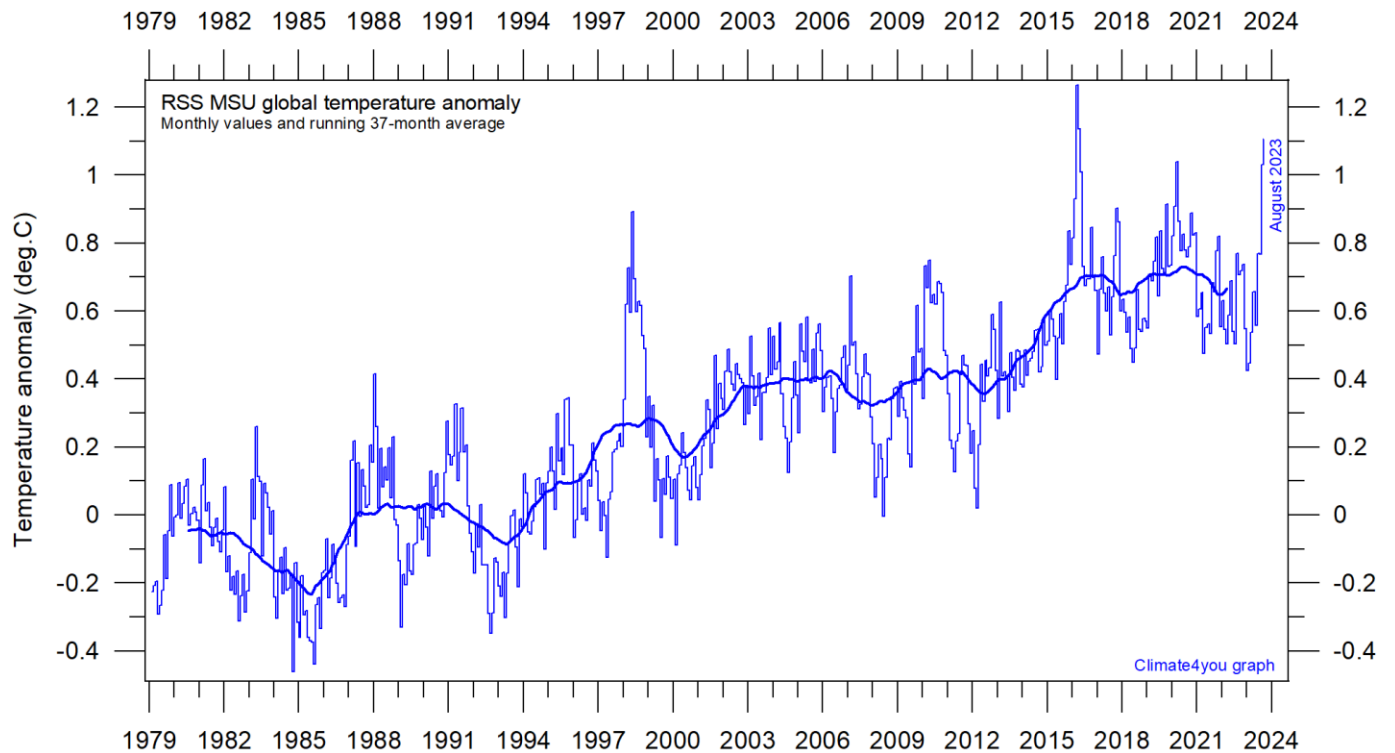
September 2023 surface air temperature compared to September 2022. Green-yellow-red colours indicate regions where the present month was warmer than last year, while blue colours indicate regions where the present month was cooler than last year. Variations in monthly temperature from one year to the next has no tangible climatic importance but may nevertheless be interesting to study. Data source: Remote Sensed Surface Temperature Anomaly, AIRS/Aqua L3 Monthly Standard Physical Retrieval 1-degree x 1-degree V006 (<https://airs.jpl.nasa.gov/>), obtained from the GISS data portal (https://data.giss.nasa.gov/gistemp/maps/index_v4.html).

Temperature quality class 1: Lower troposphere temperature from satellites, updated to September 2023 (see page 9 for definition of classes)



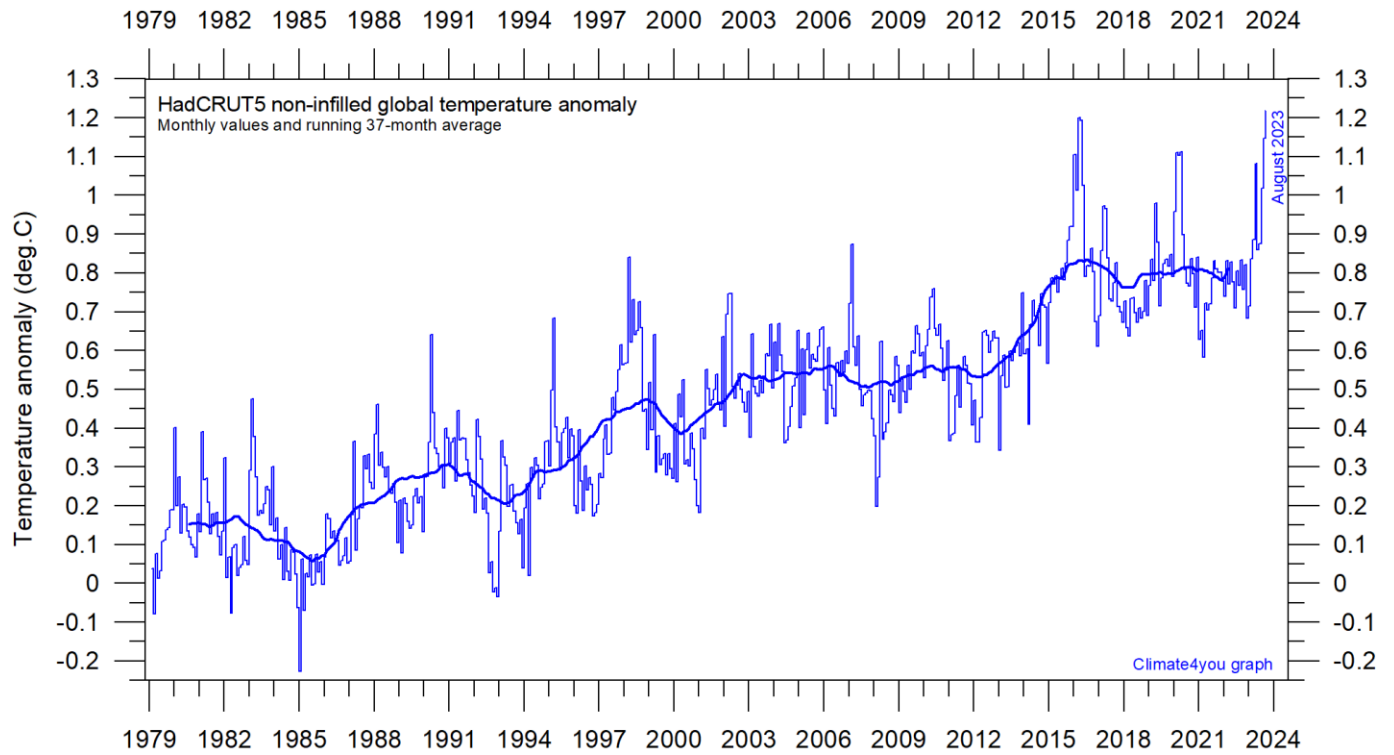
Global monthly average lower troposphere temperature (thin line) since 1979 according to [University of Alabama](#) at Huntsville, USA. The thick line is the simple running 37-month average. Reference period 1991-2020.

6



Global monthly average lower troposphere temperature (thin line) since 1979 according to according to [Remote Sensing Systems](#) (RSS), USA. The thick line is the simple running 37-month average.

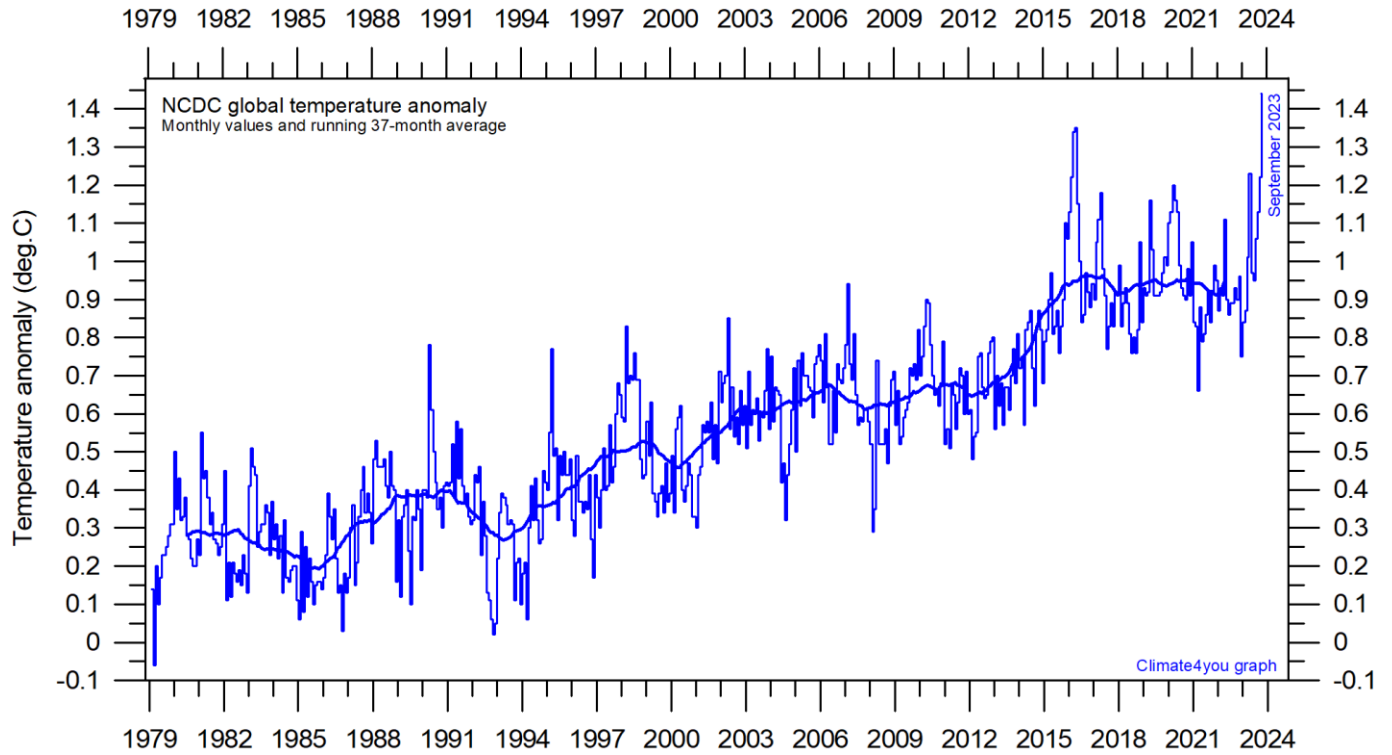
Temperature quality class 2: HadCRUT global surface air temperature, updated to August 2023



7

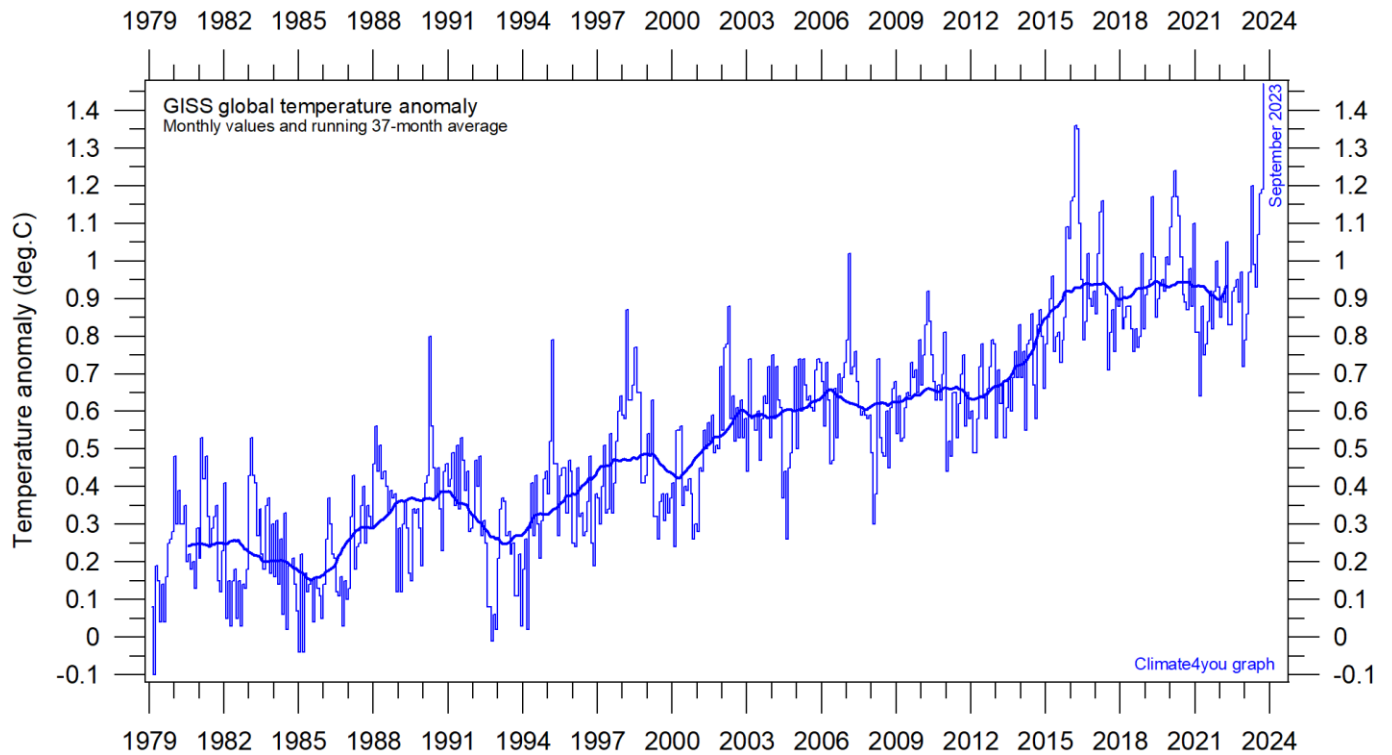
Global monthly average surface air temperature (thin line) since 1979 according to the Hadley Centre for Climate Prediction and Research and the University of East Anglia's [Climatic Research Unit \(CRU\)](#), UK. The thick line is the simple running 37-month average.

Temperature quality class 3: GISS and NCDC global surface air temperature, updated to September 2023



Global monthly average surface air temperature since 1979 according to according to the [National Climatic Data Center](#) (NCDC), USA. The thick line is the simple running 37-month average.

8



Global monthly average surface air temperature (thin line) since 1979 according to according to the [Goddard Institute for Space Studies](#) (GISS), at Columbia University, New York City, USA, using ERSST_v4 ocean surface temperatures. The thick line is the simple running 37-month average.

A note on data record stability and -quality:

The temperature diagrams shown above all have 1979 as starting year. This roughly marks the beginning of the recent episode of global warming, after termination of the previous episode of global cooling from about 1940. In addition, the year 1979 also represents the starting date for the satellite-based global temperature estimates (UAH and RSS). For the three surface air temperature records (HadCRUT, NCDC and GISS), they begin much earlier (in 1850 and 1880, respectively), as can be inspected on www.climate4you.com.

For all three surface air temperature records, but especially NCDC and GISS, administrative changes to anomaly values are quite often introduced, even affecting observations many years back in time. Some changes from the recent past may be due to the delayed addition of new station data or change of station location, while others probably have their origin in changes of the technique implemented to calculate average values from the raw data. It is clearly impossible to evaluate the validity of such administrative changes for the outside user of these records; it is only possible to note that such changes quite often are introduced (see example diagram next page).

In addition, the three surface records represent a blend of sea surface data collected by moving ships or by other means, plus data from land stations of partly unknown quality and unknown degree of representativeness for their region. Many of the land stations also has been moved geographically during their period of operation, instrumentation have been changed, and they are influenced by changes in their near surroundings (vegetation, buildings, etc.). The surface network is inherently heterogeneous (dense over continents but sparse over oceans) and probably contaminated by urbanization surrounding many measurement sites.

The satellite temperature records also have their problems, but these are generally of a more technical nature and probably therefore better correctable. In

addition, the temperature sampling by satellites is more regular and complete on a global basis than that represented by the surface records. It is also important that the sensors on satellites measure temperature directly by microwave radiance (thereby unobstructed by clouds), while most modern surface temperature measurements are indirect, using electronic resistance.

Everybody interested in climate science should gratefully acknowledge the big efforts put into maintaining the different temperature databases referred to in the present newsletter. At the same time, however, it is also important to realise that all temperature records cannot be of equal scientific quality. The simple fact that they to some degree differ shows that they cannot all be correct.

On this background, and for practical reasons, Climate4you therefore operates with three quality classes (1-3) for global temperature records, with 1 representing the highest quality level:

Quality class 1: The satellite records (UAH and RSS).

Quality class 2: The HadCRUT surface record.

Quality class 3: The NCDC and GISS surface records.

The main reason for discriminating between the three surface records is the following:

While both NCDC and GISS often experience quite large administrative changes (see example on p.10), and therefore essentially must be considered as unstable records, the changes introduced to HadCRUT are fewer and smaller. For obvious reasons, as the past does not change, any record undergoing continuing changes cannot describe the past correctly all the time. Frequent and large corrections in a database unavoidably signal a fundamental uncertainty about what is likely to represent the correct values.

You can find more on the issue of lack of temporal stability on www.climate4you.com (go to: *Global Temperature*, and then proceed to *Temporal Stability*).

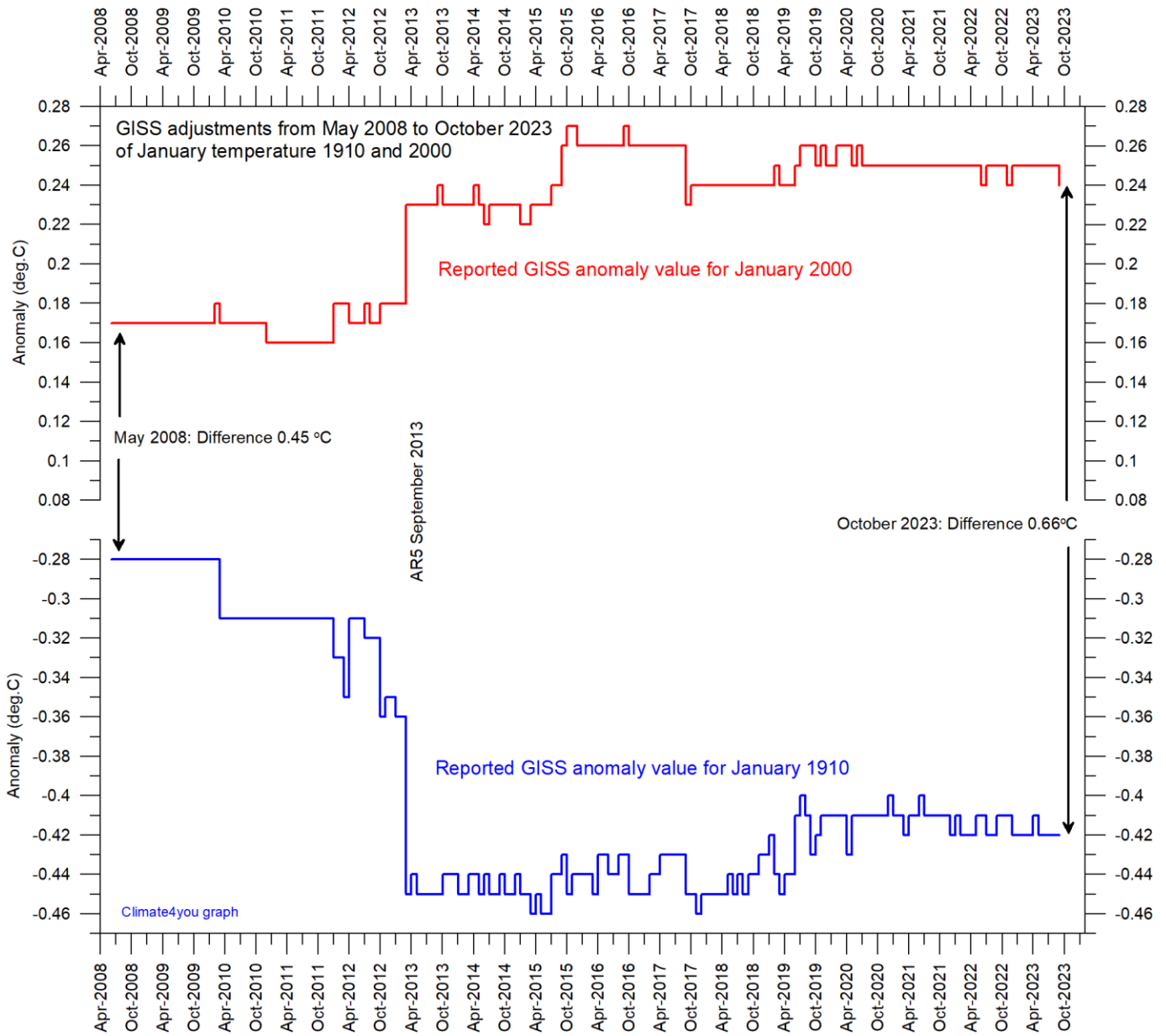
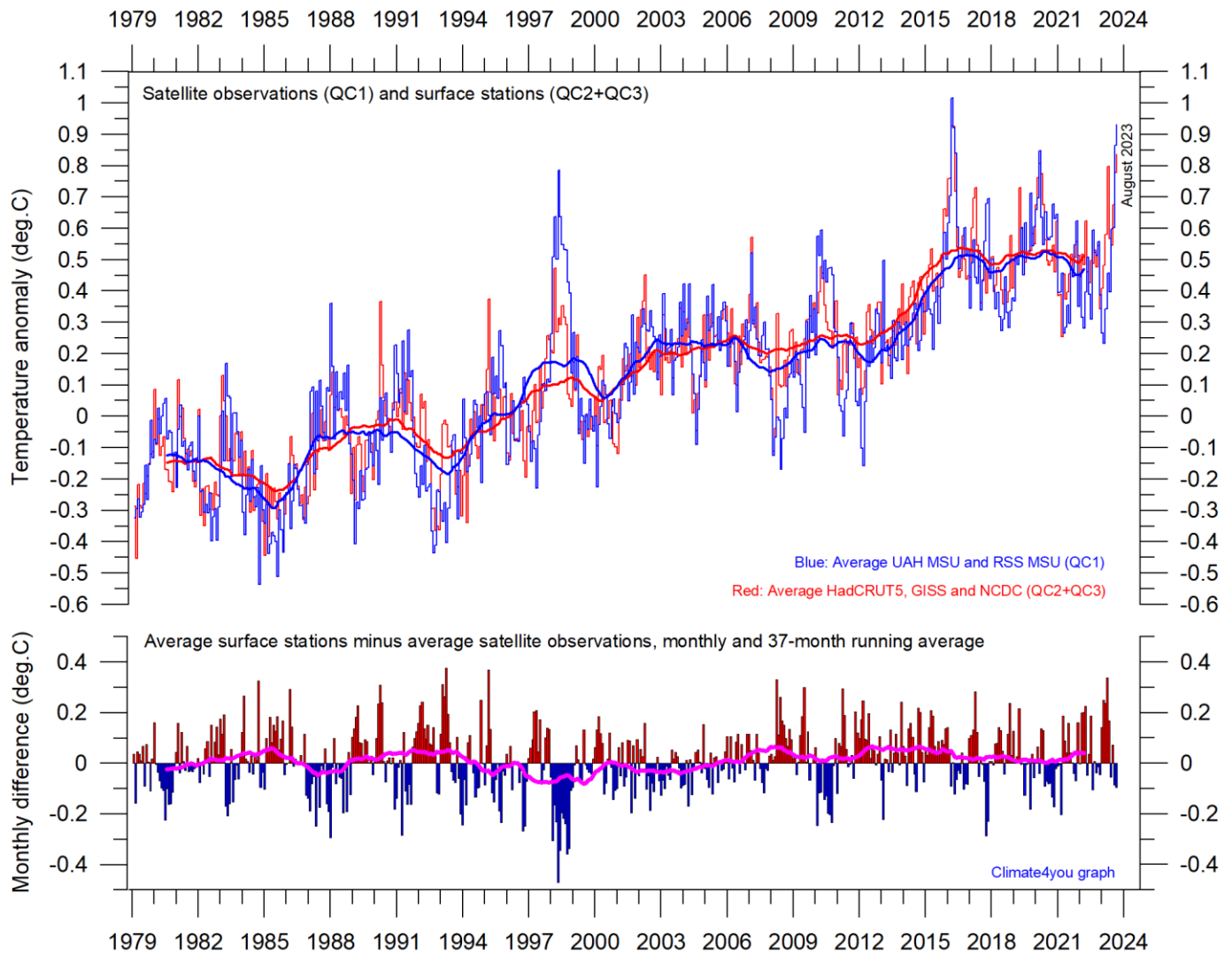


Diagram showing the monthly adjustments made since May 2008 by the [Goddard Institute for Space Studies](#) (GISS), USA, as recorded by published anomaly values for the two months January 1910 and January 2000. AR5 indicates timing of publication of IPCC report AR5 *Climate Change 2013: The Physical Science Basis*.

The administrative upsurge of the temperature increase from January 1915 to January 2000 has grown from 0.45 (reported May 2008) to 0.66°C (reported September 2023). This represents an about 47% administrative temperature increase over this

period, meaning that a significant part (nearly half) of the apparent global temperature increase from January 1910 to January 2000 (as reported by GISS) is caused by administrative changes of the original data since May 2008.

Comparing global surface air temperature and lower troposphere satellite temperatures; updated to August 2023



11

Plot showing the average of monthly global surface air temperature estimates (HadCRUT5, GISS and NCDC) and satellite-based temperature estimates (RSS MSU and UAH MSU). The thin lines indicate the monthly value, while the thick lines represent the simple running 37-month average, nearly corresponding to a running 3-yr average. The lower panel shows the monthly difference between average surface air temperature and satellite temperatures. As the base period differs for the different temperature estimates, they have all been normalised by comparing to the average value of 30 years from January 1979 to December 2008.

Global air temperature linear trends updated to August 2023

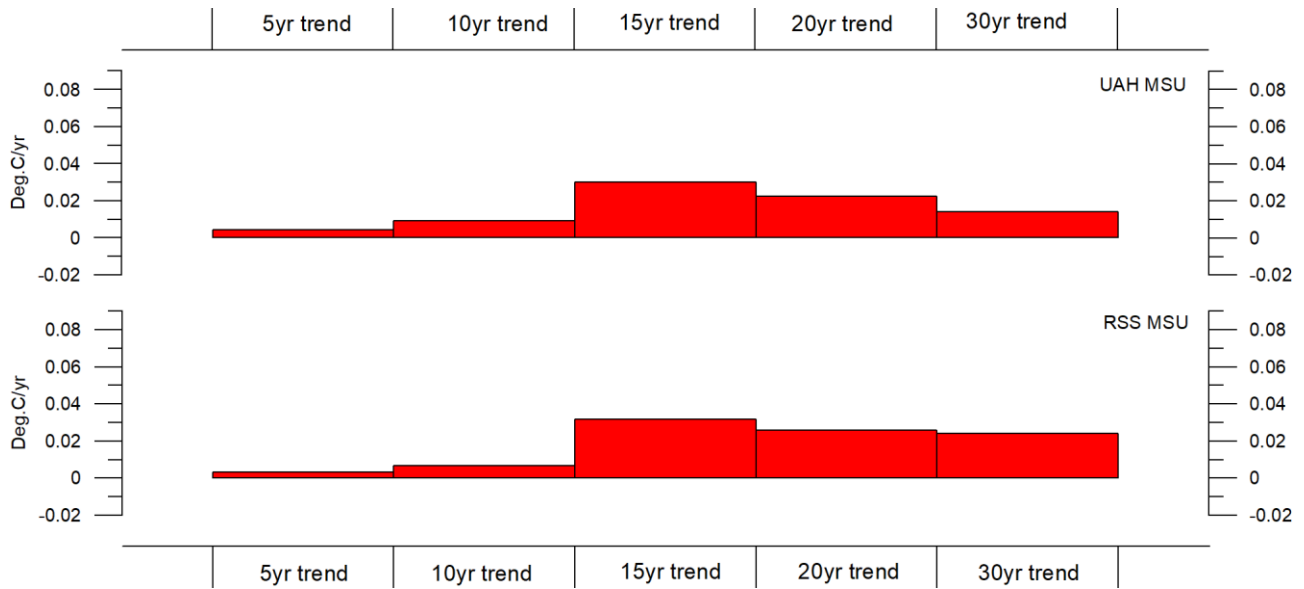


Diagram showing the latest 5, 10, 20 and 30-yr linear annual global temperature trend, calculated as the slope of the linear regression line through the data points, for two satellite-based temperature estimates (UAH MSU and RSS MSU).

12

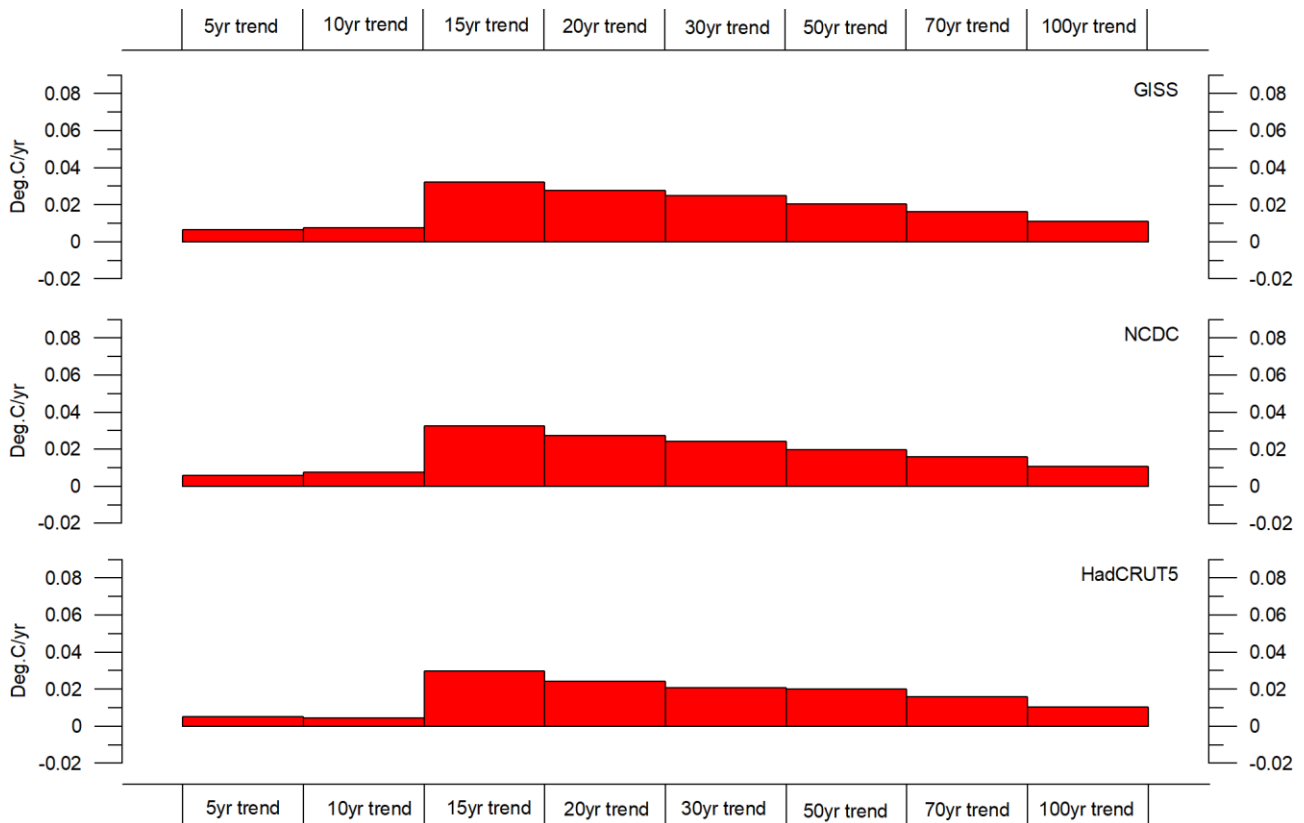
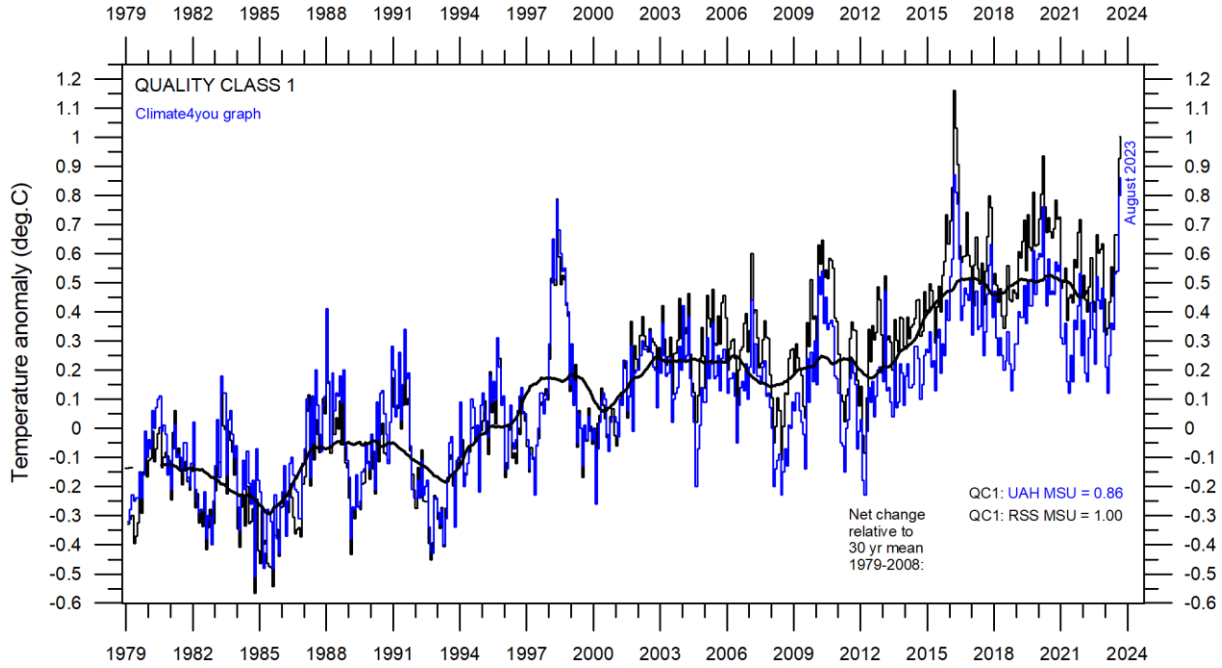


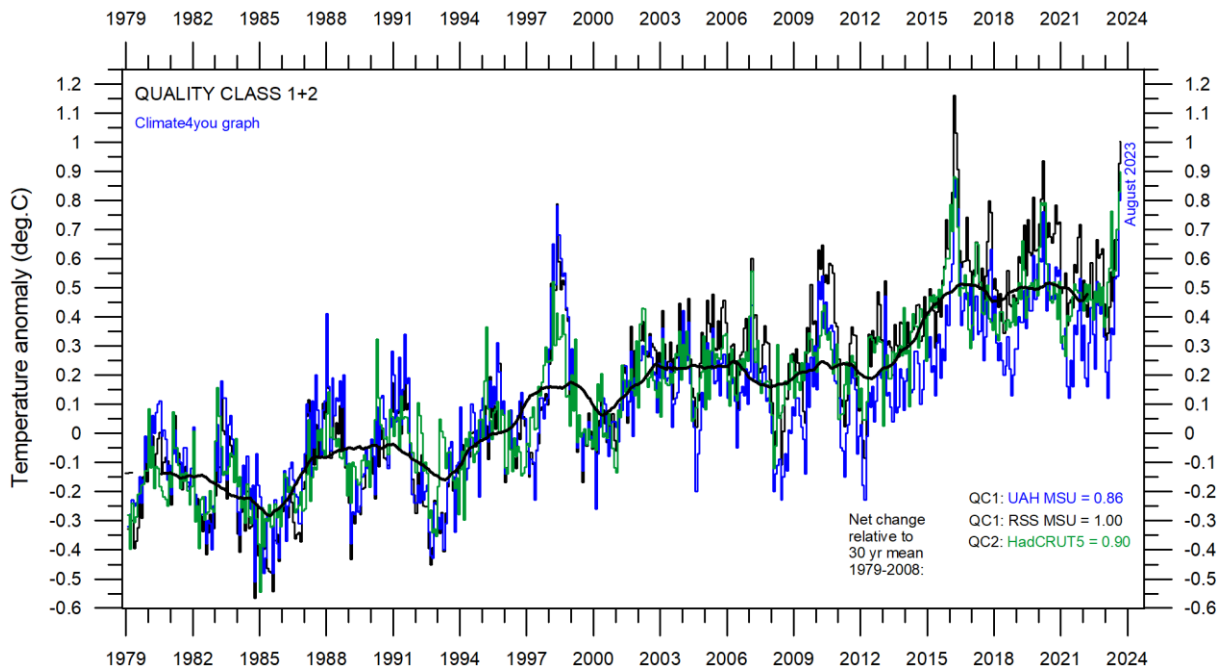
Diagram showing the latest 5, 10, 20, 30, 50, 70 and 100-year linear annual global temperature trend, calculated as the slope of the linear regression line through the data points, for three surface-based temperature estimates (GISS, NCDC and HadCRUT5).

All in one, Quality Class 1, 2 and 3; updated to August 2023

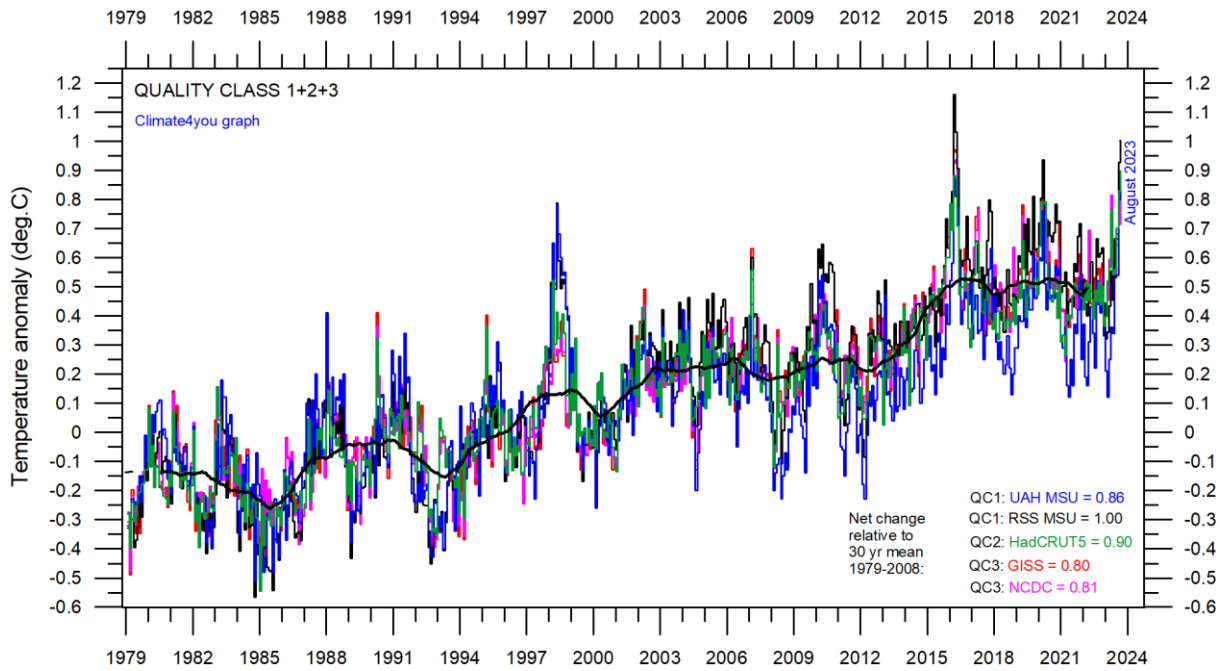


Superimposed plot of Quality Class 1 (UAH and RSS) global monthly temperature estimates. As the base period differs for the individual temperature estimates, they have all been normalised by comparing with the average value of the initial 120 months (30 years) from January 1979 to December 2008. The heavy black line represents the simple running 37 month (c. 3 year) mean of the average of both temperature records. The numbers shown in the lower right corner represent the temperature anomaly relative to the individual 1979-2008 averages.

13



Superimposed plot of Quality Class 1 and 2 (UAH, RSS and HadCRUT) global monthly temperature estimates. As the base period differs for the individual temperature estimates, they have all been normalised by comparing with the average value of the initial 120 months (30 years) from January 1979 to December 2008. The heavy black line represents the simple running 37 month (c. 3 year) mean of the average of all three temperature records. The numbers shown in the lower right corner represent the temperature anomaly relative to the individual 1979-2008 averages.



Superimposed plot of Quality Class 1, 2 and 3 global monthly temperature estimates (UAH, RSS, HadCRUT, GISS and NCDC). As the base period differs for the individual temperature estimates, they have all been normalised by comparing with the average value of the initial 120 months (30 years) from January 1979 to December 2008. The heavy black line represents the simple running 37 month (c. 3 year) mean of the average of all five temperature records. The numbers shown in the lower right corner represent the temperature anomaly relative to the individual 1979-2008 averages.

14 Please see reflections on page 9 relating to the above three quality classes.

Satellite- and surface-based temperature estimates are derived from different types of measurements and comparing them directly as in the above diagrams therefore may be somewhat ambiguous.

However, as both types of estimates often are discussed together in various news media, the above composite diagrams may nevertheless be of some interest.

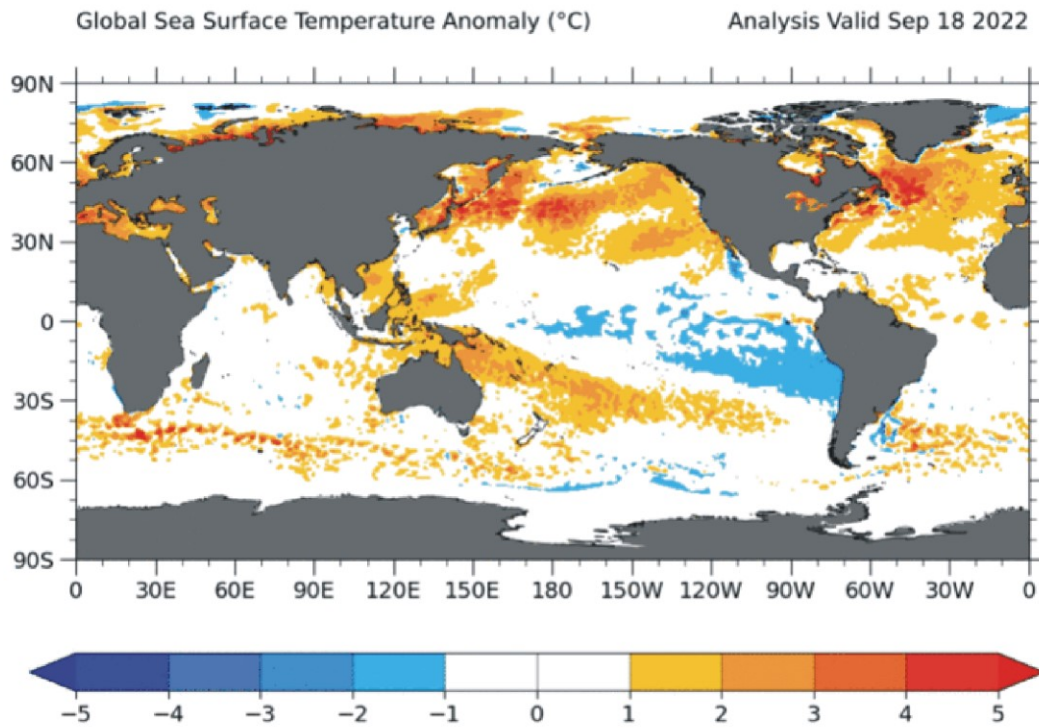
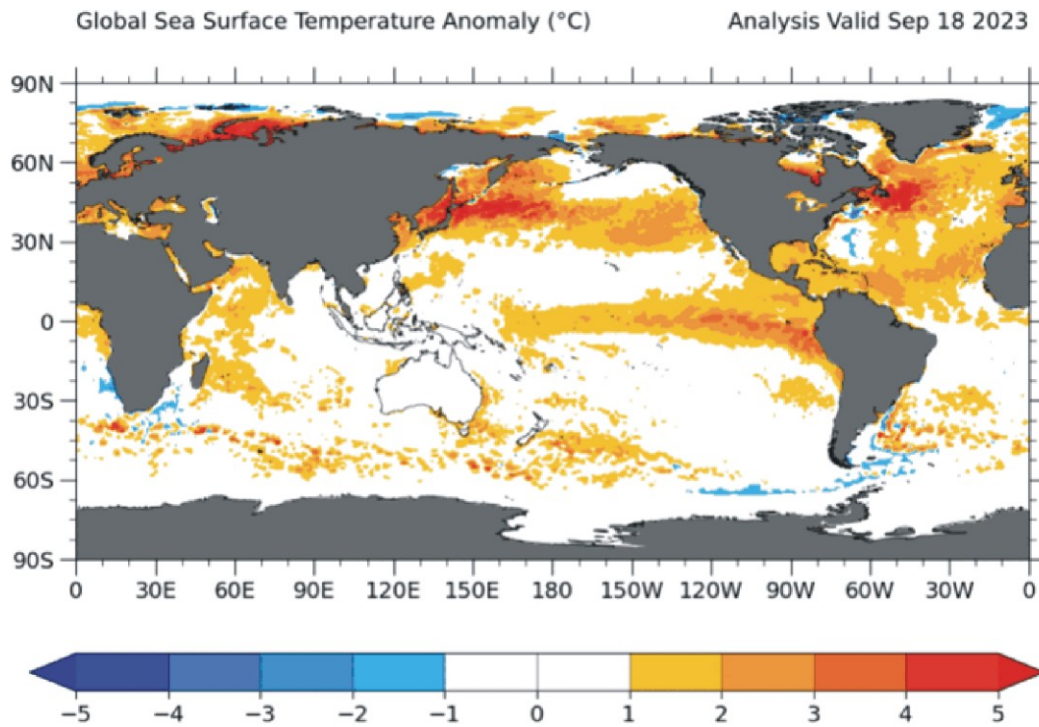
In fact, the different types of temperature estimates appear to agree as to the overall temperature variations on a 2-3-year scale, although on a shorter time scale there are often considerable differences between the individual records. However, since about 2003 the surface records used to be drifting towards higher temperatures than the combined satellite record, but this overall tendency was much removed by the major adjustment of the RSS satellite series in 2015 (see lower diagram on page 6).

The combined records (diagram above) suggest a modest global air temperature increase over the last 30 years, about 0.22°C per decade. It should be noted that the apparent temperature increases since about 2003 at least partly is the result of ongoing administrative adjustments (page 9-10). At the same time, none of the temperature records considered here indicates any overall temperature decrease during the last 20 years.

The present temperature development does not exclude the possibility that global temperatures may begin to increase significantly later. On the other hand, it also remains a possibility that Earth just now is passing an overall temperature peak, and that global temperatures may begin to decrease during the coming 5-10 years.

As always, time will show which of these possibilities is correct.

Global sea surface temperature, updated to September 2023



Plymouth State Weather Center

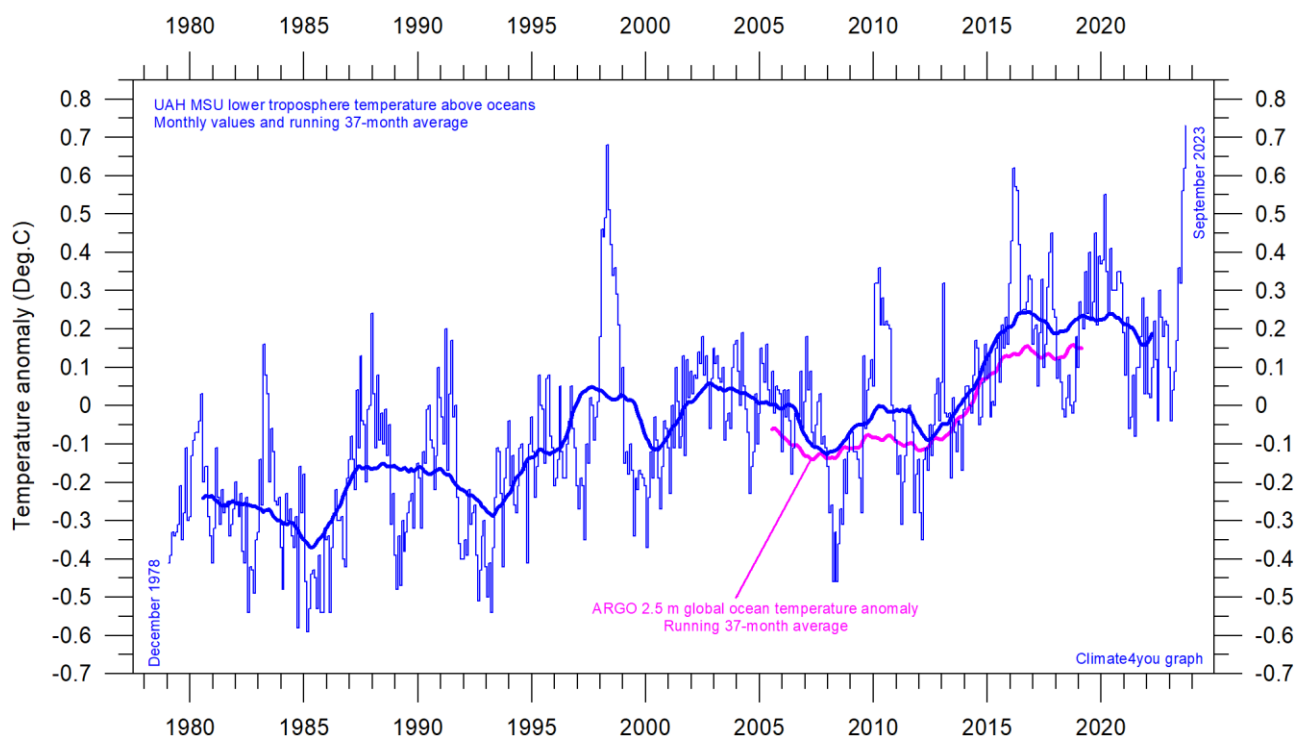
Sea surface temperature anomaly on 18 September 2023 (upper map) and 2022 (lower map). Map source: Plymouth State Weather Center. Reference period: 1977-1991.

Because of the large surface areas near Equator, the temperature of the surface water in these regions is especially important for the global atmospheric temperature (p. 6-8). In fact, no less than 50% of planet Earth's surface area is located within 30°N and 30°S.

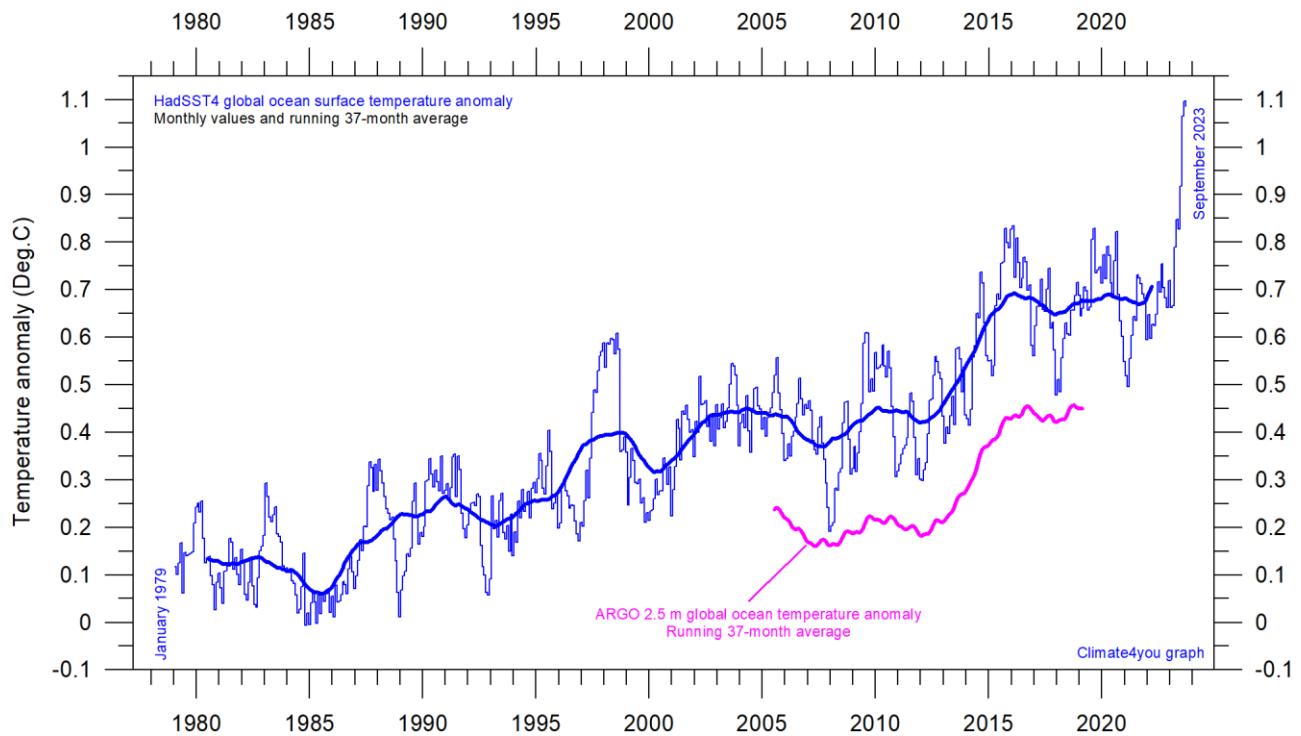
A mixture of relatively warm and cold water presently dominates much of the global ocean surface, but with notable variations from month to month. All such ocean surface temperature changes will be influencing global air temperatures in the months to come. A cold La Niña episode (Pacific Ocean) has recently ended and is now being followed by a warm El Niño episode (maps p.15 and diagram p.25).

The significance of short-term cooling or warming reflected in air temperatures should never be overstated. Whenever Earth experiences cold La Niña or warm El Niño episodes major heat exchanges take place between the Pacific Ocean and the atmosphere above, sooner or later showing up in estimates of the global air temperature.

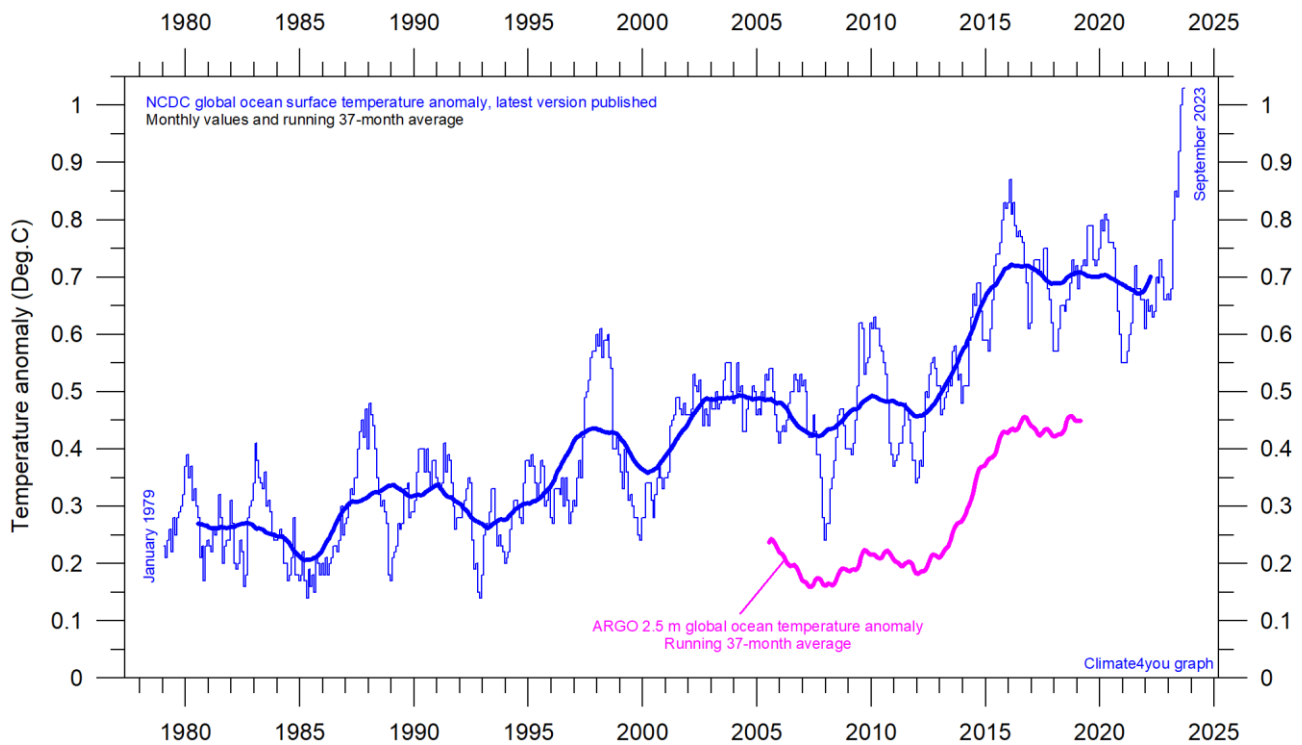
However, this does not necessarily reflect similar changes in the total heat content of the atmosphere-ocean system. In fact, global net changes can be small and such heat exchanges may mainly reflect redistribution of energy between ocean and atmosphere. What matters is the overall temperature development when seen over several years.



Global monthly average lower troposphere temperature over oceans (thin line) since 1979 according to [University of Alabama](#) at Huntsville, USA. The thick line is the simple running 37-month average. Insert: Argo global ocean temperature anomaly from floats, displaced vertically to make visual comparison easier. UAH reference period: 1991-2020.

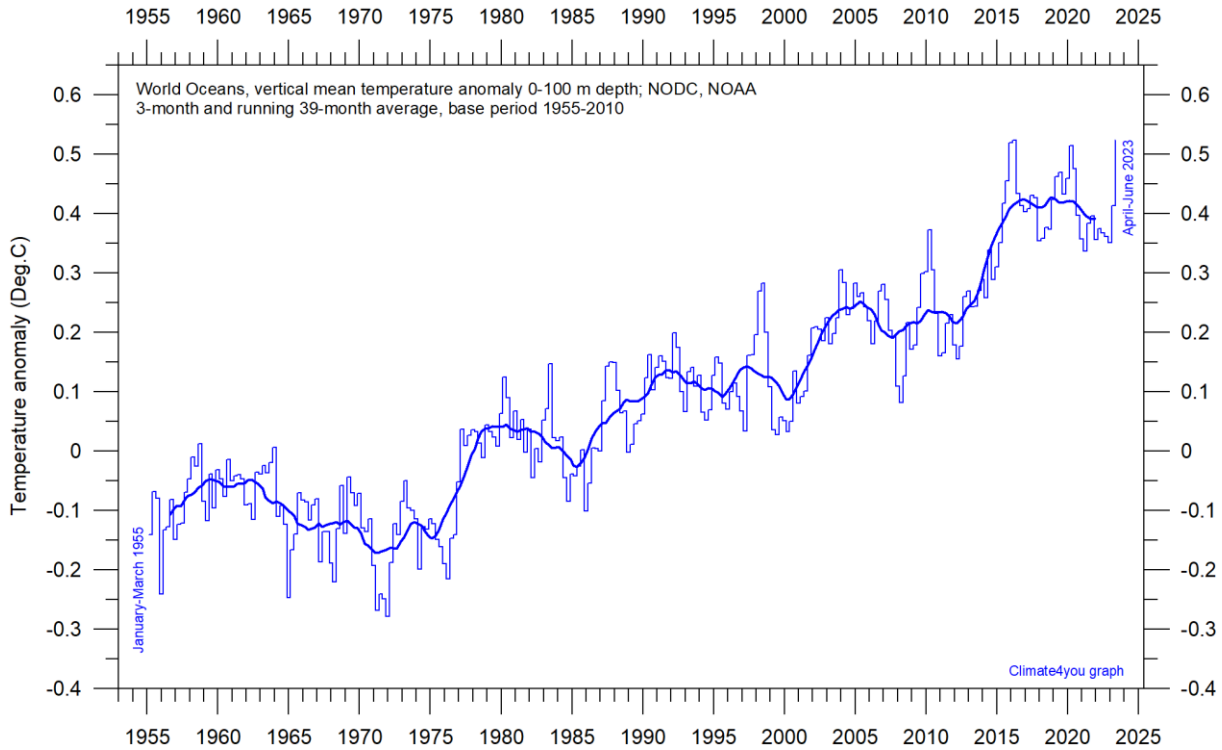


Global monthly average sea surface temperature since 1979 according to University of East Anglia's [Climatic Research Unit \(CRU\)](#), UK. Base period: 1961-1990. The thick line is the simple running 37-month average. Insert: Argo global ocean temperature anomaly from floats, displaced vertically to make visual comparison easier.



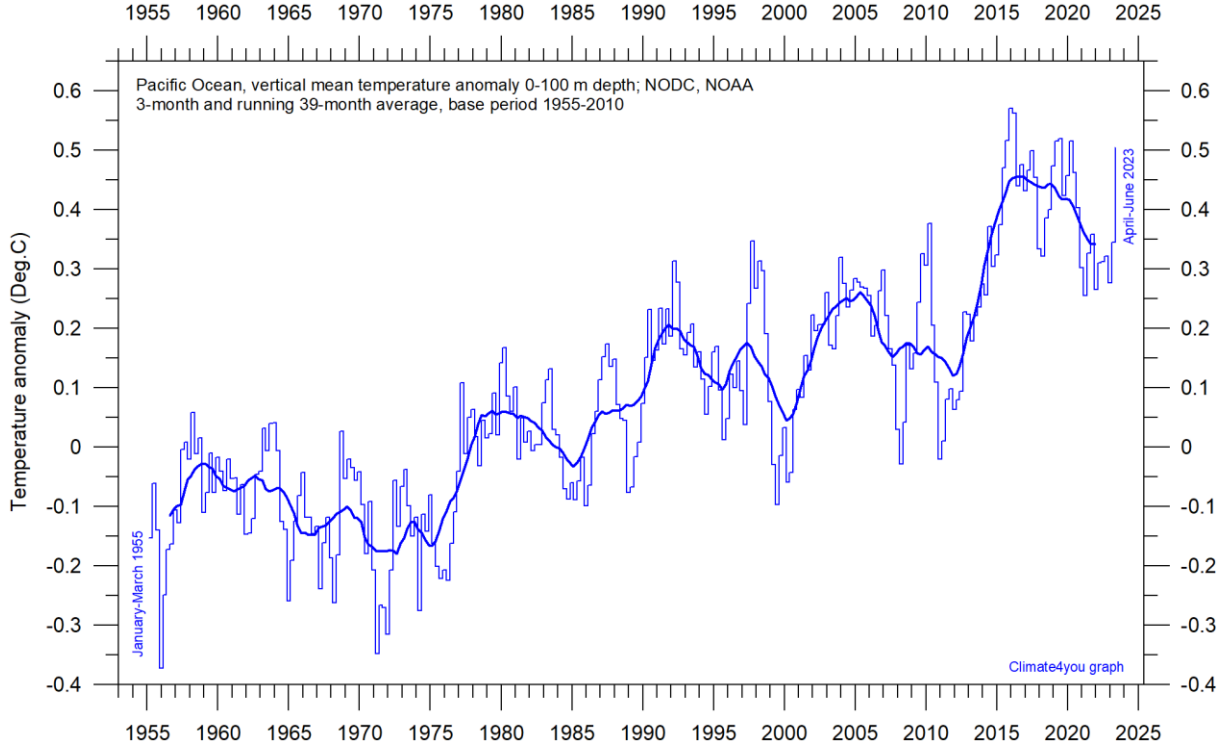
Global monthly average sea surface temperature since 1979 according to the [National Climatic Data Center \(NCDC\)](#), USA. Base period: 1901-2000. The thick line is the simple running 37-month average. Insert: Argo global ocean temperature anomaly from floats, displaced vertically to make visual comparison easier.

Ocean temperature in uppermost 100 m, updated to June 2023

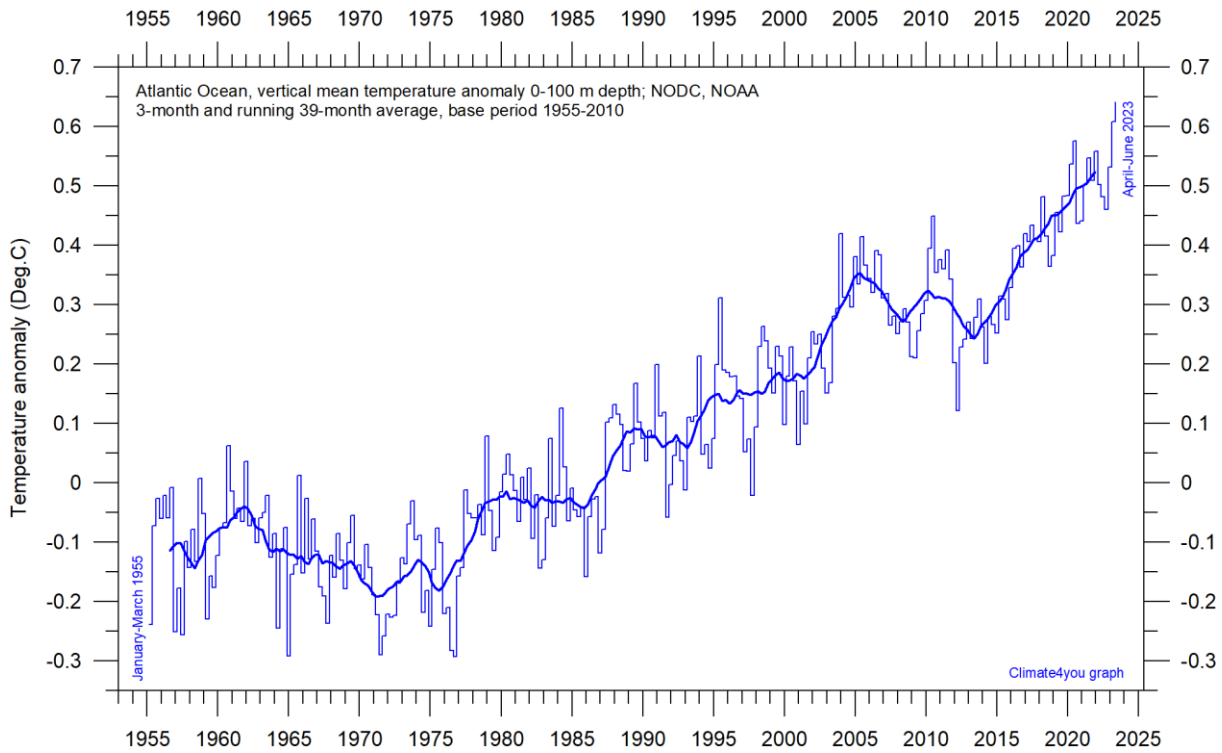


World Oceans vertical average temperature 0-100 m depth since 1955. The thin line indicates 3-month values, and the thick line represents the simple running 39-month (c. 3 year) average. Data source: [NOAA National Oceanographic Data Center](#) (NODC). Base period 1955-2010.

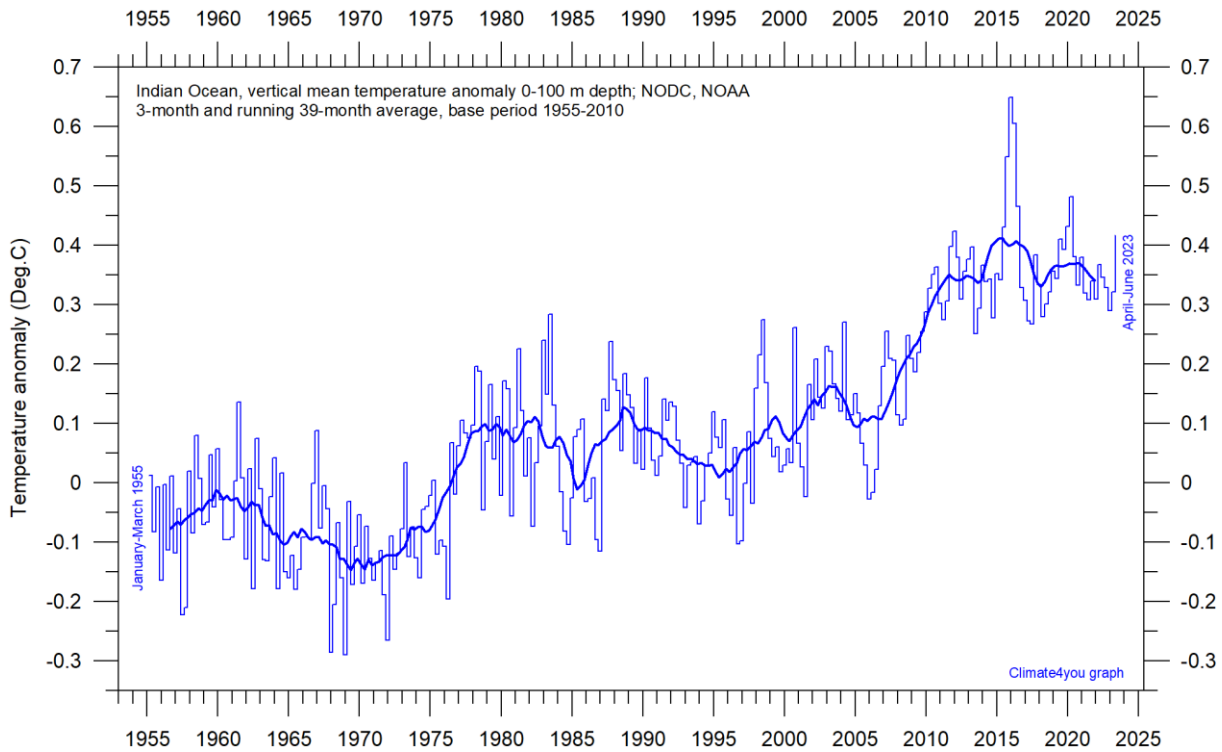
18



Pacific Ocean vertical average temperature 0-100 m depth since 1955. The thin line indicates 3-month values, and the thick line represents the simple running 39-month (c. 3 year) average. Data source: [NOAA National Oceanographic Data Center](#) (NODC). Base period 1955-2010.

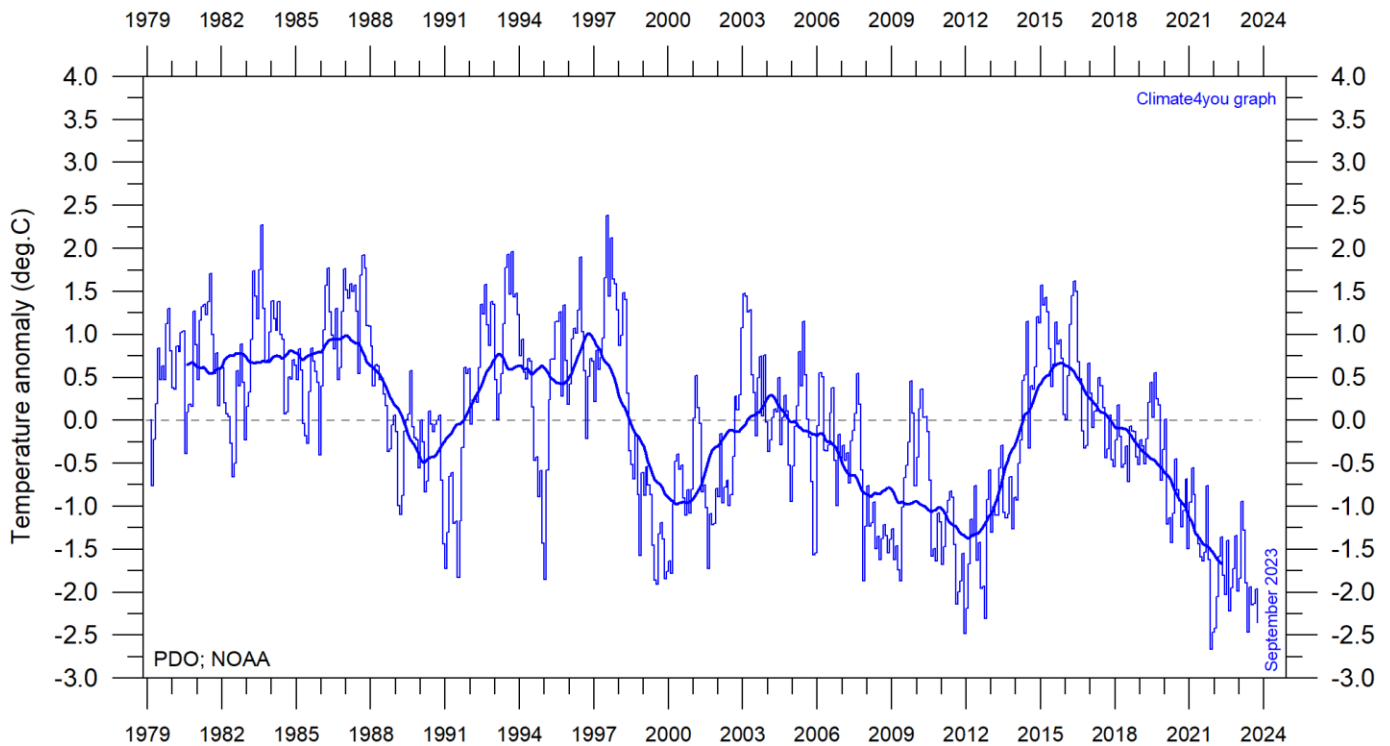


Atlantic Ocean vertical average temperature 0-100 m depth since 1955. The thin line indicates 3-month values, and the thick line represents the simple running 39-month (c. 3 year) average. Data source: [NOAA National Oceanographic Data Center](#) (NODC). Base period 1955-2010.



Indian Ocean vertical average temperature 0-100 m depth since 1955. The thin line indicates 3-month values, and the thick line represents the simple running 39-month (c. 3 year) average. Data source: [NOAA National Oceanographic Data Center](#) (NODC). Base period 1955-2010.

Pacific Decadal Oscillation (PDO), updated to September 2023



20

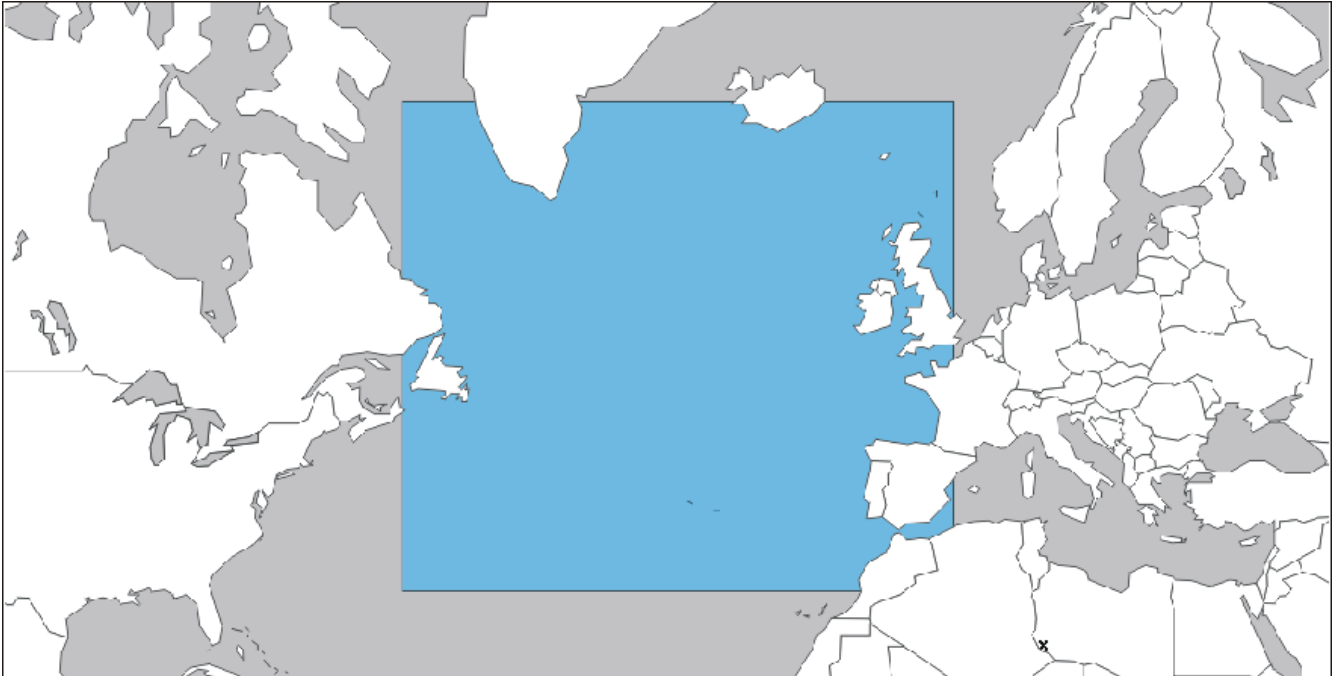
Monthly values of the Pacific Decadal Oscillation (PDO) since January 1979. The PDO is a long-lived El Niño-like pattern of Pacific climate variability, and the data series goes back to January 1854. Base period: 1982-2002. The thin line indicates monthly PDO values, and the thick line is the simple running 37-month average. Data source: [NOAA Physical Science Laboratory](#) (version PDO ERSST V5 plotted above).

The PDO is a long-lived El Niño-like pattern of Pacific climate variability, with data extending back to January 1854. Causes for PDO are not currently known, but even in the absence of a theoretical understanding, PDO climate information improves season-to-season and year-to-year climate forecasts for North America because of its strong tendency for multi-season and multi-year persistence. The PDO also appears to be roughly in phase with global temperature changes. Thus, from a societal impact's perspective, recognition of PDO is important because it shows that "normal" climate conditions can vary over time periods comparable to the length of a human's lifetime.

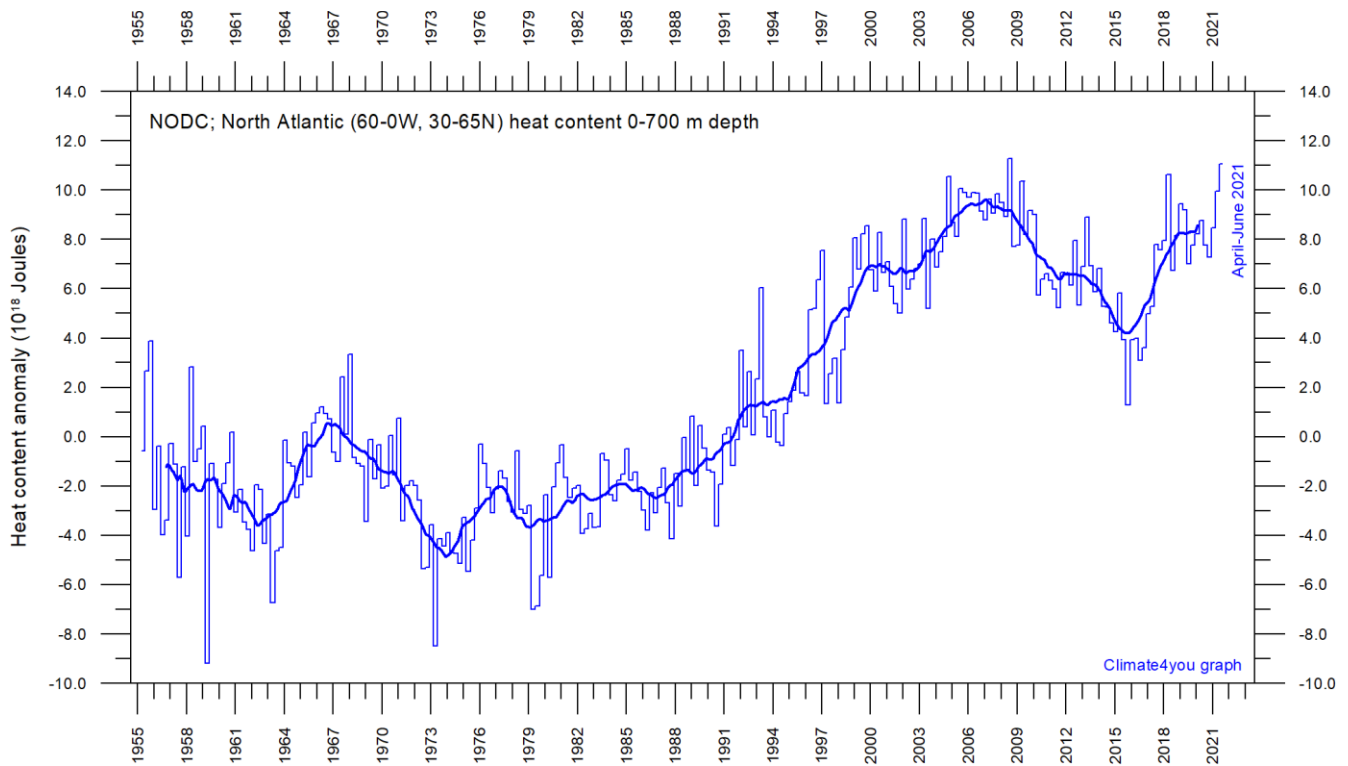
The PDO illustrates how global temperatures are tied to sea surface temperatures in the Pacific Ocean, the largest ocean on Earth. When sea surface temperatures are relatively low (negative phase PDO), as it was from 1945 to 1977, global air temperature often decreases. When Pacific Ocean surface temperatures are high (positive phase PDO), as from 1977 to 1998, global surface air temperature often increases.

A Fourier frequency analysis (not shown here) shows the entire PDO record since 1854 to be influenced by a 5.7-year cycle, and possibly also by a longer about 53-year long cycle.

North Atlantic heat content uppermost 700 m, updated to June 2021

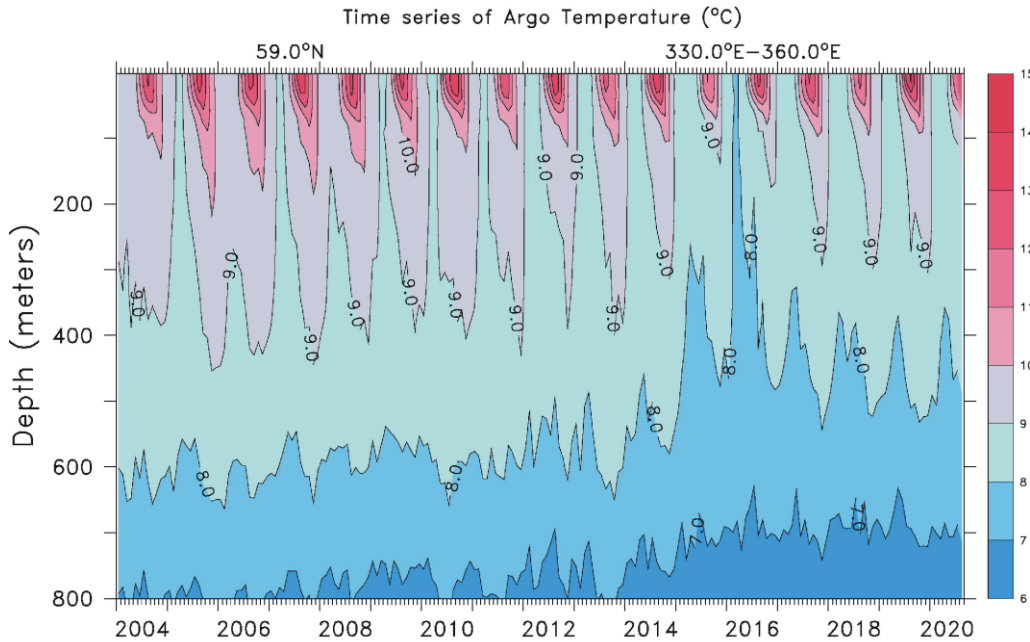


21

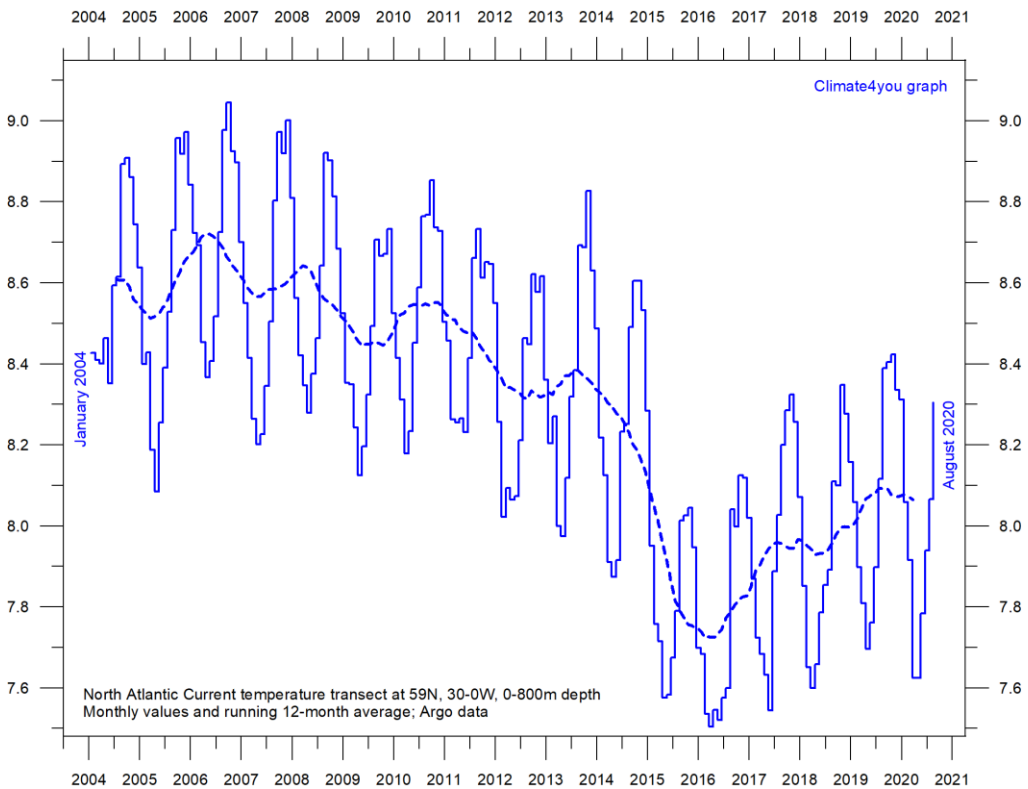


Global monthly heat content anomaly (10^{18} Joules) in the uppermost 700 m of the North Atlantic (60-0W, 30-65N; see map above) ocean since January 1955. The thin line indicates monthly values, and the thick line represents the simple running 37-month (c. 3 year) average. Data source: [National Oceanographic Data Center](https://www.nodc.noaa.gov/) (NODC).

North Atlantic temperatures 0-800 m depth along 59°N, 30-0W, updated to August 2020

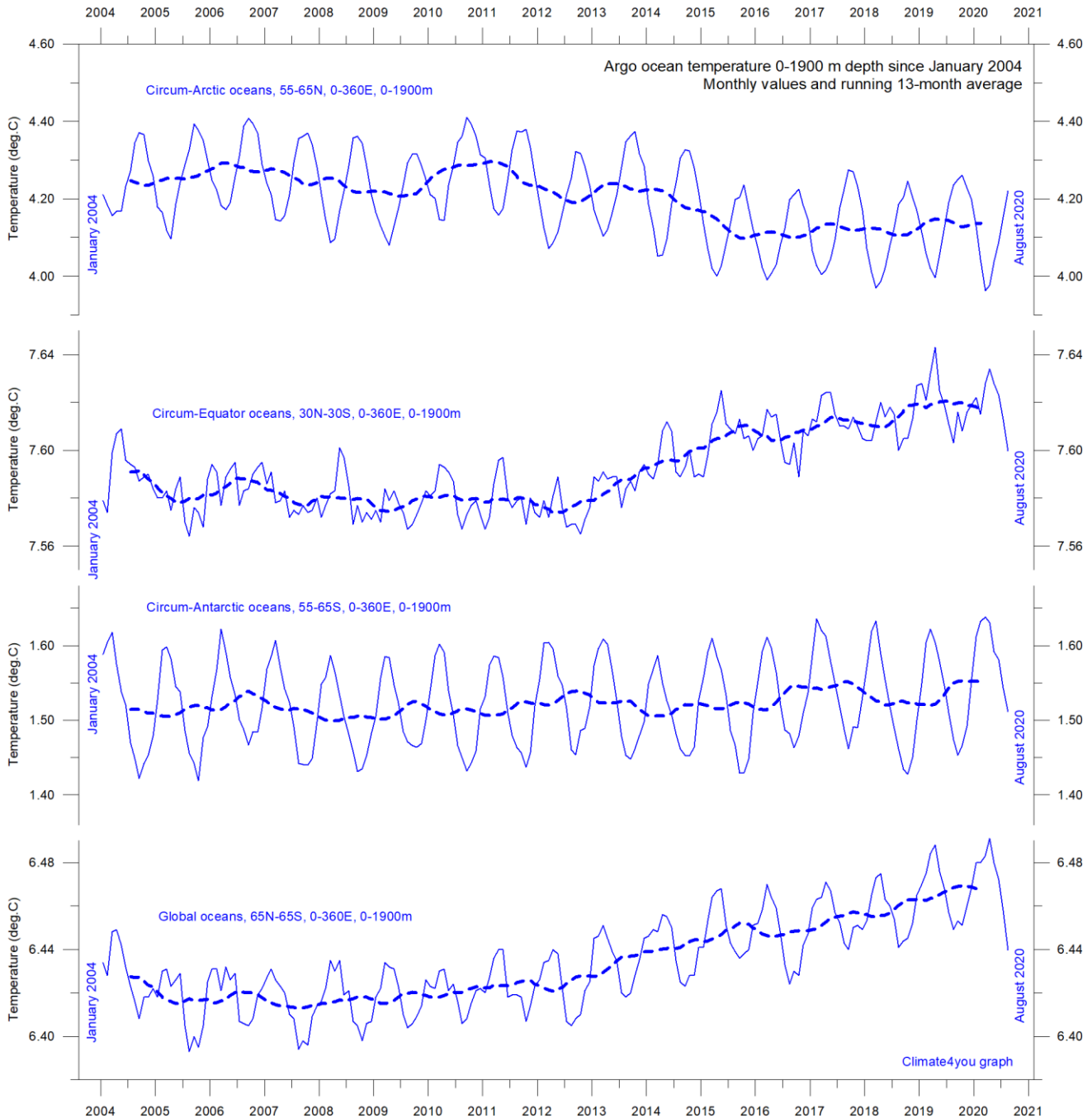


Time series depth-temperature diagram along 59 N across the North Atlantic Current from 30°W to 0°W, from surface to 800 m depth. Source: [Global Marine Argo Atlas](#). See also the diagram below.



Average temperature along 59 N, 30-0W, 0-800m depth, corresponding to the main part of the North Atlantic Current, using [Argo](#)-data. Source: [Global Marine Argo Atlas](#). Additional information can be found in: Roemmich, D. and J. Gilson, 2009. The 2004-2008 mean and annual cycle of temperature, salinity, and steric height in the global ocean from the Argo Program. [Progress in Oceanography](#), 82, 81-100.

Global ocean temperature 0-1900 m depth summary, updated to August 2020

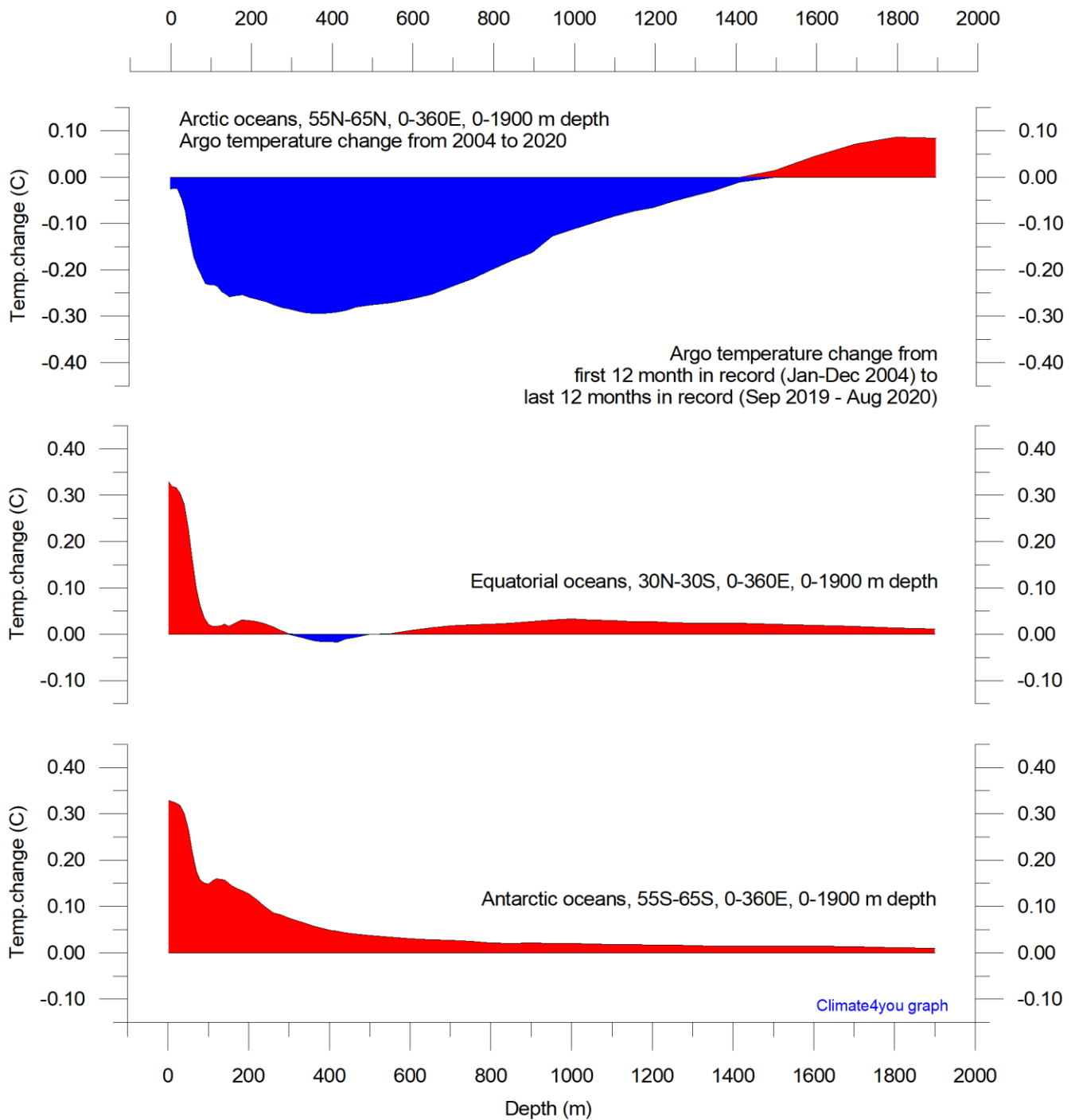


Summary of average temperature in uppermost 1900 m in different parts of the global oceans, using [Argo](#)-data. Source: [Global Marine Argo Atlas](#). Additional information can be found in: Roemmich, D. and J. Gilson, 2009. The 2004-2008 mean and annual cycle of temperature, salinity, and steric height in the global ocean from the Argo Program. [Progress in Oceanography](#), 82, 81-100.

The global summary diagram above shows that, on average, the temperature of the global oceans down to 1900 m depth has been increasing since about 2011. It is also seen that this increase since 2013 dominantly is due to oceanic changes occurring near the Equator, between 30°N

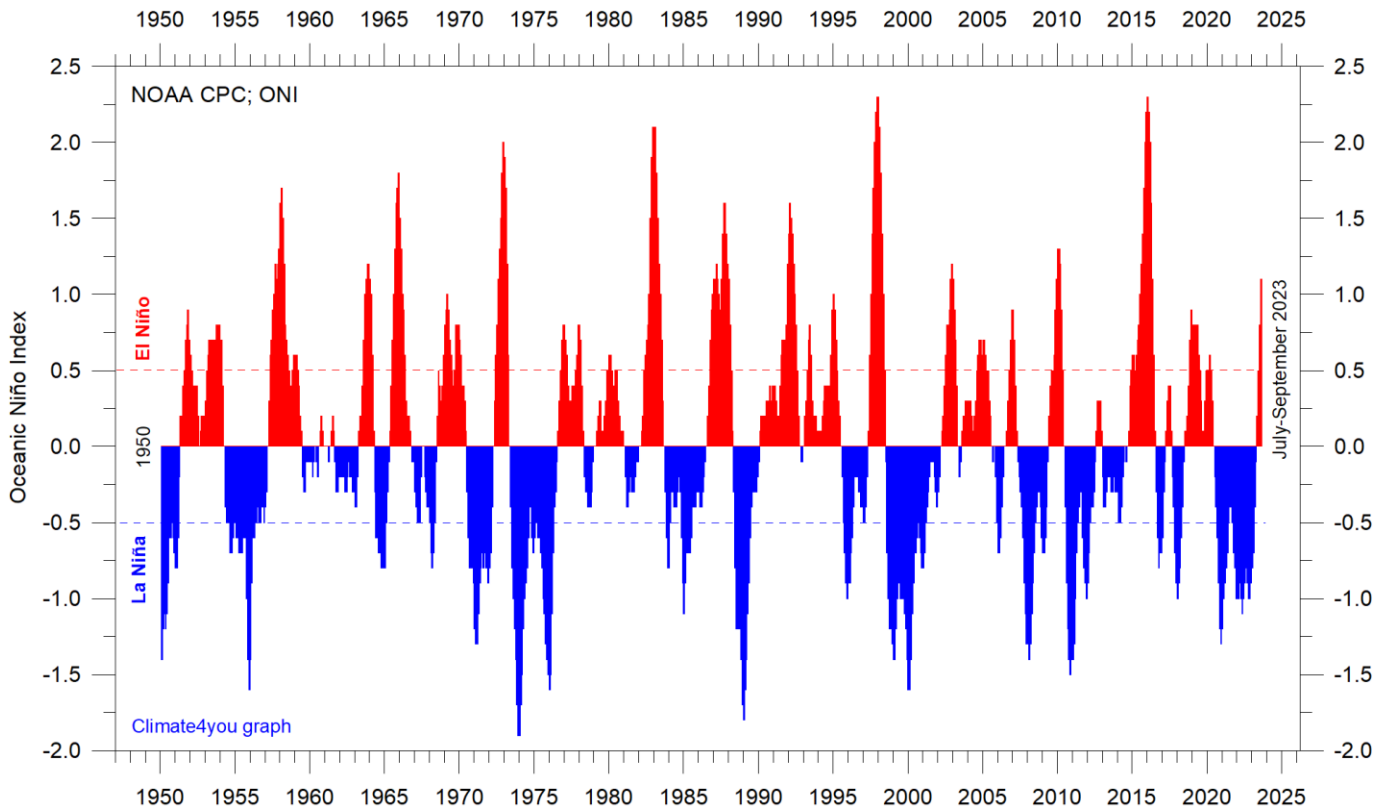
and 30°S. In contrast, for the circum-Arctic oceans north of 55°N, depth-integrated ocean temperatures have been decreasing since 2011. Near the Antarctic, south of 55°S, temperatures have essentially been stable. At most latitudes, a clear annual rhythm is evident.

Global ocean net temperature change since 2004 at different depths, updated to August 2020



Net temperature change since 2004 from surface to 1900 m depth in different parts of the global oceans, using [Argo-data](#). Source: [Global Marine Argo Atlas](#). Additional information can be found in: Roemmich, D. and J. Gilson, 2009. The 2004-2008 mean and annual cycle of temperature, salinity, and steric height in the global ocean from the Argo Program. [Progress in Oceanography](#), 82, 81-100. Please note that due to the spherical form of Earth, northern and southern latitudes represent only small ocean volumes, compared to latitudes near the Equator.

La Niña and El Niño episodes, Oceanic Niño Index (ONI), updated to September 2023



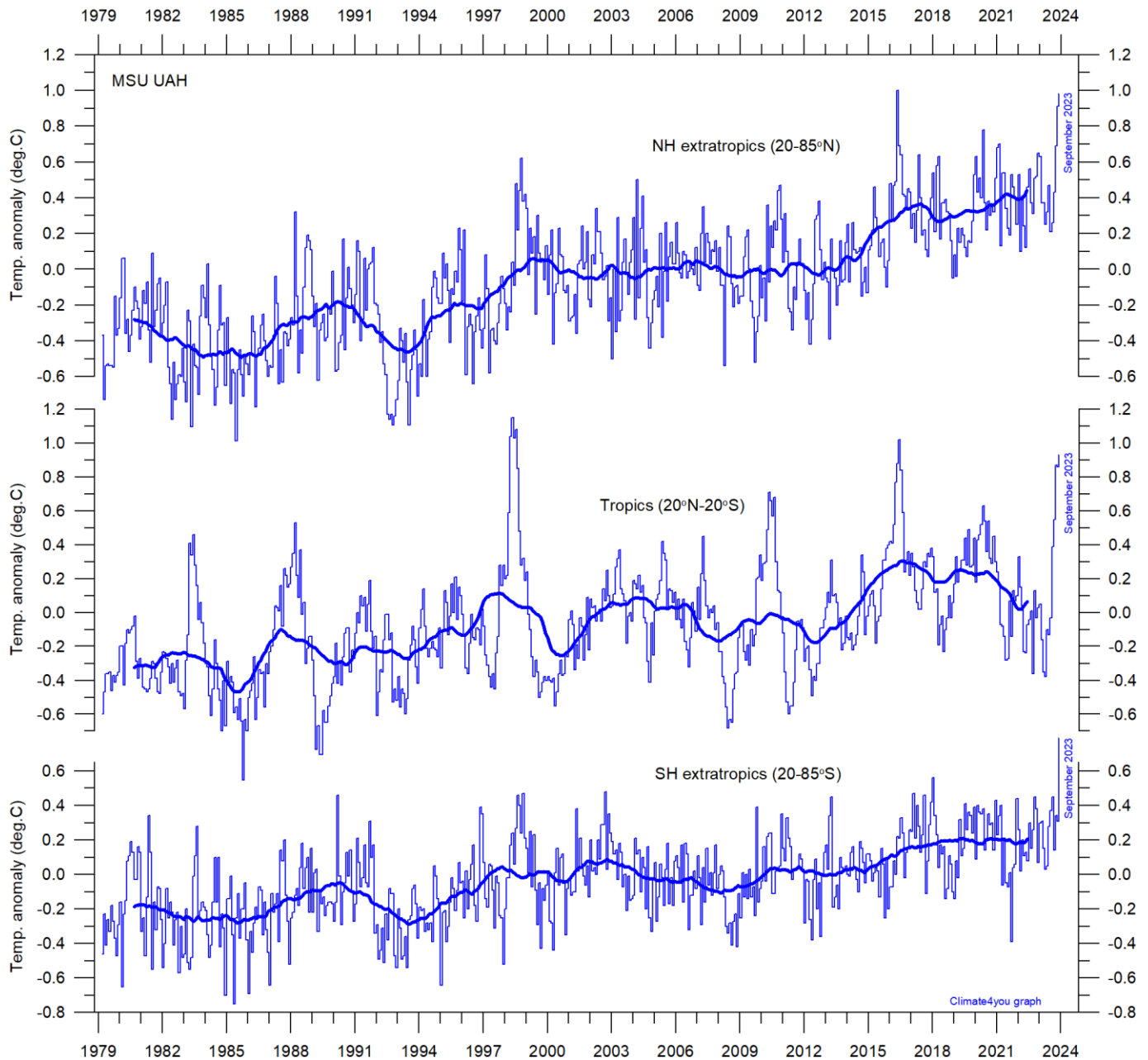
25

Warm ($>+0.5^{\circ}\text{C}$) and cold ($<0.5^{\circ}\text{C}$) episodes for the [Oceanic Niño Index \(ONI\)](#), defined as 3 month running mean of ERSSTv4 SST anomalies in the Niño 3.4 region (5°N - 5°S , 120° - 170°W). For historical purposes cold and warm episodes are defined when the threshold is met for a minimum of 5 consecutive over-lapping seasons. Anomalies are centred on 30-yr base periods updated every 5 years.

The 2015-16 El Niño episode is among the strongest since the beginning of the record in 1950. Considering the entire record, however, recent variations

between El Niño and La Niña episodes do not appear abnormal in any way. See also diagrams on pages 44 and 53.

Zonal lower troposphere temperatures from satellites, updated to September 2023

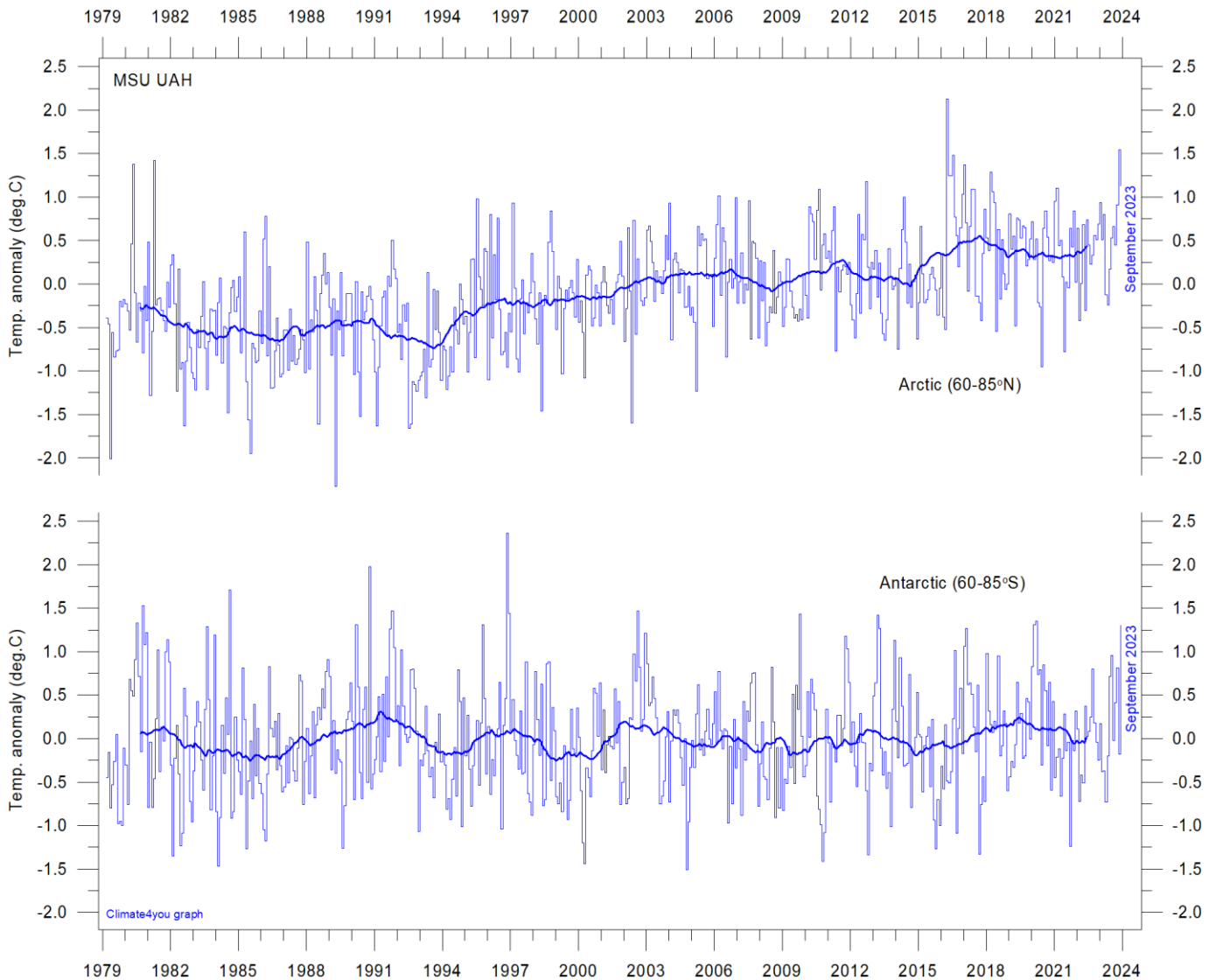


Global monthly average lower troposphere temperature since 1979 for the tropics and the northern and southern extratropics, according to University of Alabama at Huntsville, USA. Thin lines show the monthly temperature. Thick lines represent the simple running 37-month average, nearly corresponding to a running 3-year average. Reference period 1981-2010.

The overall warming since 1980 has dominantly been a northern hemisphere phenomenon, and mainly played out as a marked change between 1994 and 1999. However, this rather rapid temperature change is probably influenced by the Mt. Pinatubo eruption 1992-93 and the subsequent 1997 El Niño episode. The diagram also shows the

temperature effects of the strong Equatorial El Niño's in 1997 and 2015-16, as well as the moderate El Niño in 2019. Apparently, these effects were spreading to higher latitudes in both hemispheres with some delay. Just now a new El Niño has begun in the Pacific Ocean (p.25), as indicated by tropics surface air temperatures.

Arctic and Antarctic lower troposphere temperature, updated to September 2023



Global monthly average lower troposphere temperature since 1979 for the North Pole and South Pole regions, based on satellite observations ([University of Alabama](#) at Huntsville, USA). Thin lines show the monthly temperature. The thick line is the simple running 37-month average, nearly corresponding to a running 3-year average. Reference period 1991-2020.

In the Arctic region, warming mainly took place 1994-96, and less so subsequently. In 2016, however, temperatures peaked for several months, presumably because of oceanic heat given off to the atmosphere during the 2015-15 El Niño (see also diagram on page 25) and subsequently advected to higher latitudes.

This underscores how Arctic air temperatures may be affected not only by variations in local conditions but also by variations playing out in geographically remote regions.

A slight, but persistent, temperature decrease has characterised the Arctic since the 2016 peak (see also diagrams on page 28-30).

In the Antarctic region, temperatures have basically remained stable since the onset of the satellite record in 1979. In 2016-17 a small temperature peak visible in the monthly record may be interpreted as the subdued effect of the recent El Niño episode.

Arctic and Antarctic surface air temperature, updated to December 2021

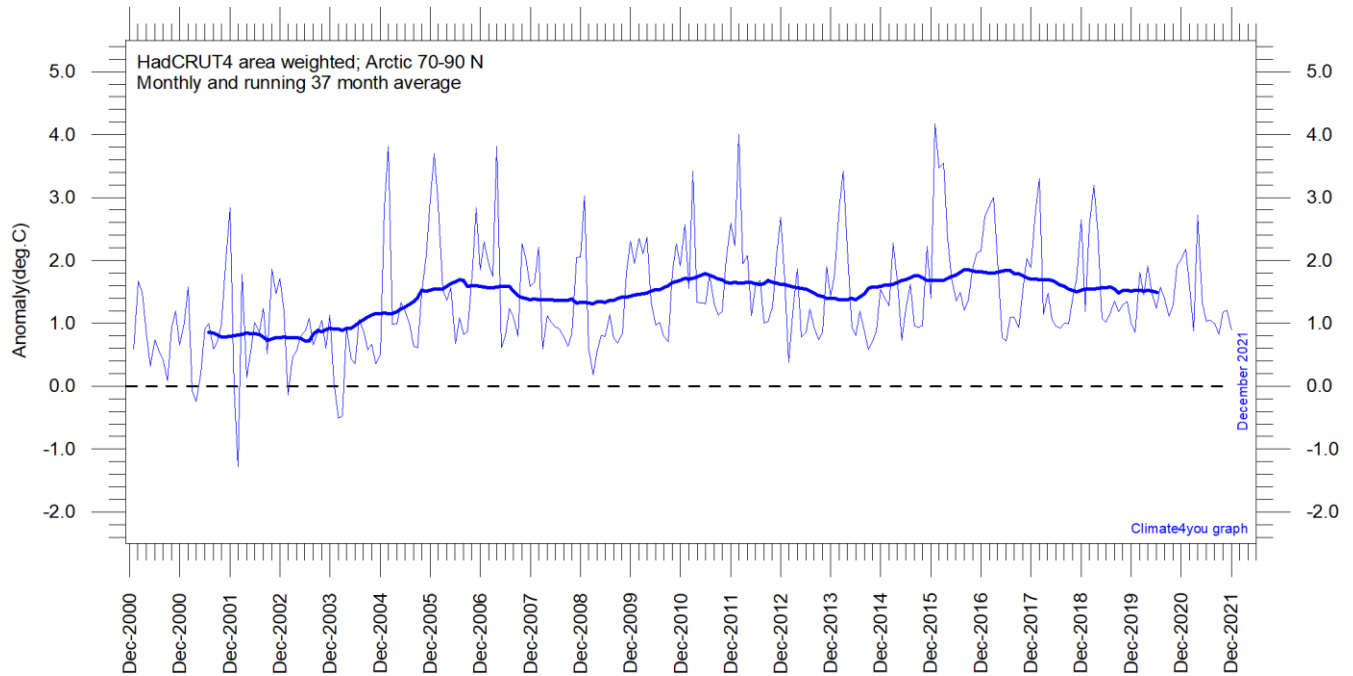


Diagram showing area weighted Arctic (70-90°N) monthly surface air temperature anomalies ([HadCRUT4](#)) since January 2000, in relation to the WMO [normal period](#) 1961-1990. The thin line shows the monthly temperature anomaly, while the thicker line shows the running 37-month (c. 3 year) average.

28

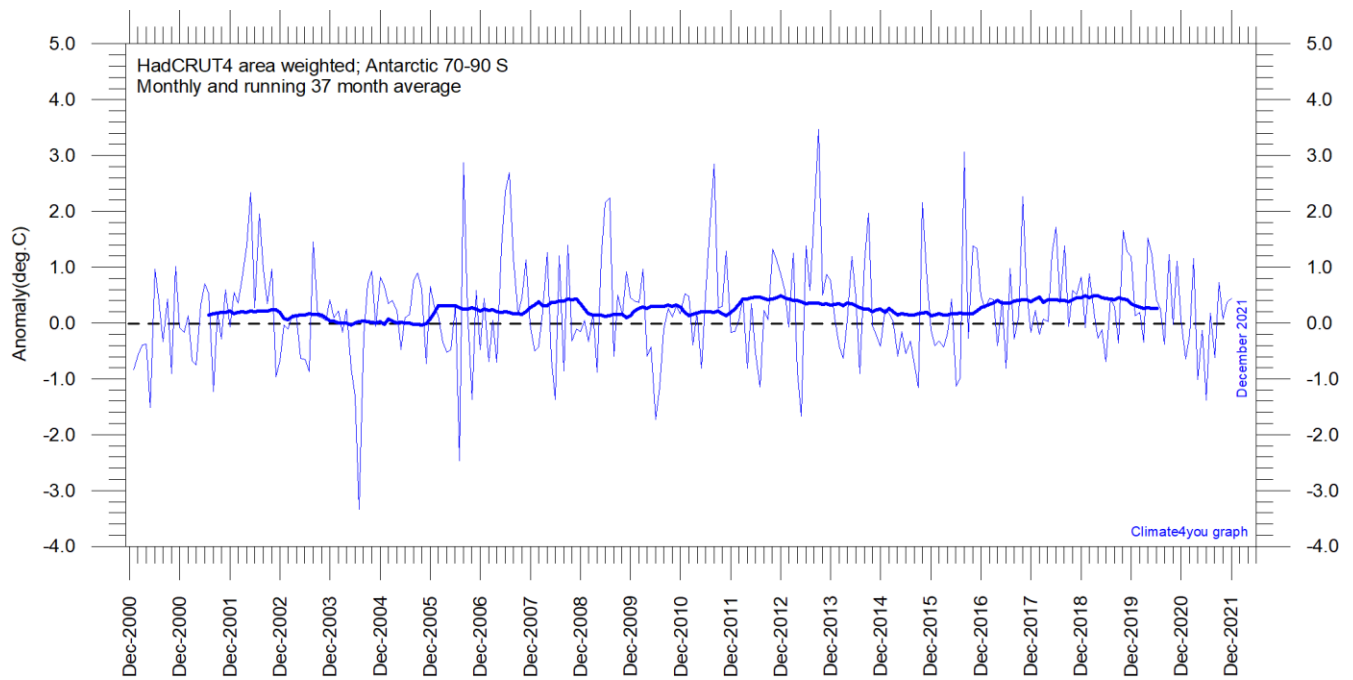


Diagram showing area weighted Antarctic (70-90°S) monthly surface air temperature anomalies ([HadCRUT4](#)) since January 2000, in relation to the WMO [normal period](#) 1961-1990. The thin line shows the monthly temperature anomaly, while the thicker line shows the running 37-month (c. 3 year) average.

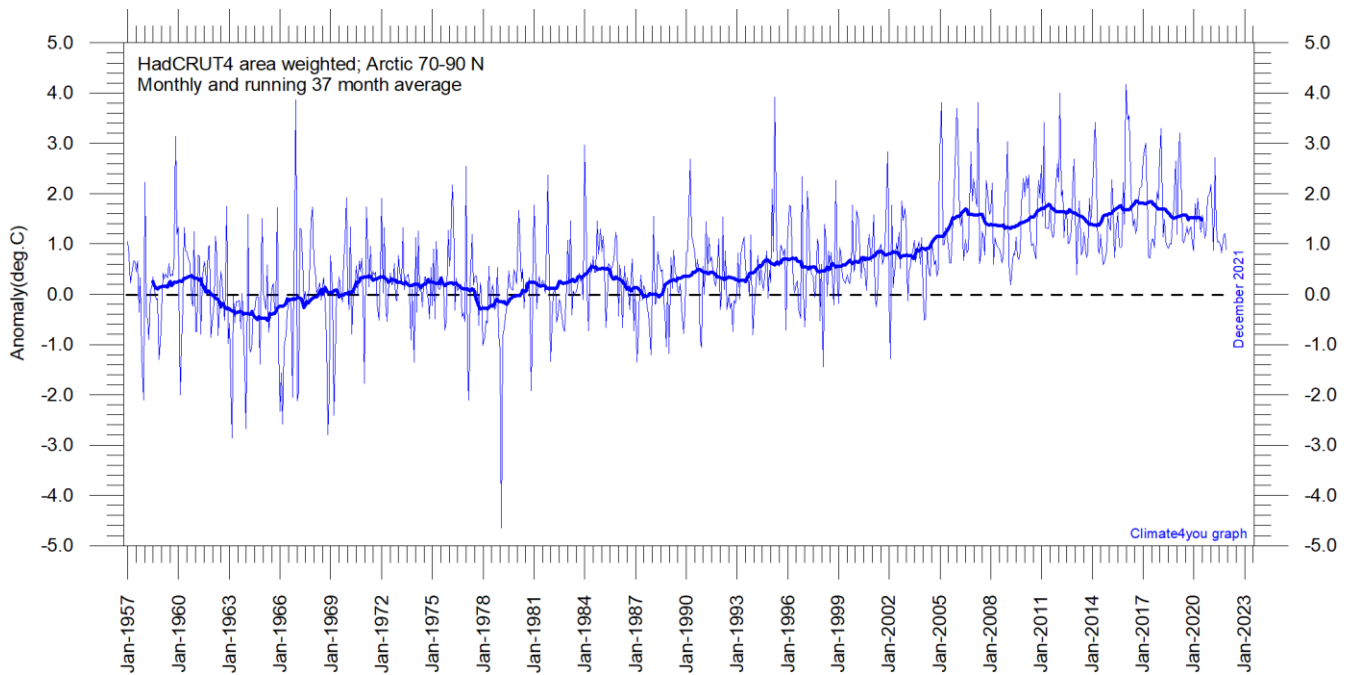


Diagram showing area weighted Arctic (70-90°N) monthly surface air temperature anomalies ([HadCRUT4](#)) since January 1957, in relation to the WMO [normal period](#) 1961-1990. The thin line shows the monthly temperature anomaly, while the thicker line shows the running 37-month (c. 3 year) average.

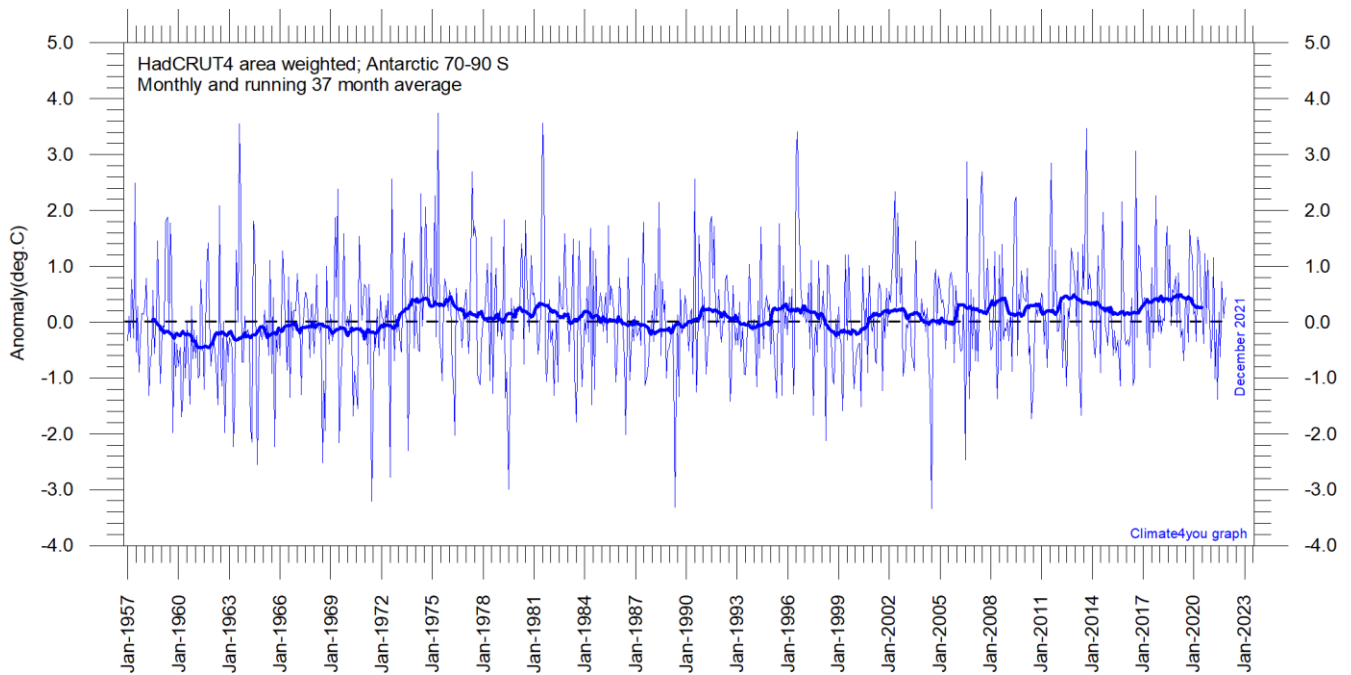


Diagram showing area weighted Antarctic (70-90°S) monthly surface air temperature anomalies ([HadCRUT4](#)) since January 1957, in relation to the WMO [normal period](#) 1961-1990. The thin line shows the monthly temperature anomaly, while the thicker line shows the running 37-month (c. 3 year) average.

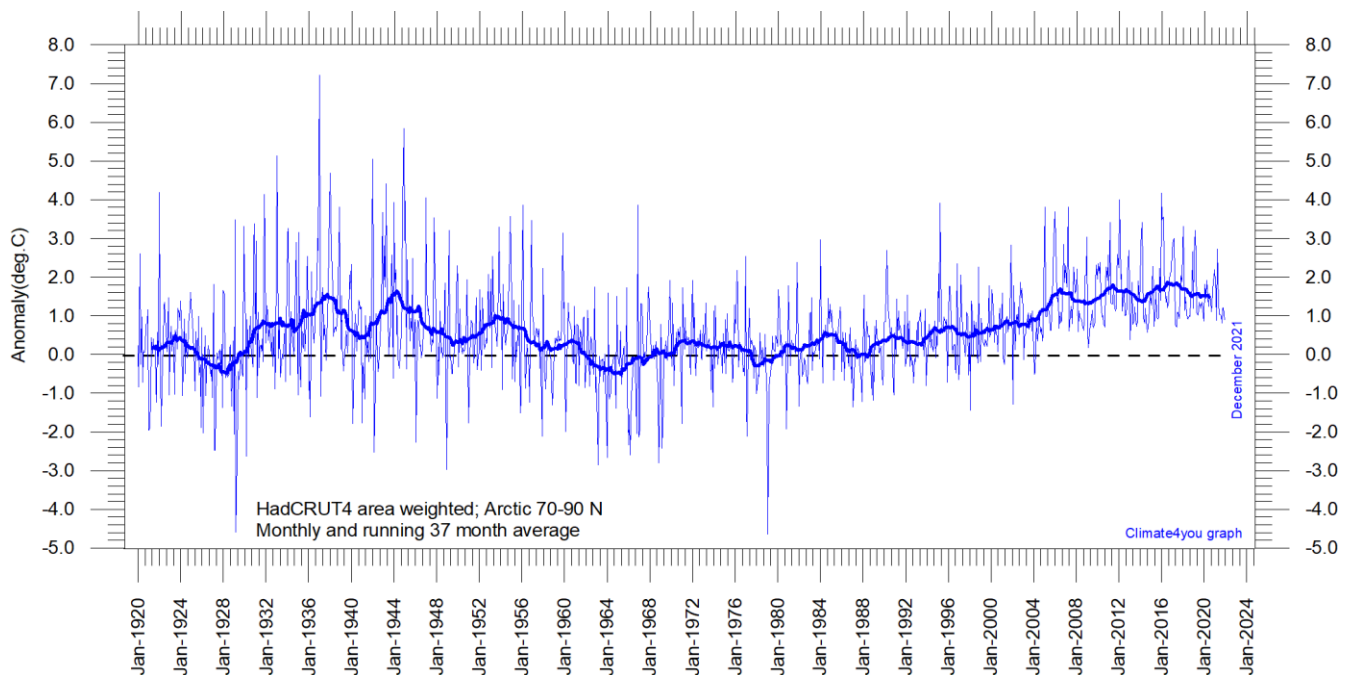


Diagram showing area-weighted Arctic (70-90°N) monthly surface air temperature anomalies ([HadCRUT4](#)) since January 1920, in relation to the WMO [normal period](#) 1961-1990. The thin line shows the monthly temperature anomaly, while the thicker line shows the running 37-month (c. 3 year) average.

Because of the relatively small number of Arctic stations before 1930, month-to-month variations in the early part of the Arctic temperature record 1920-2018 are higher than later (diagram above).

The period from about 1930 saw the establishment of many new Arctic meteorological stations, first in Russia and Siberia, and following the 2nd World War, also in North America, explaining the above difference.

The period since 2005 is warm, about as warm as the period 1930-1940.

As the HadCRUT4 data series has improved high latitude coverage data coverage (compared to the HadCRUT3 series), the individual 5°x5° grid cells have been weighted according to their surface area. This area correction is especially important for polar

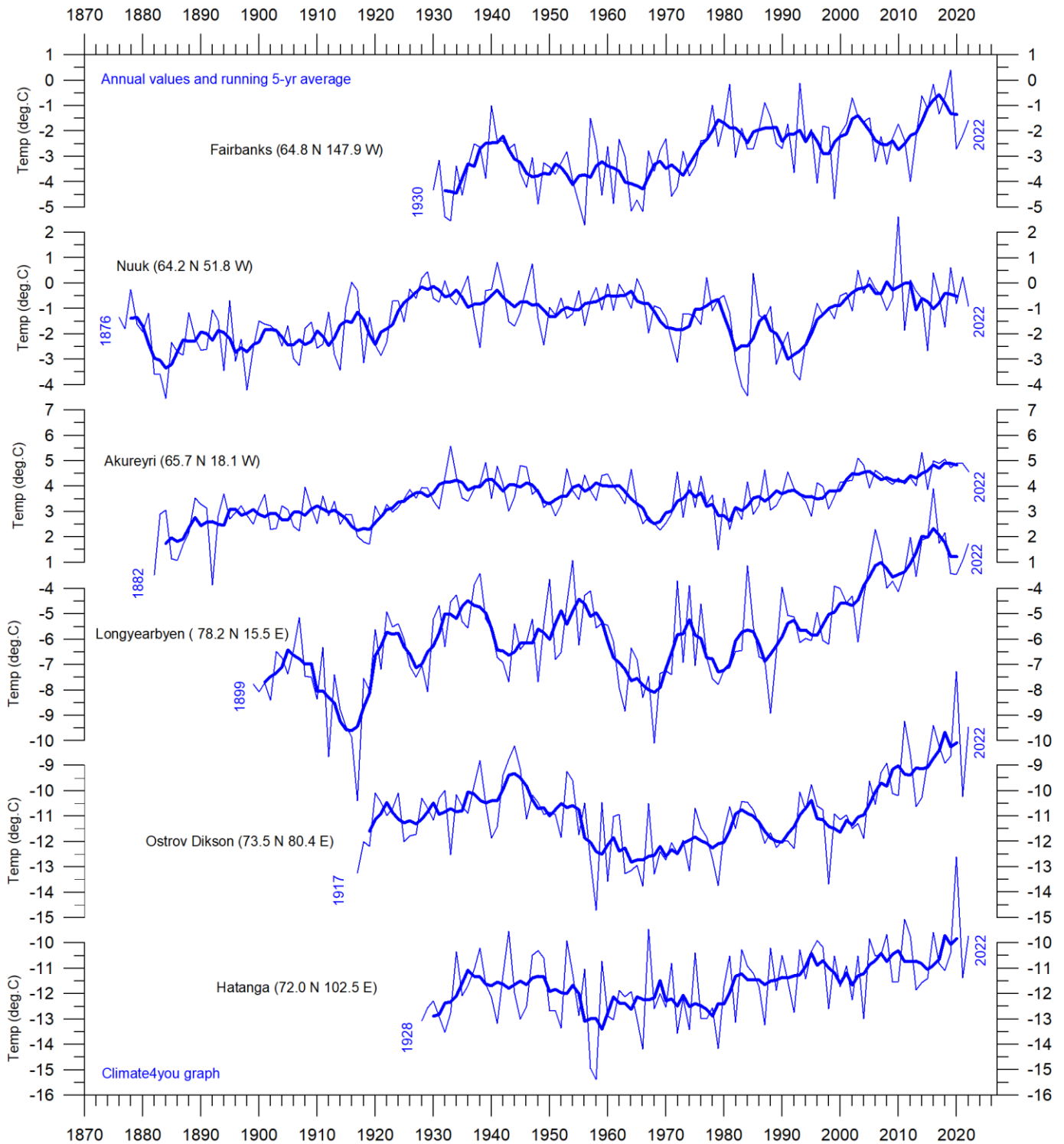
regions, where longitudes converge rapidly. This approach differs from the approach used by Gillett et al. 2008, which calculated a simple average, with no correction for the substantial latitudinal surface area effect in polar regions.

The area weighted Arctic HadCRUT4 surface air temperature anomalies (p.28-30) correspond rather well to the lower troposphere temperature anomalies recorded by satellites (p.27).

Literature:

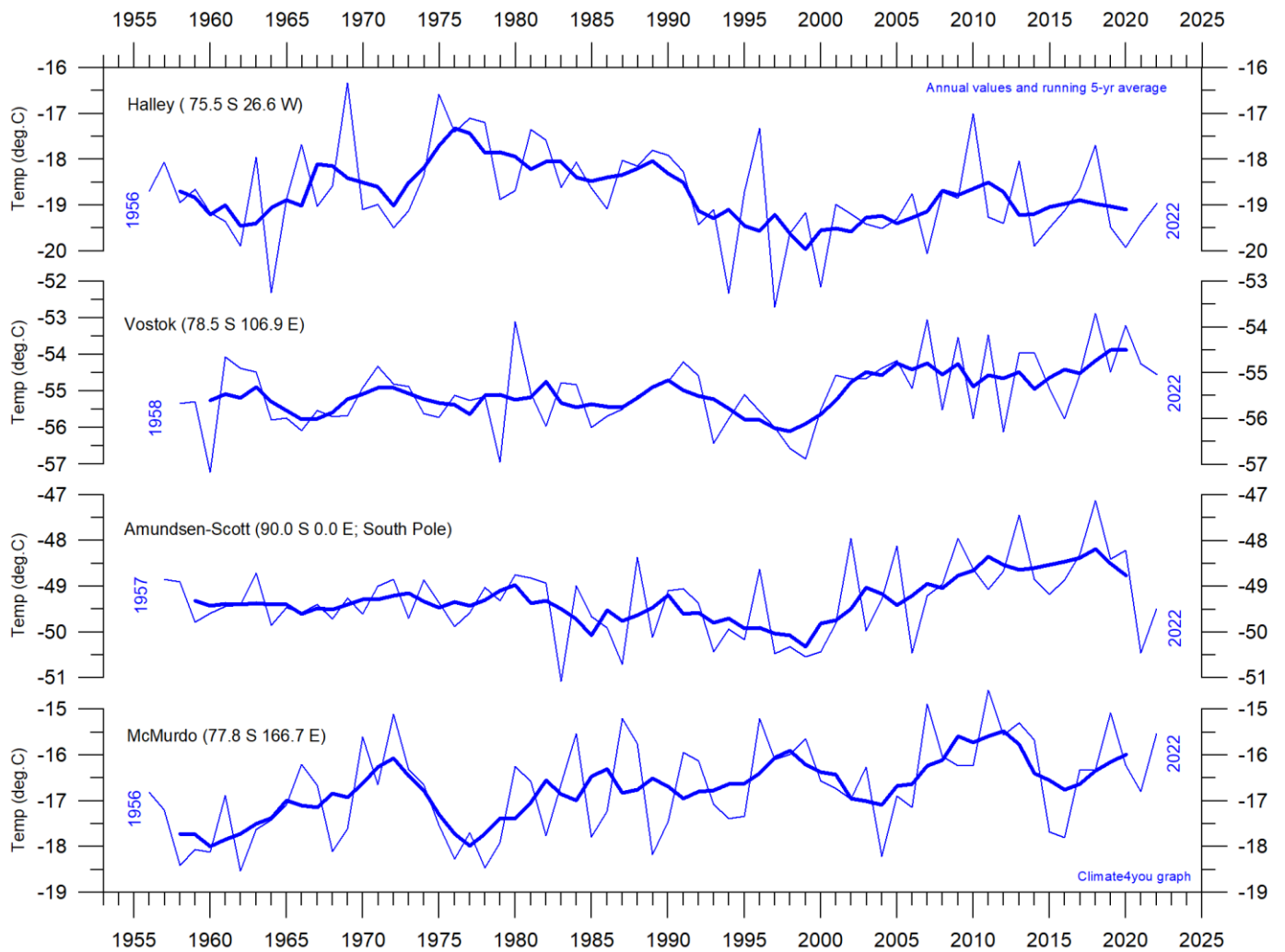
Gillett, N.P., Stone, D.A., Stott, P.A., Nozawa, T., Karpechko, A.Y.U., Hegerl, G.C., Wehner, M.F. and Jones, P.D. 2008. Attribution of polar warming to human influence. *Nature Geoscience* 1, 750-754.

Long Arctic annual surface air temperature series, updated to year 2022



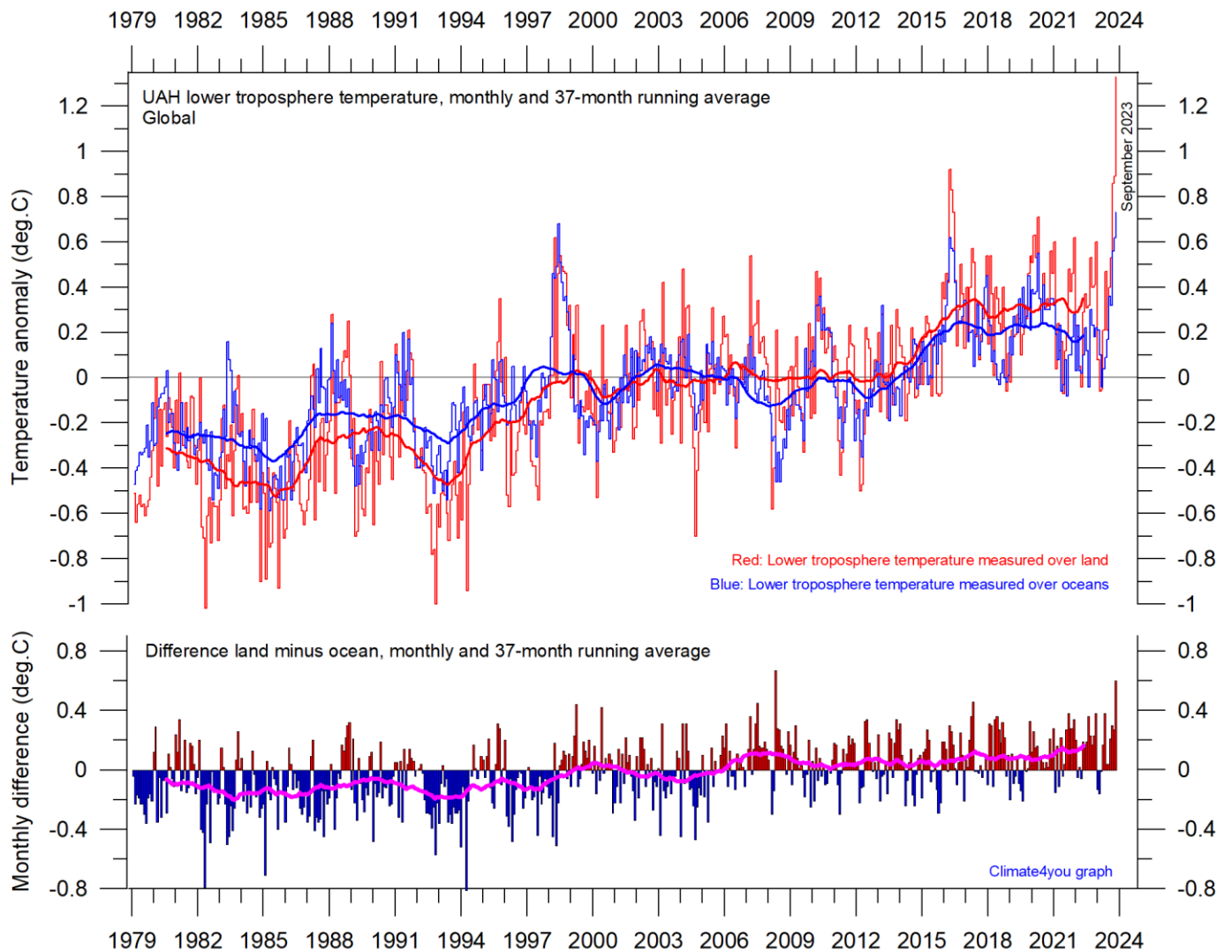
Arctic annual surface air temperature series, selected because of their length of observation time. The thin blue line represents the mean annual air temperature, and the thick blue line is the running 5-year average. Annual values were calculated from monthly average temperatures. More info on [Climate4you](#).

Long Antarctic annual surface air temperature series, updated to year 2022



Antarctic annual surface air temperature series, selected because of their length of observation time. The thin blue line represents the mean annual air temperature, and the thick blue line is the running 5-year average. Annual values were calculated from monthly average temperatures. More info on [Climate4you](https://climate4you.com).

Temperature over land versus over oceans, updated to September 2023

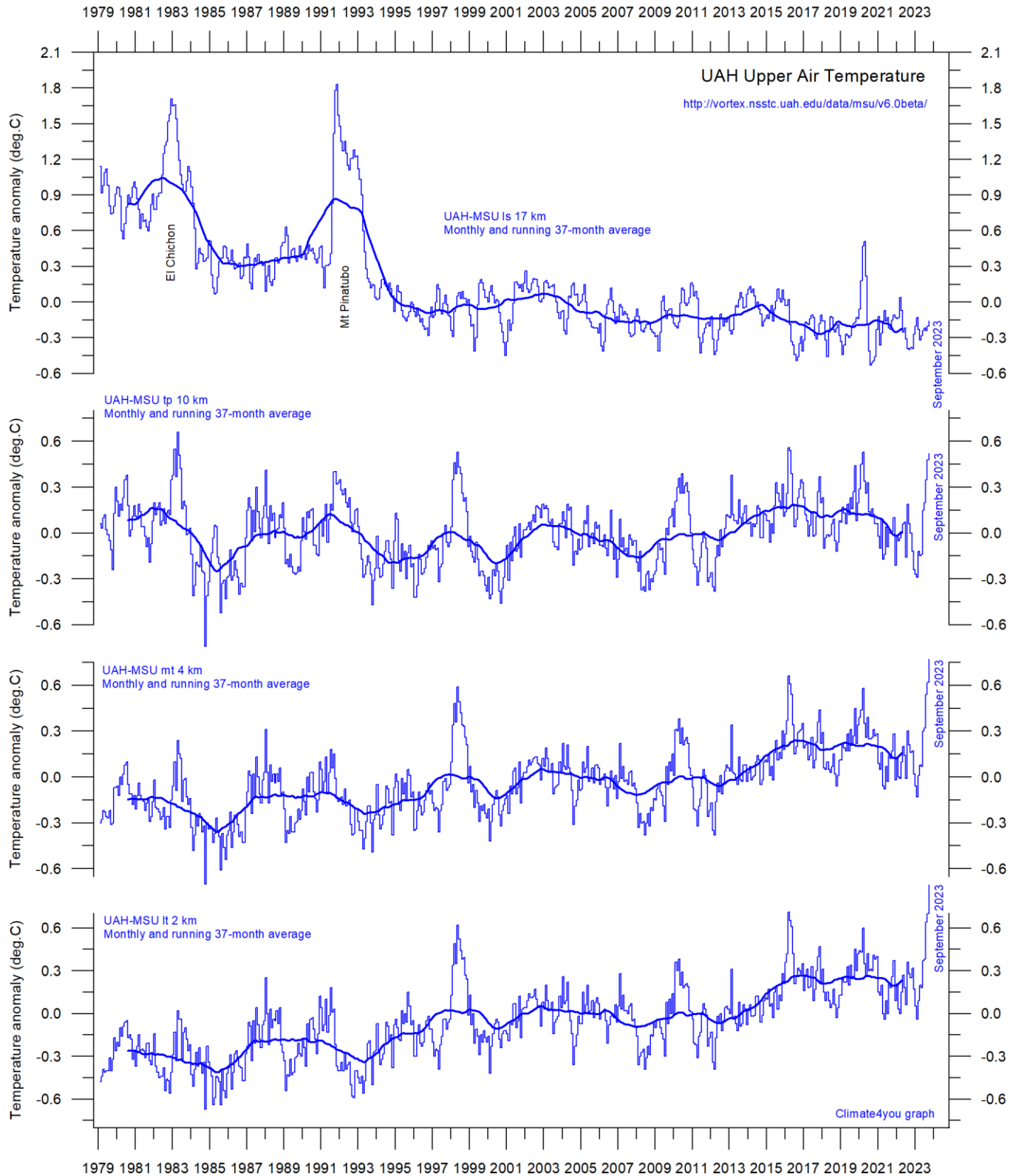


Global monthly average lower troposphere temperature since 1979 measured over land and oceans, respectively, according to [University of Alabama](#) at Huntsville, USA. Thick lines are the simple running 37-month average, nearly corresponding to a running 3-year average. Reference period 1991-2020.

Since 1979, the lower troposphere over land has warmed much more than over oceans, suggesting that the overall warming is derived mainly from

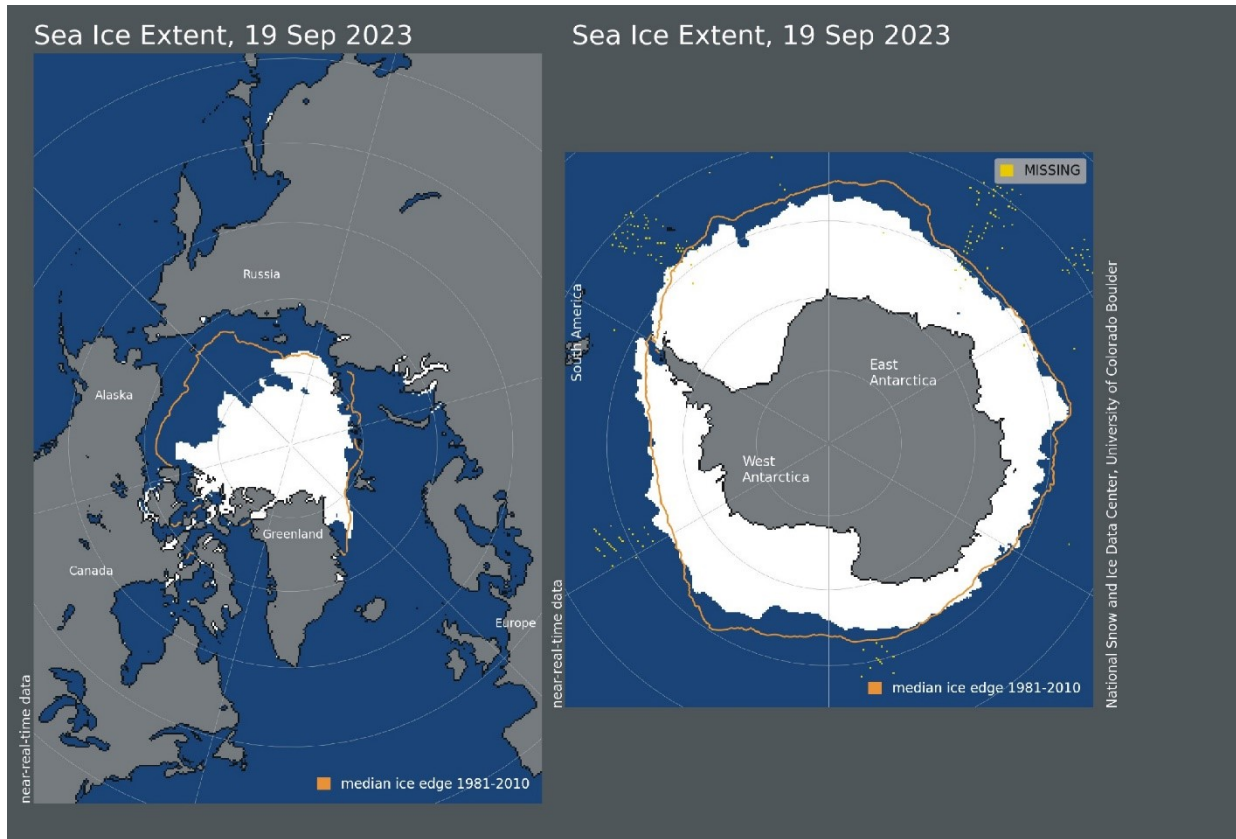
incoming solar radiation. In addition, there may be supplementary reasons for this divergence, such as, e.g., variations in cloud cover and changes in land use.

Troposphere and stratosphere temperatures from satellites, updated to September 2023



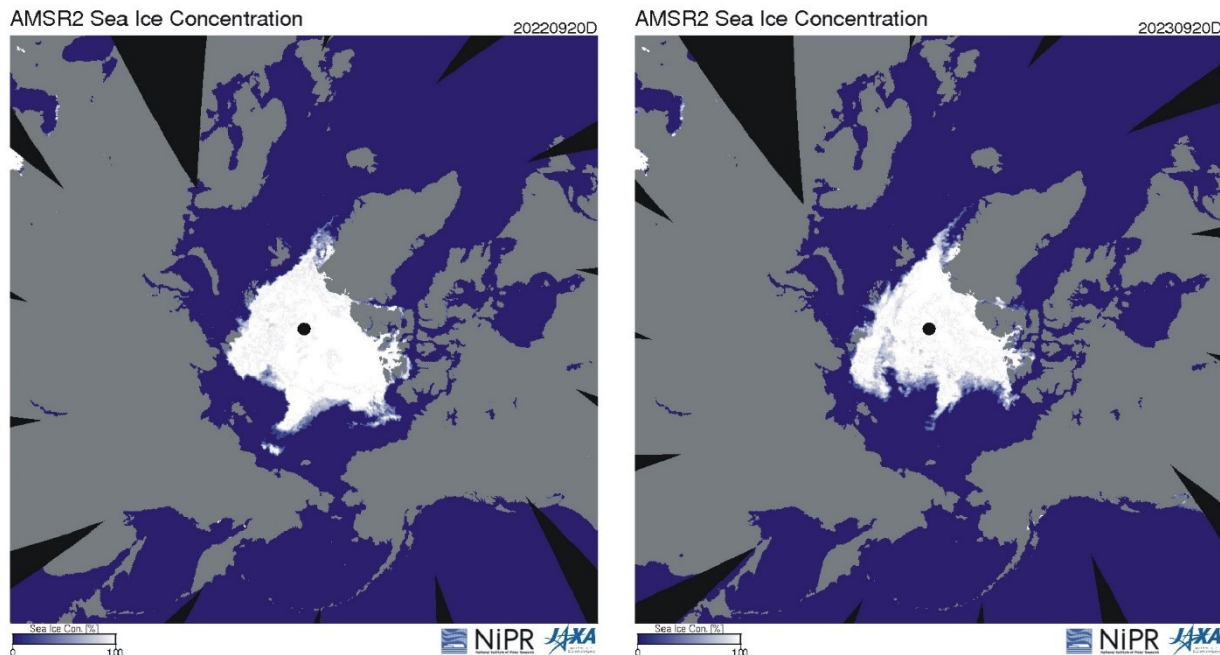
Global monthly average temperature in different according to University of Alabama at Huntsville, USA. The thin lines represent the monthly average, and the thick line the simple running 37-month average, nearly corresponding to a running 3-year average. Reference period 1991-2020.

Arctic and Antarctic sea ice, updated to September 2023

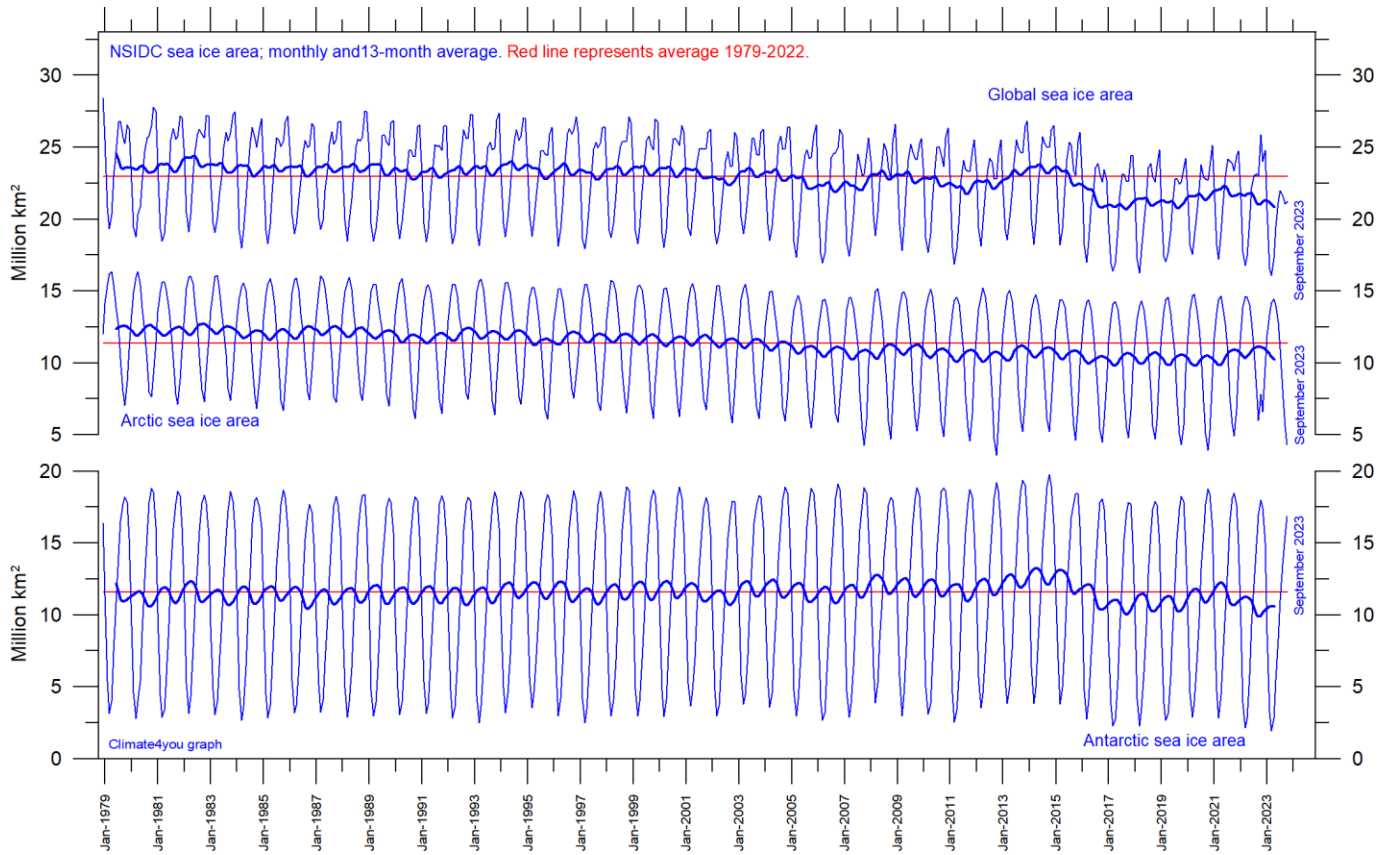


35

Sea ice extent 19 September 2023. The median limit of sea ice (orange line) is defined as 15% sea ice cover, according to the average of satellite observations 1981-2010 (both years included). Sea ice may therefore well be encountered outside and open water areas inside the limit shown in the diagrams above. Map source: National Snow and Ice Data Center (NSIDC).



Diagrams showing Arctic sea ice extent and concentration 20 September 2022 (left) and 2023 (right), according to the Japan Aerospace Exploration Agency (JAXA).



Graphs showing monthly Antarctic, Arctic, and global sea ice extent since November 1978, according to the [National Snow and Ice data Center \(NSIDC\)](#).

36

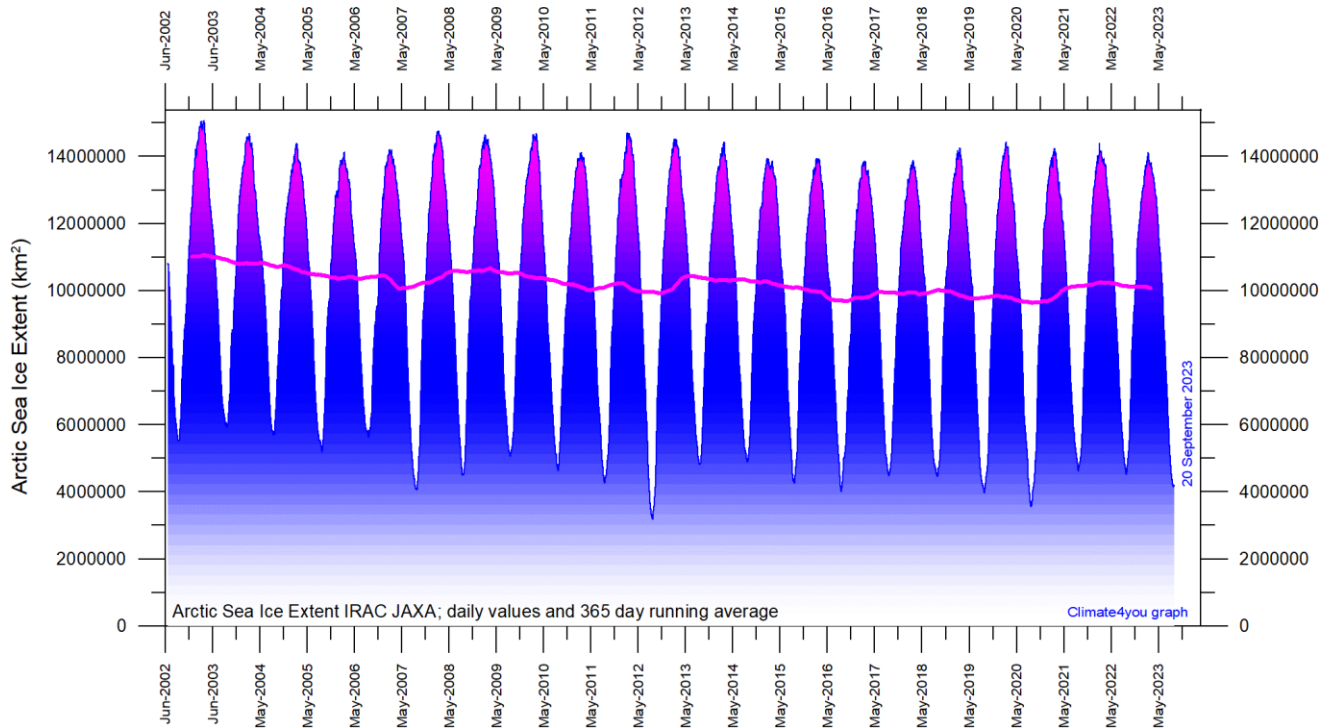
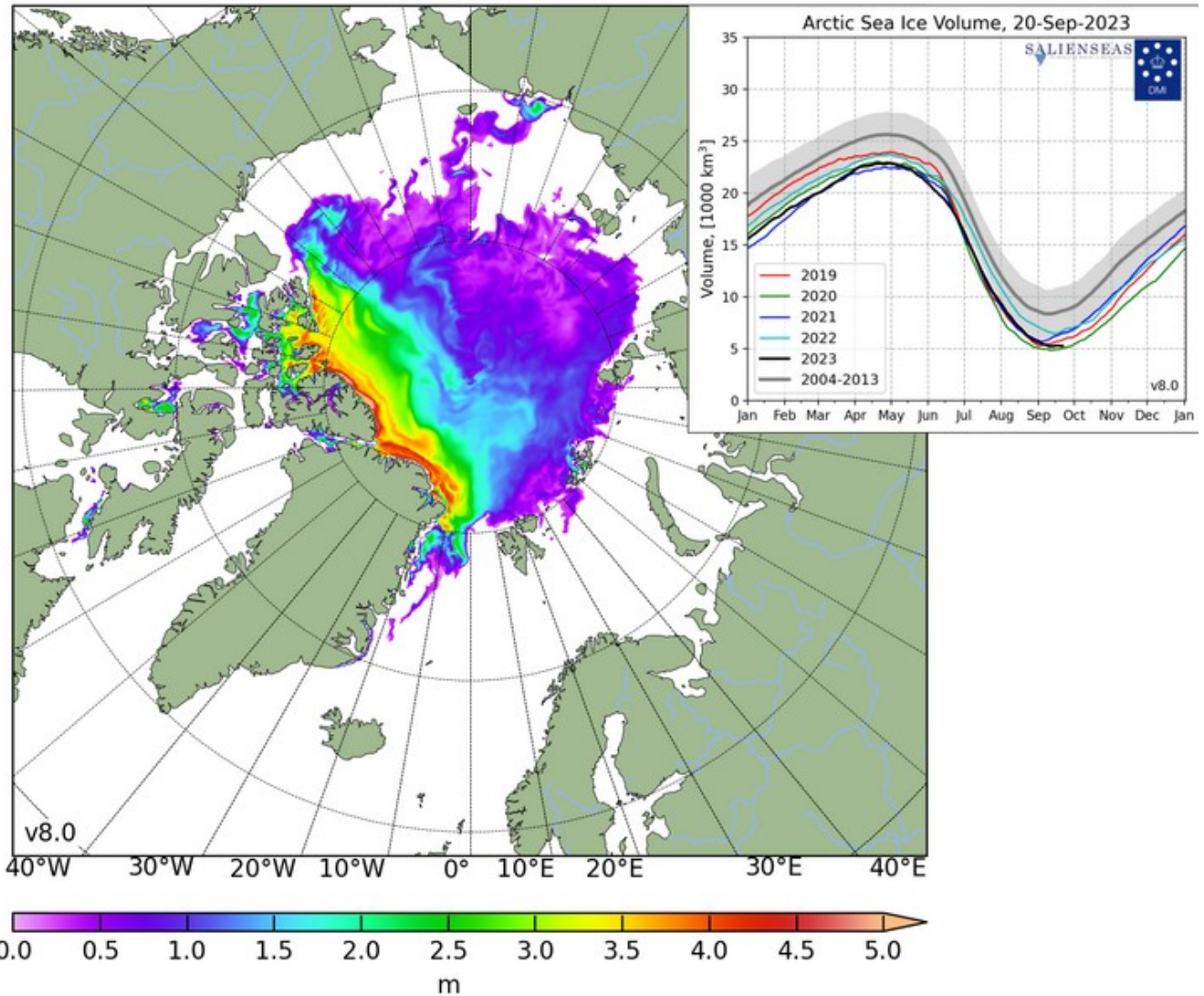
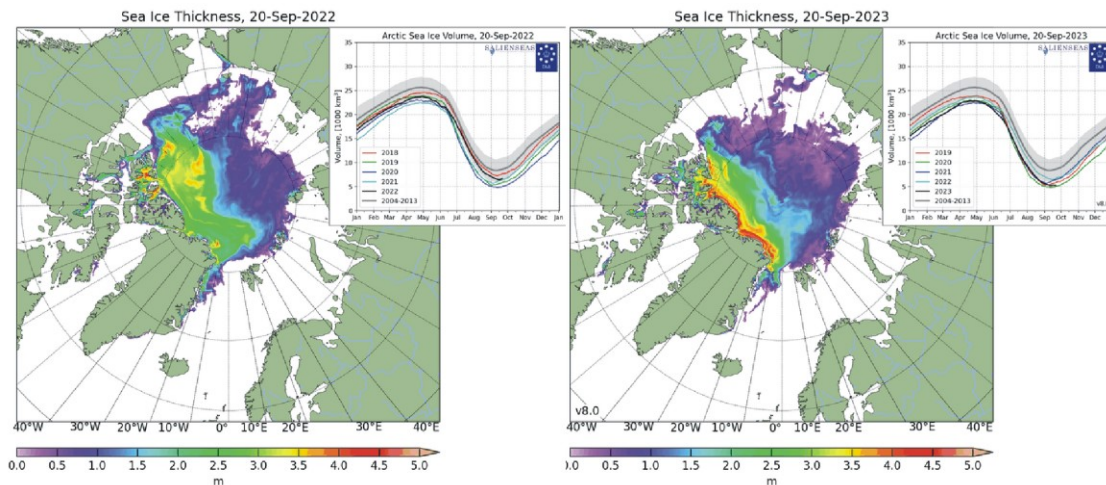


Diagram showing daily Arctic sea ice extent since June 2002, to 20 September 2023, data courtesy of [Japan Aerospace Exploration Agency \(JAXA\)](#).

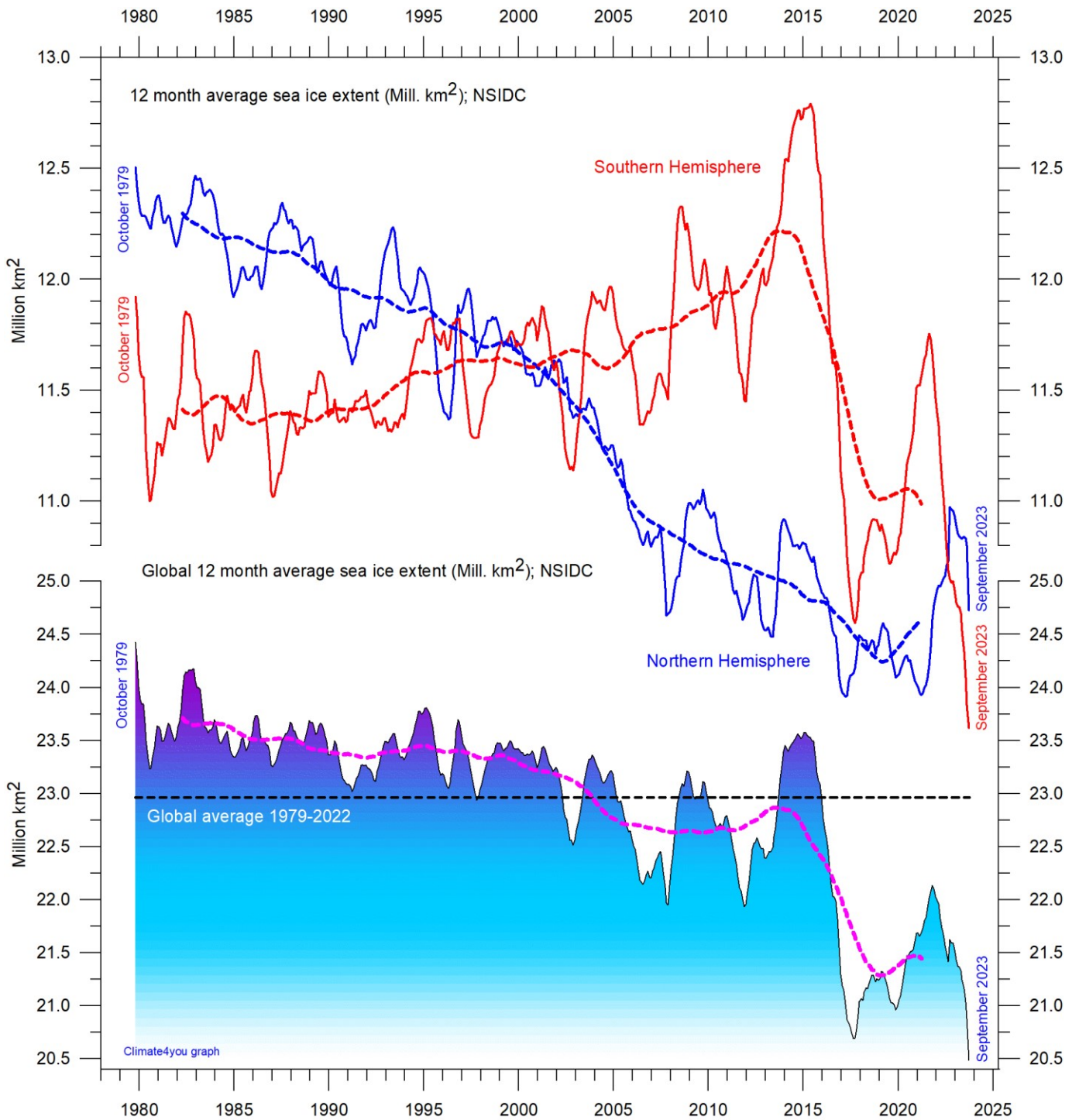
Sea Ice Thickness, 20-Sep-2023



37



Diagrams showing Arctic sea ice extent and thickness 20 September 2022 (left) and 2023 (right and above) and the seasonal cycles of the calculated total arctic sea ice volume, according to [The Danish Meteorological Institute \(DMI\)](http://www.dmi.dk/). The mean sea ice volume and standard deviation for the period 2004-2013 are shown by grey shading. Please note that DMI on 7 December 2021 changed their sea ice calculation model. DMI's description of the model version change can be read here: <http://polarportal.dk/en/sea-ice-and-icebergs/sea-ice-thickness-and-volume/>



12 month running average sea ice extension, global and in both hemispheres since 1979, the satellite-era. The October 1979 value represents the monthly 12-month average of November 1978 - October 1979, the November 1979 value represents the average of December 1978 - November 1979, etc. The stippled lines represent a 61-month (ca. 5 years) average. Data source: National Snow and Ice Data Center (NSIDC).

Sea level in general

Global (or eustatic) sea-level change is measured relative to an idealised reference level, the geoid, which is a mathematical model of planet Earth's surface (Carter et al. 2014). Global sea-level is a function of the volume of the ocean basins and the volume of water they contain. Changes in global sea-level are caused by – but not limited to - four main mechanisms:

1. Changes in local and regional air pressure and wind, and tidal changes introduced by the Moon.
2. Changes in ocean basin volume by tectonic (geological) forces.
3. Changes in ocean water density caused by variations in currents, water temperature and salinity.
4. Changes in the volume of water caused by changes in the mass balance of terrestrial glaciers.

In addition to these there are other mechanisms influencing sea-level, such as storage of ground water, storage in lakes and rivers, evaporation, etc.

Mechanism 1 is controlling sea-level at many sites on a time scale from months to several years. As an example, many coastal stations show a pronounced annual variation reflecting seasonal changes in air pressures and wind speed. Longer-term climatic changes playing out over decades or centuries will also affect measurements of sea-level changes. Hansen et al. (2011, 2015) provide excellent analyses of sea-level changes caused by recurrent changes of the orbit of the Moon and other phenomena.

Mechanism 2 – with the important exception of earthquakes and tsunamis - typically operates over long (geological) time scales and is not significant on human time scales. It may relate to variations in the seafloor spreading rate, causing volume changes in mid-ocean mountain ridges, and to the slowly changing configuration of land and oceans. Another effect may be the slow rise of basins due to isostatic offloading by deglaciation after an ice age. The floor of the Baltic Sea and the Hudson Bay are

presently rising, causing a slow net transfer of water from these basins into the adjoining oceans. Slow changes of excessively big glaciers (ice sheets) and movements in the mantle will affect the gravity field and thereby the vertical position of the ocean surface. Any increase of the total water mass as well as sediment deposition into oceans increase the load on their bottom, generating sinking by viscoelastic flow in the mantle below. The mantle flow is directed towards the surrounding land areas, which will rise, thereby partly compensating for the initial sea level increase induced by the increased water mass in the ocean.

Mechanism 3 (temperature-driven expansion) only affects the uppermost part of the oceans on human time scales. Usually, temperature-driven changes in density are more important than salinity-driven changes. Seawater is characterised by a relatively small coefficient of expansion, but the effect should however not be overlooked, especially when interpreting satellite altimetry data. Temperature-driven expansion of a column of seawater will not affect the total mass of water within the column considered and will therefore not affect the potential at the top of the water column. Temperature-driven ocean water expansion will therefore not in itself lead to any lateral displacement of water, but only locally lift the ocean surface. Near the coast, where people are living, the depth of water approaches zero, so no measurable temperature-driven expansion will take place here (Mörner 2015). Mechanism 3 is for that reason not important for coastal regions.

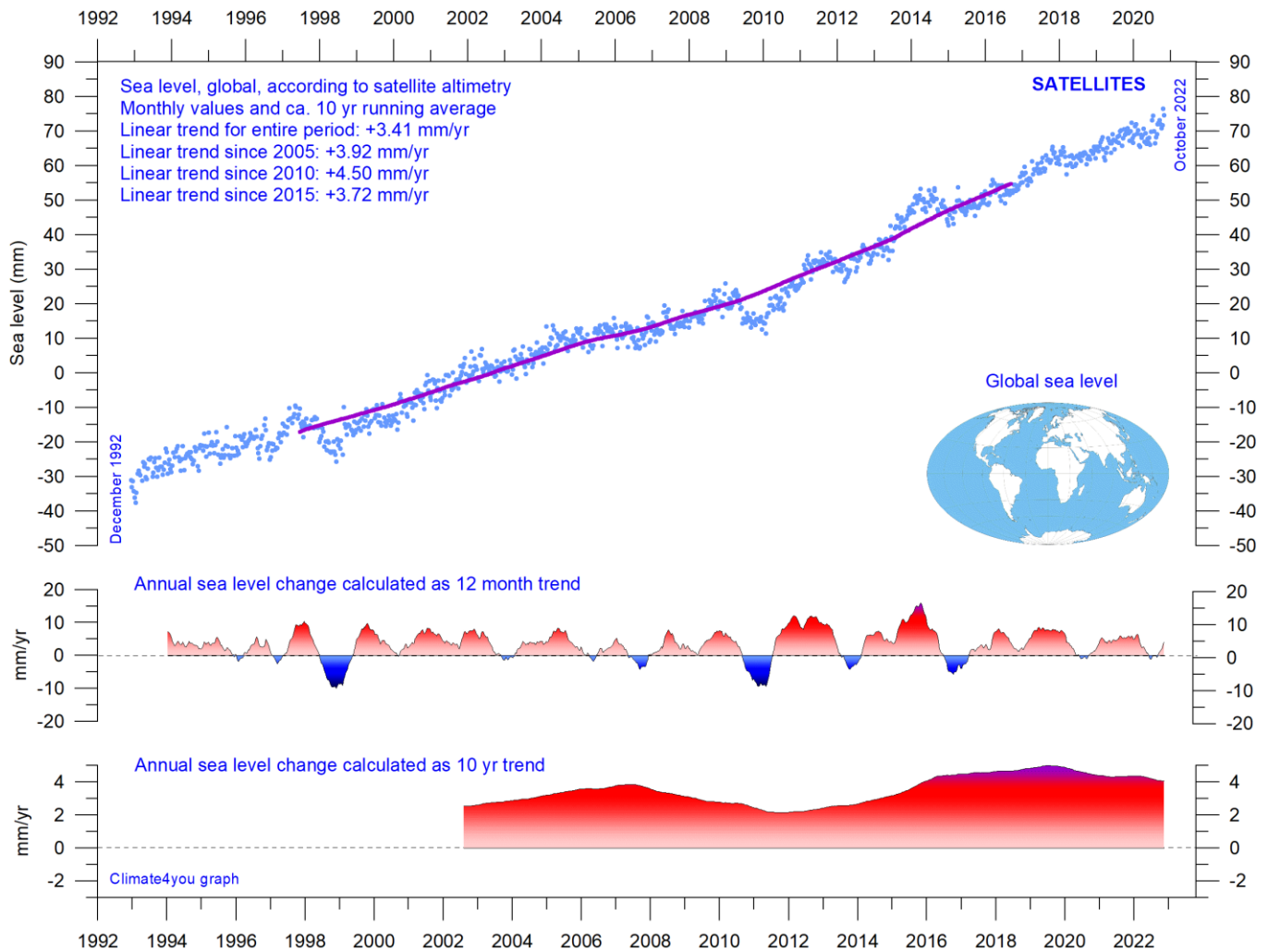
Mechanism 4 (changes in glacier mass balance) is an important driver for global sea-level changes along coasts, for human time scales. Volume changes of floating glaciers – ice shelves – has no influence on the global sea-level, just like volume changes of floating sea ice has no influence. Only the mass-balance of grounded or land-based glaciers is important for the global sea-level along coasts.

Summing up: Presumably, mechanism 1 and 4 are the most important for understanding sea-level changes along coasts.

References:

- Carter R.M., de Lange W., Hansen, J.M., Humlum O., Idso C., Kear, D., Legates, D., Mörner, N.A., Ollier C., Singer F. & Soon W. 2014. Commentary and Analysis on the Whitehead& Associates 2014 NSW Sea-Level Report. Policy Brief, NIPCC, 24. September 2014, 44 pp. <http://climatechangereconsidered.org/wp-content/uploads/2014/09/NIPCC-Report-on-NSW-Coastal-SL-9z-corrected.pdf>
- Hansen, J.-M., Aagaard, T. and Binderup, M. 2011. Absolute sea levels and isostatic changes of the eastern North Sea to central Baltic region during the last 900 years. *Boreas*, 10.1111/j.1502-3885.2011.00229.x. ISSN 0300–9483.
- Hansen, J.-M., Aagaard, T. and Huijpers, A. 2015. Sea-Level Forcing by Synchronization of 56- and 74-Year Oscillations with the Moon's Nodal Tide on the Northwest European Shelf (Eastern North Sea to Central Baltic Sea). *Journ. Coastal Research*, 16 pp.
- Mörner, Nils-Axel 2015. Sea Level Changes as recorded in nature itself. *Journal of Engineering Research and Applications*, Vol.5, 1, 124-129.

Global sea level from satellite altimetry, updated to October 2022



Global sea level since December 1992 according to the Colorado Center for Astrodynamics Research at University of Colorado at Boulder. The blue dots are the individual observations, and the purple line represents the running 121-month (ca. 10 year) average. The two lower panels show the annual sea level change, calculated for 1 and 10-year time windows, respectively. These values are plotted at the end of the interval considered.

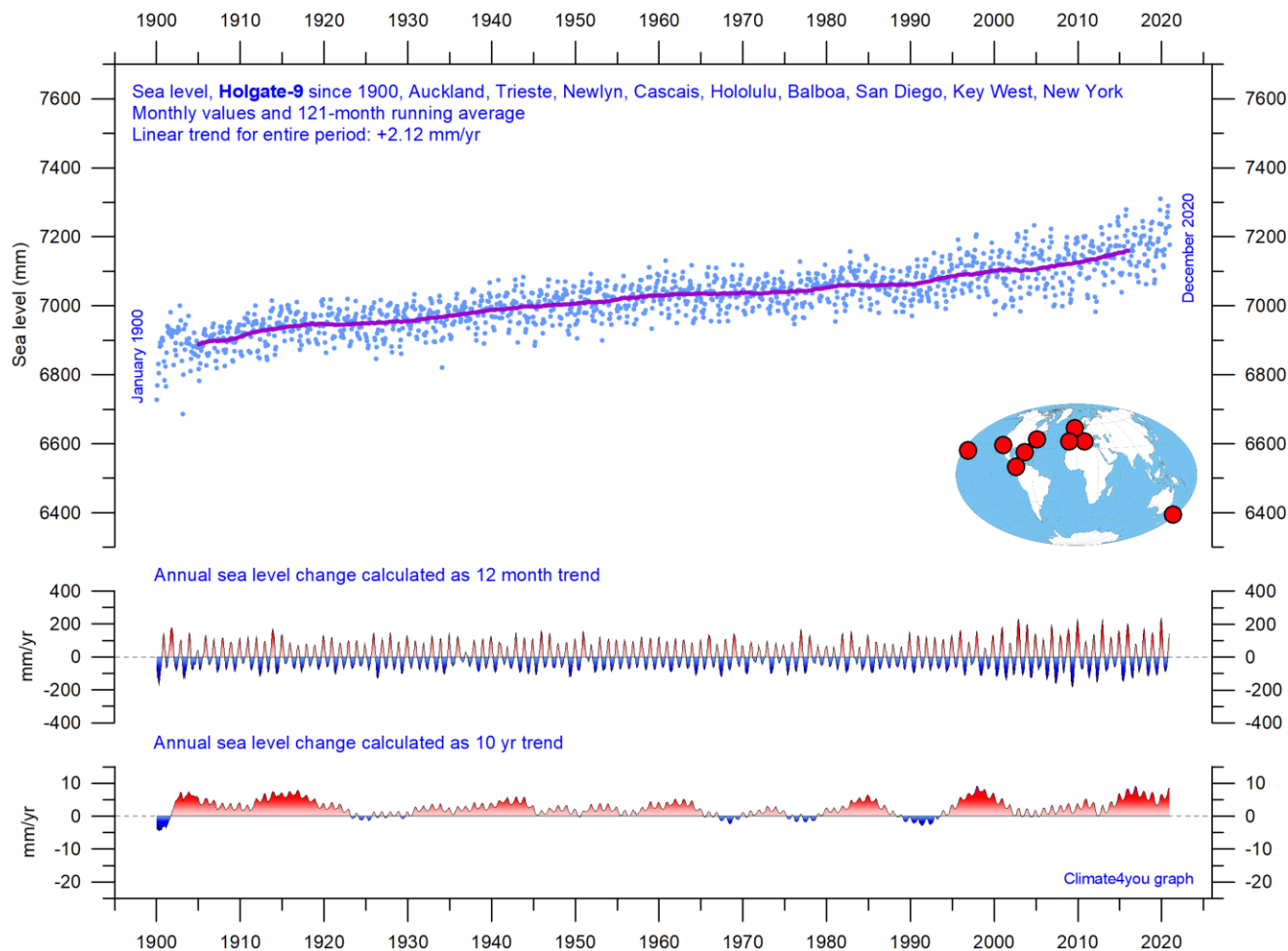
Ground truth is a term used in various fields to refer to information provided by direct observation as opposed to information provided by inference, such as, e.g., by satellite observations.

In remote sensing using satellite observations, ground truth data refers to information collected on location. Ground truth allows the satellite data to be related to real features observed on the planet surface. The collection of ground truth data enables calibration of remote-sensing data, and

aids in the interpretation and analysis of what is being sensed or recorded by satellites. Ground truth sites allow the remote sensor operator to correct and improve the interpretation of satellite data.

For satellite observations on sea level ground true data are provided by the classical tide gauges (example diagram on next page), that directly measures the local sea level many places distributed along the coastlines on the surface of the planet.

Global sea level from tide-gauges, updated to December 2020



Holgate-9 monthly tide gauge data from PSMSL Data Explorer. Holgate (2007) suggested the nine stations listed in the diagram to capture the variability found in a larger number of stations over the last half century studied previously. For that reason, average values of the Holgate-9 group of tide gauge stations are interesting to follow, even though Auckland (New Zealand) has not reported data since 2000, and Cascais (Portugal) not since 1993. Unfortunately, by this data loss the Holgate-9 series since 2000 is underrepresented with respect to the southern hemisphere and should therefore not be overinterpreted. The blue dots are the individual average monthly observations, and the purple line represents the running 121-month (ca. 10 year) average. The two lower panels show the annual sea level change, calculated for 1 and 10-year windows, respectively. These values are plotted at the end of the interval considered.

Data from tide-gauges all over the world suggest an average global sea-level rise of 1-2 mm/year, while the satellite-derived record (page 37) suggest a rise of about 3.3 mm/year, or more. The noticeable difference (about 1:2) between the two data sets is remarkable but has no

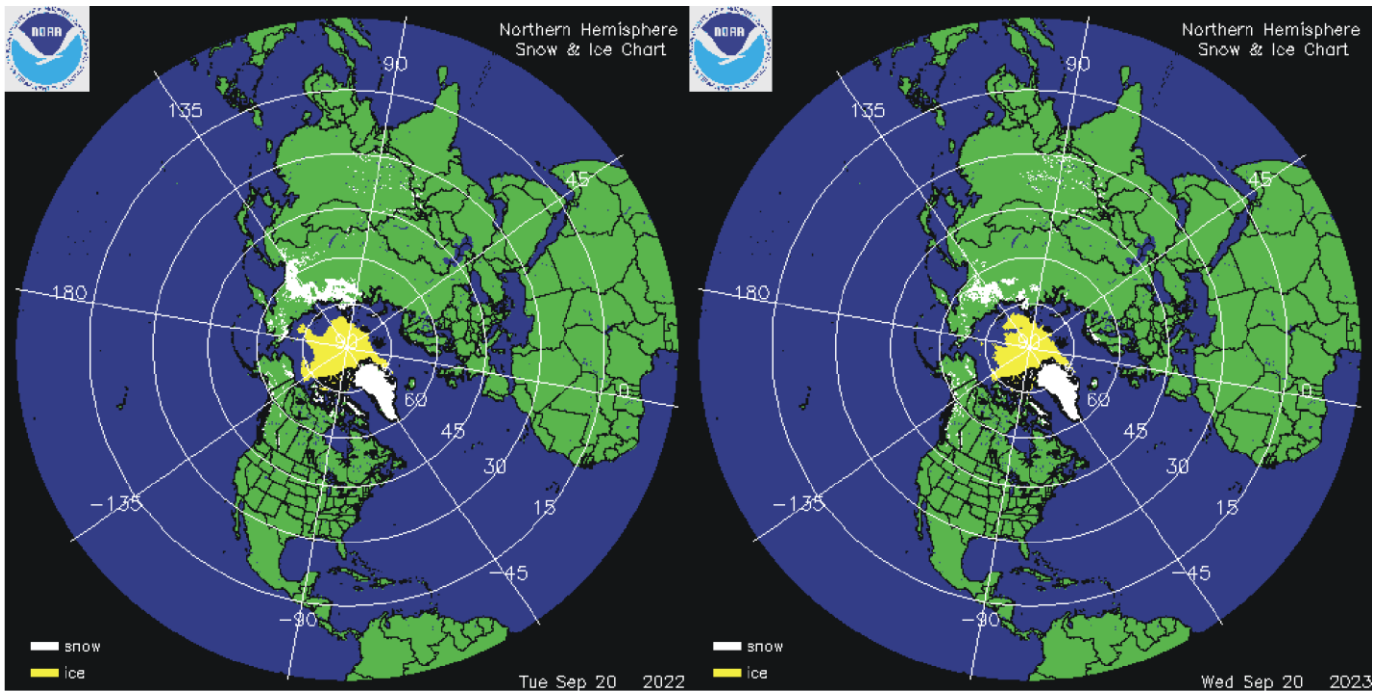
generally accepted explanation. It is however known that satellite observations are facing several complications in areas near the coast. Vignudelli et al. (2019) provide an updated overview of the current limitations of classical satellite altimetry in coastal regions.

References:

Holgate, S.J. 2007. On the decadal rates of sea level change during the twentieth century. *Geophys. Res. Letters*, 34, L01602, doi:10.1029/2006GL028492

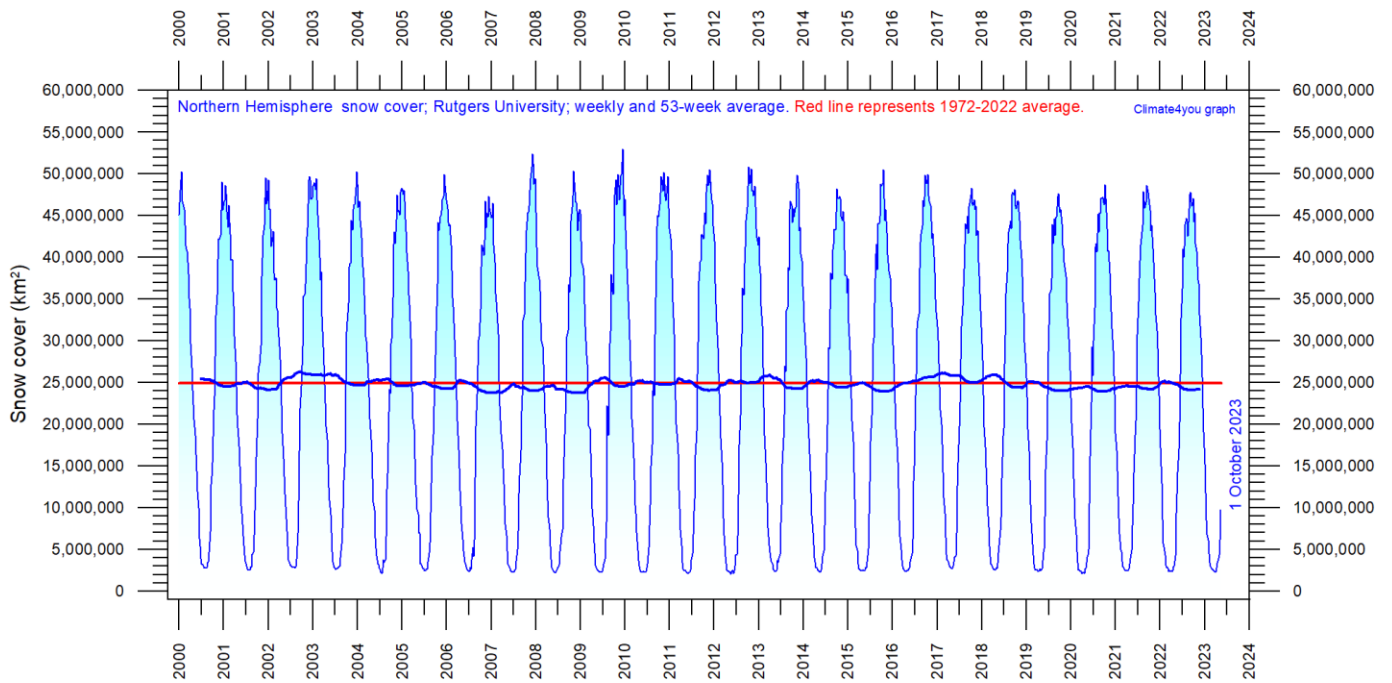
Vignudelli et al. 2019. Satellite Altimetry Measurements of Sea Level in the Coastal Zone. *Surveys in Geophysics*, Vol. 40, p. 1319–1349. <https://link.springer.com/article/10.1007/s10712-019-09569-1>

Northern Hemisphere weekly and seasonal snow cover, updated to September 2023

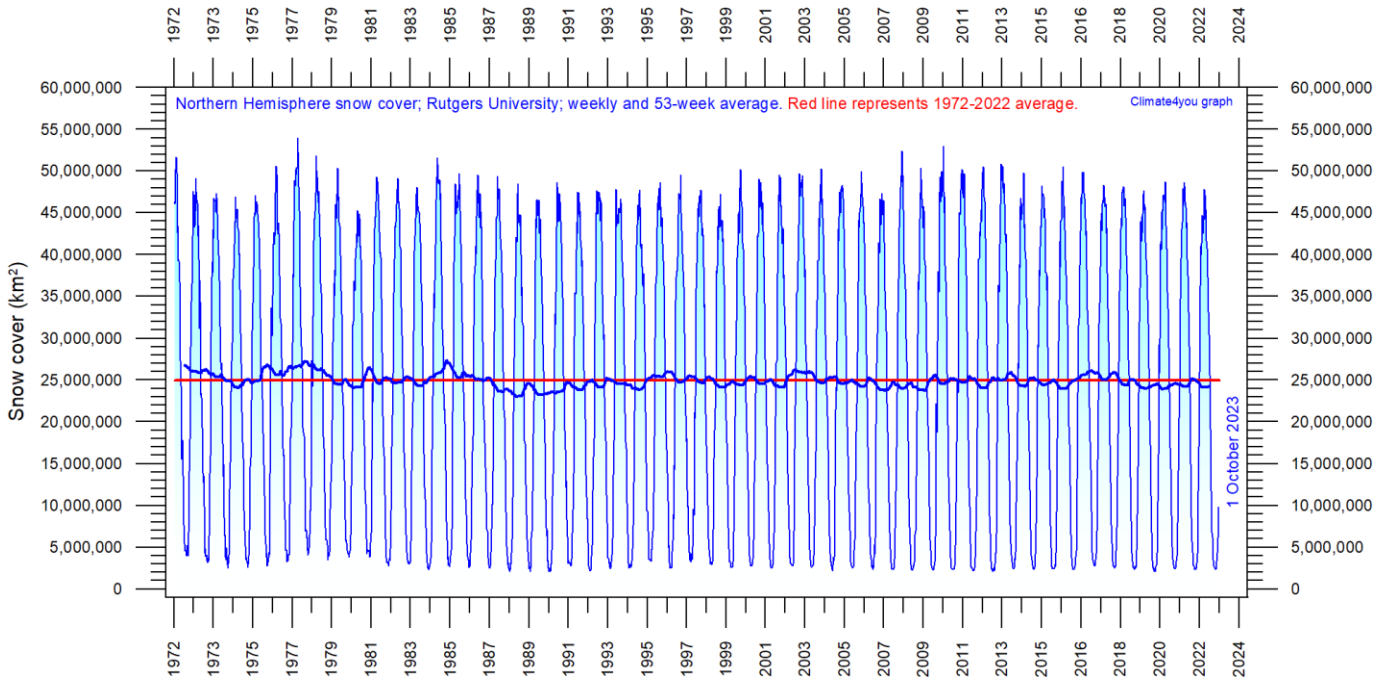


Northern hemisphere snow cover (white) and sea ice (yellow) 20 September 2022 (left) and 2023 (right). Map source: [National Ice Center \(NIC\)](#).

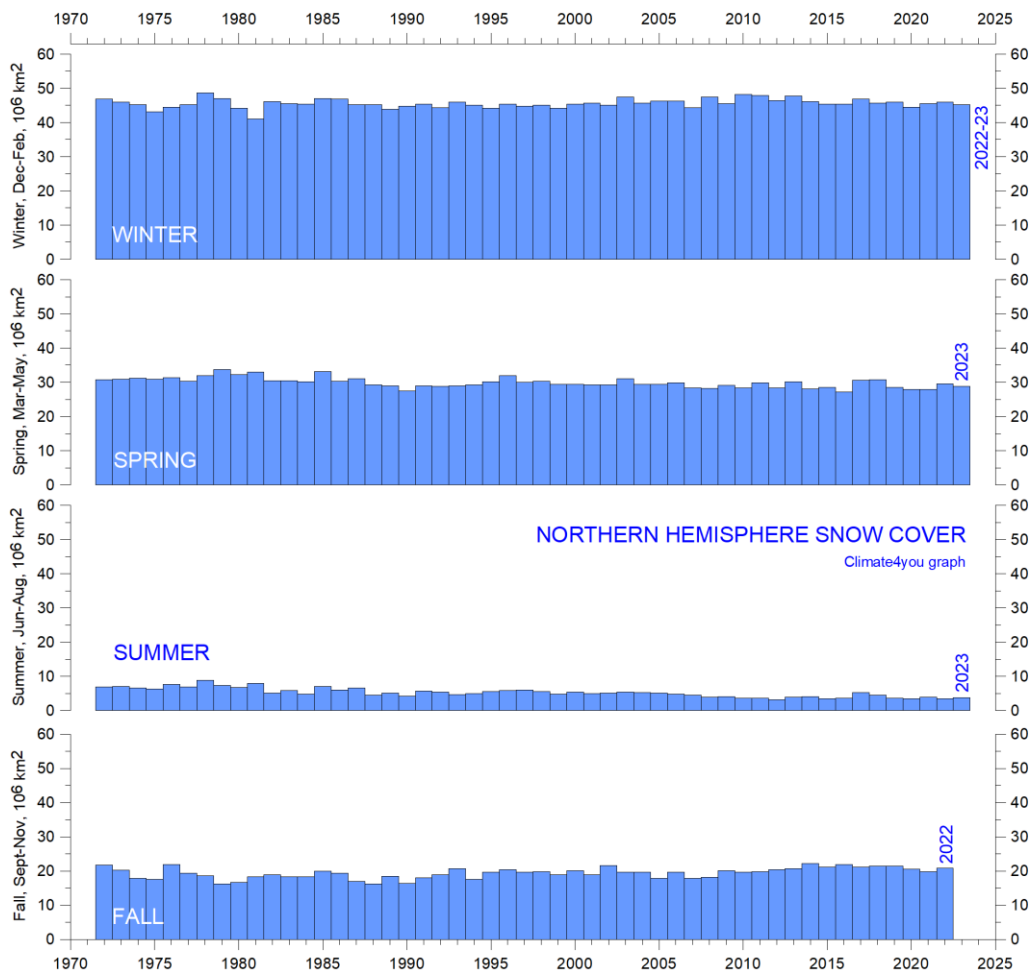
42



Northern hemisphere weekly snow cover since January 2000 according to Rutgers University Global Snow Laboratory. The thin blue line is the weekly data, and the thick blue line is the running 53-week average (approximately 1 year). The horizontal red line is the 1972-2022 average.



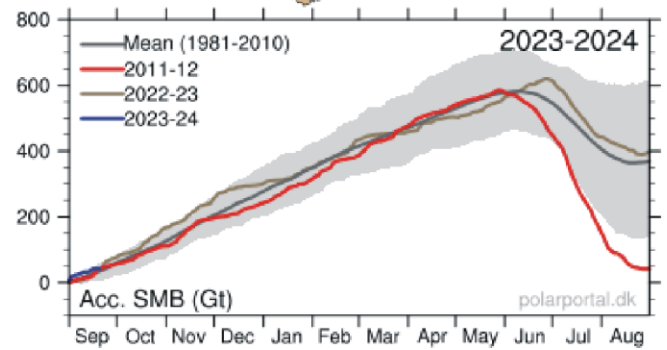
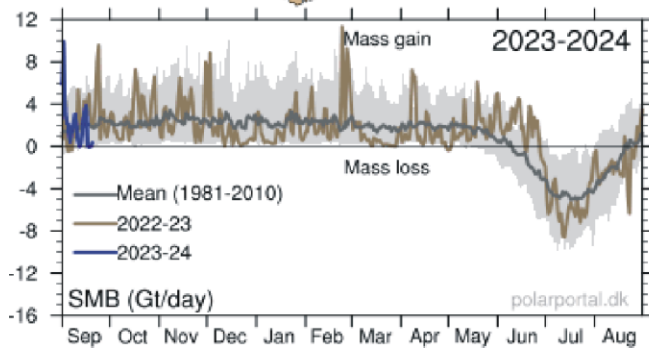
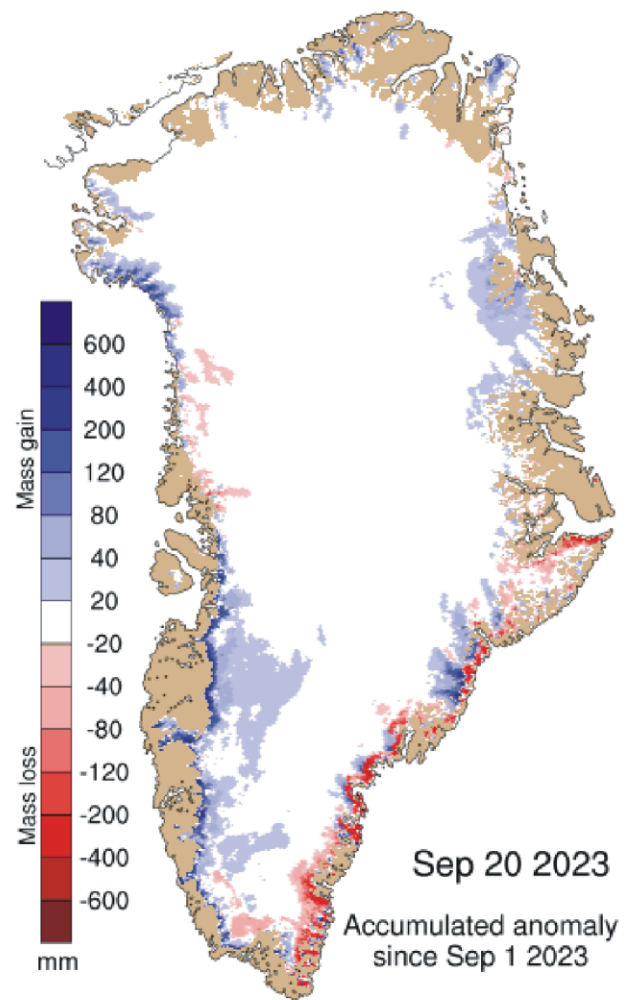
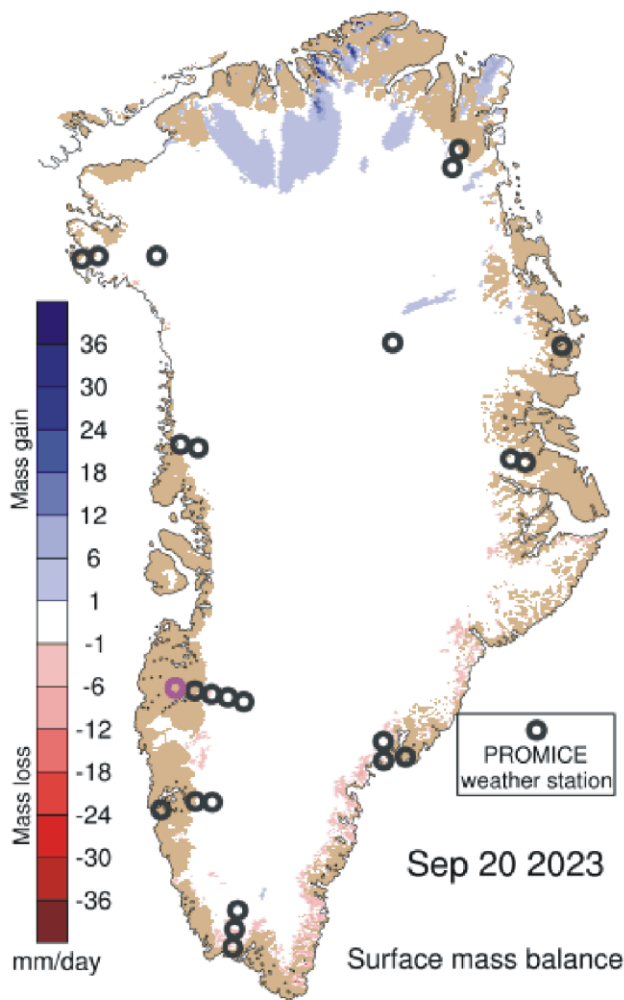
Northern hemisphere weekly snow cover since January 1972 according to Rutgers University Global Snow Laboratory. The thin blue line is the weekly data, and the thick blue line is the running 53-week average (approximately 1 year). The horizontal red line is the 1972-2022 average.



Northern hemisphere seasonal snow cover since January 1972 according to Rutgers University Global Snow Laboratory.

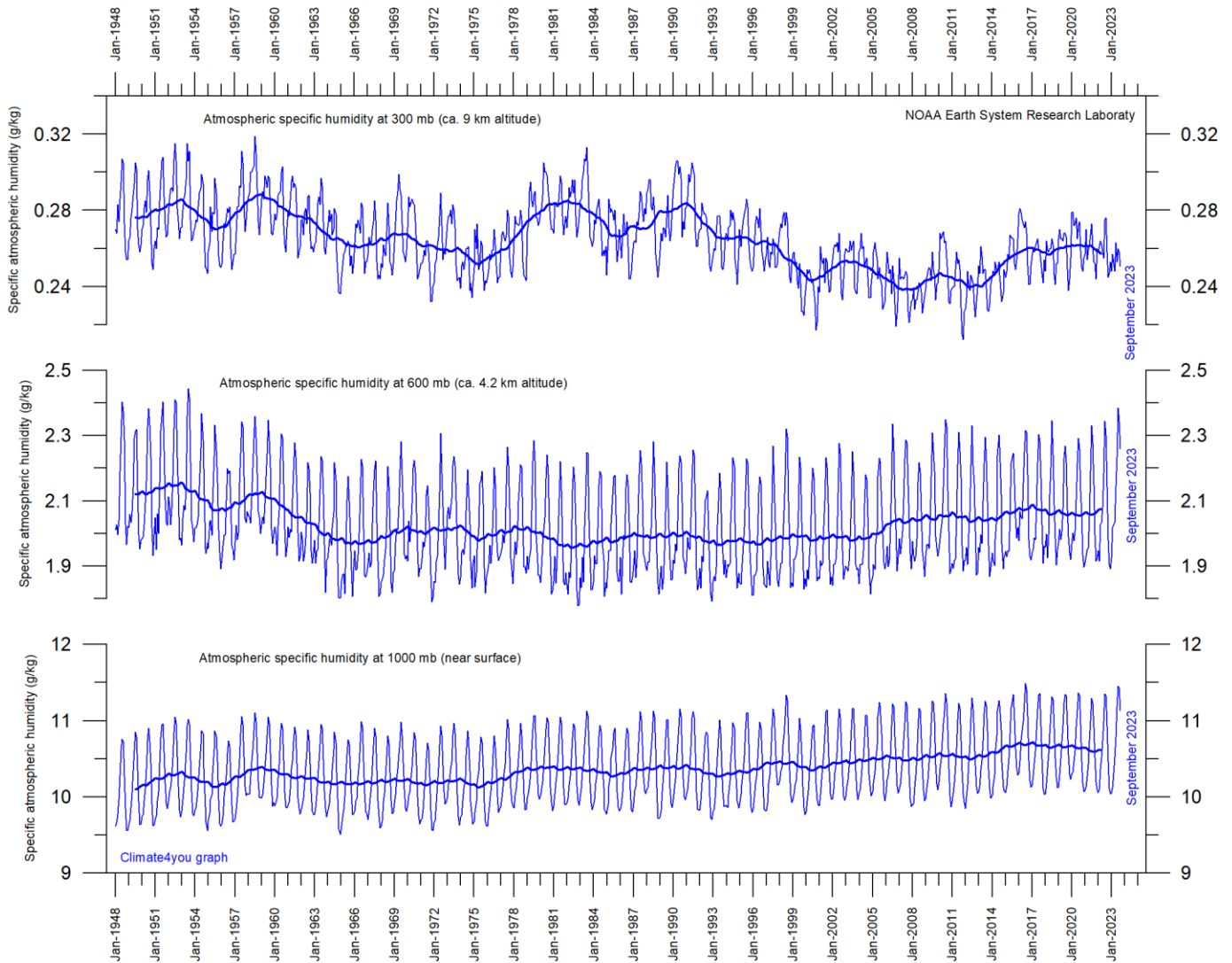
Greenland Ice Sheet net surface mass balance, updated to September 2023

44



Left: Surface mass balance 20 September 2023. Right: Net surface mass balance anomaly since September 1, 2023. Courtesy of Danish Meteorological Institute (DMI).

Atmospheric specific humidity, updated to September 2023



Specific atmospheric humidity (g/kg) at three different altitudes in the lower part of the atmosphere ([the Troposphere](#)) since January 1948 ([Kalnay et al. 1996](#)). The thin blue lines show monthly values, while the thick blue lines show the running 37-month average (about 3 years). Data source: [Earth System Research Laboratory \(NOAA\)](#).

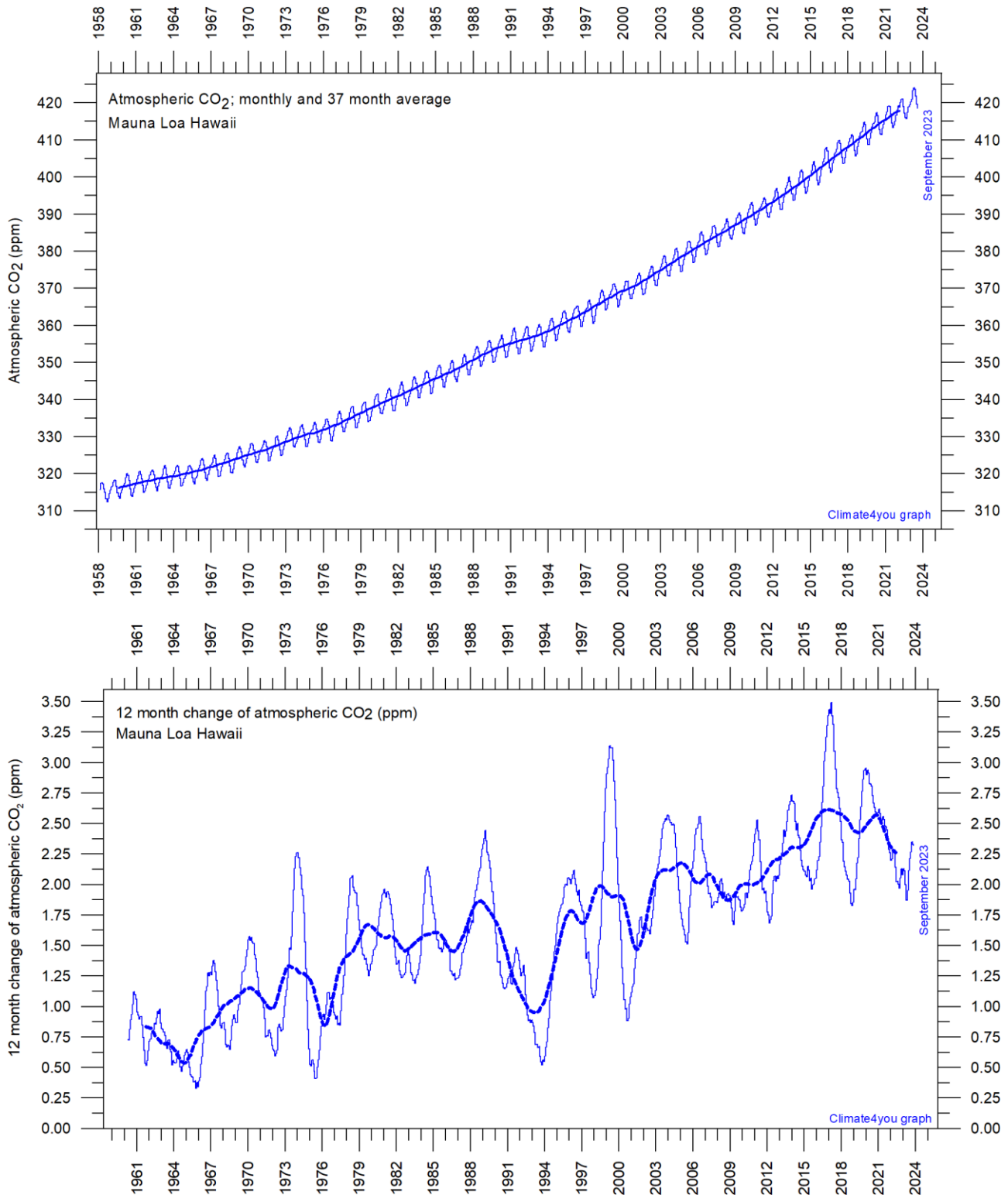
Water vapor is the most important greenhouse gas in the Troposphere. The highest concentration is found within a latitudinal range from 50°N to 60°S. The two polar regions of the Troposphere are comparatively dry.

The diagram above shows the specific atmospheric humidity to be stable or slightly increasing up to about 4-5 km altitude. At higher levels in the Troposphere (about 9 km), the specific humidity has been decreasing for the duration of the record (since 1948), but with shorter

variations superimposed on the falling trend. A Fourier frequency analysis (not shown here) shows these variations to be influenced especially by a periodic variation of about 3.7-year duration.

The persistent decrease in specific humidity at about 9 km altitude is particularly noteworthy, as this altitude roughly corresponds to the level where the theoretical temperature effect of increased atmospheric CO₂ is expected initially to play out.

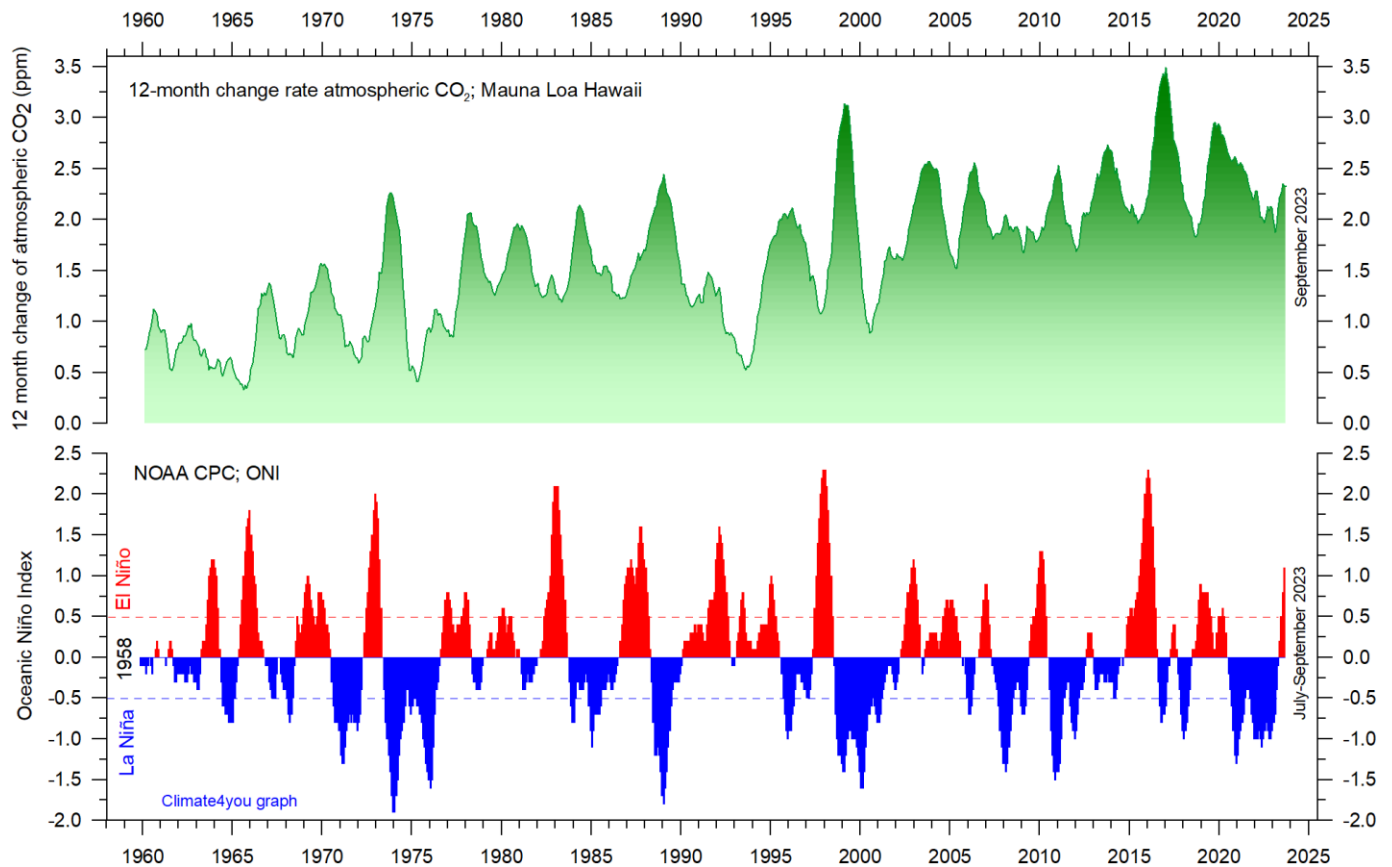
Atmospheric CO₂, updated to September 2023



46

Monthly amount of atmospheric CO₂ (upper diagram) and annual growth rate (lower diagram); average last 12 months minus average preceding 12 months, thin line) of atmospheric CO₂ since 1959, according to data provided by the [Mauna Loa Observatory](#), Hawaii, USA. The thick, stippled line is the simple running 37-observation average, nearly corresponding to a running 3-year average. A Fourier frequency analysis (not shown here) shows the 12-month change of Tropospheric CO₂ to be influenced especially by periodic variations of 2.5- and 3.8-years' duration.

The relation between annual change of atmospheric CO₂ and La Niña and El Niño episodes, updated to September 2023



Visual association between annual growth rate of atmospheric CO₂ (upper panel) and Oceanic Niño Index (lower panel). See also diagrams on page 40 and 22, respectively.

Changes in the global atmospheric CO₂ is seen to vary roughly in concert with changes in the Oceanic Niño Index. The typical sequence of events is that changes in the global atmospheric CO₂ to a certain degree follows changes in the Oceanic Niño Index, but clearly not in all details. Many processes, natural as well as anthropogenic, controls the amount of atmospheric CO₂, but oceanographic processes are clearly particularly important (see also diagram on next page).

Atmospheric CO₂ and the present coronavirus pandemic

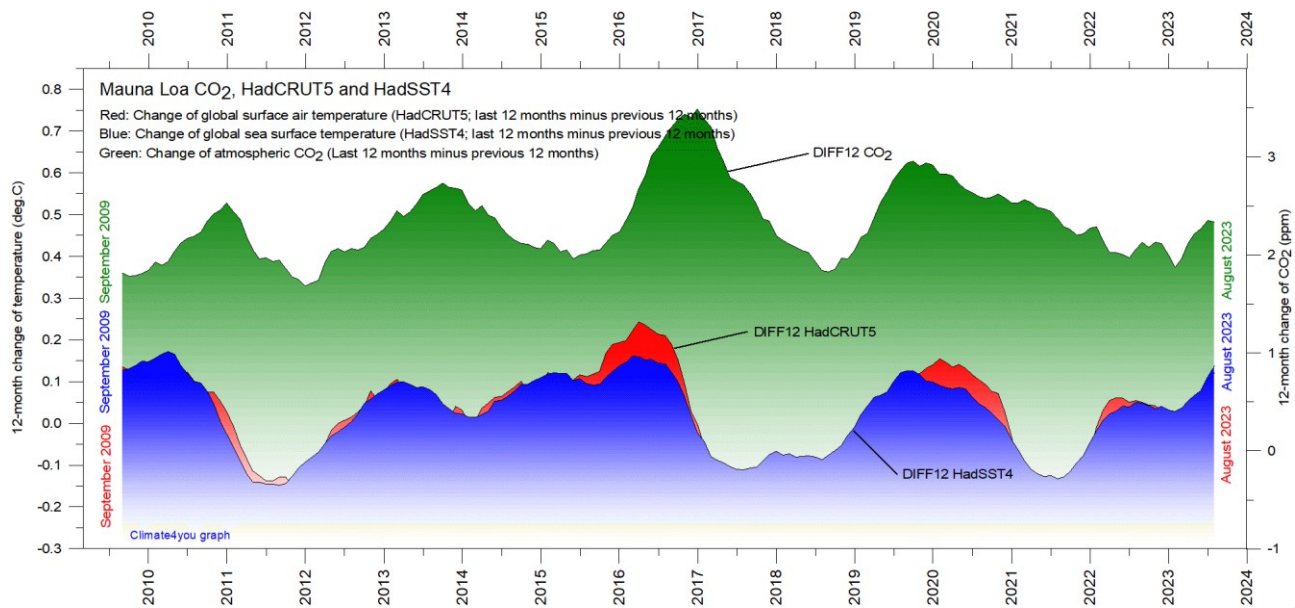
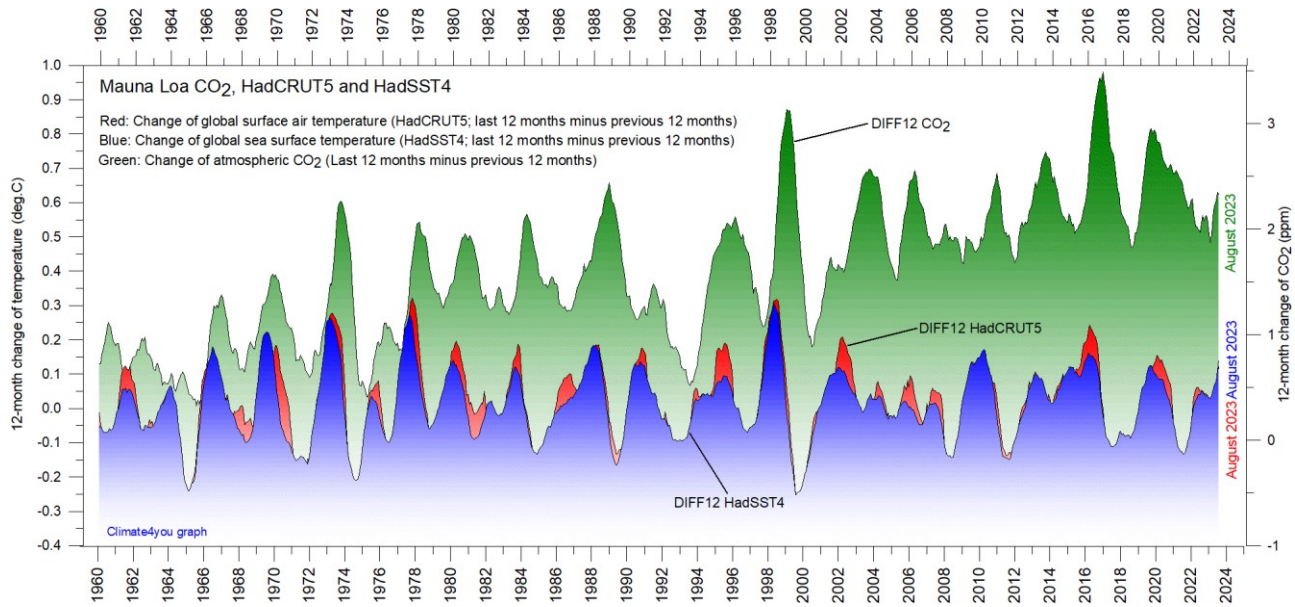
Modern political initiatives usually assume the human influence (mainly the burning of fossil fuels) to represent

the core reason for the observed increase in atmospheric CO₂ since 1958 (diagrams on page 44).

The coronavirus pandemic since January 2020 resulted in a marked reduction in the global consumption of fossil fuels. It is therefore enlightening to follow the effect of this reduction on the amount of atmospheric CO₂.

However, there is still no clear effect to be seen of the above reduction in release of CO₂ from fossil fuels. Presumably, the main explanation for this is that the human contribution is too small compared to the numerous natural sources and sinks for atmospheric CO₂ to appear in diagrams showing the amount of atmospheric CO₂ (see, e.g., diagrams on p. 44-46).

The phase relation between atmospheric CO₂ and global temperature, updated to August 2023



12-month change of global atmospheric CO₂ concentration (*Mauna Loa*; green), global sea surface temperature (*HadSST4*; blue) and global surface air temperature (*HadCRUT5*; red dotted). Entire data series since 1958 in upper figure, and last 15 years in lower figure, to enhance modern dynamics. All graphs are showing monthly values of DIFF12, the difference between the average of the last 12 month and the average for the previous 12 months for each data series.

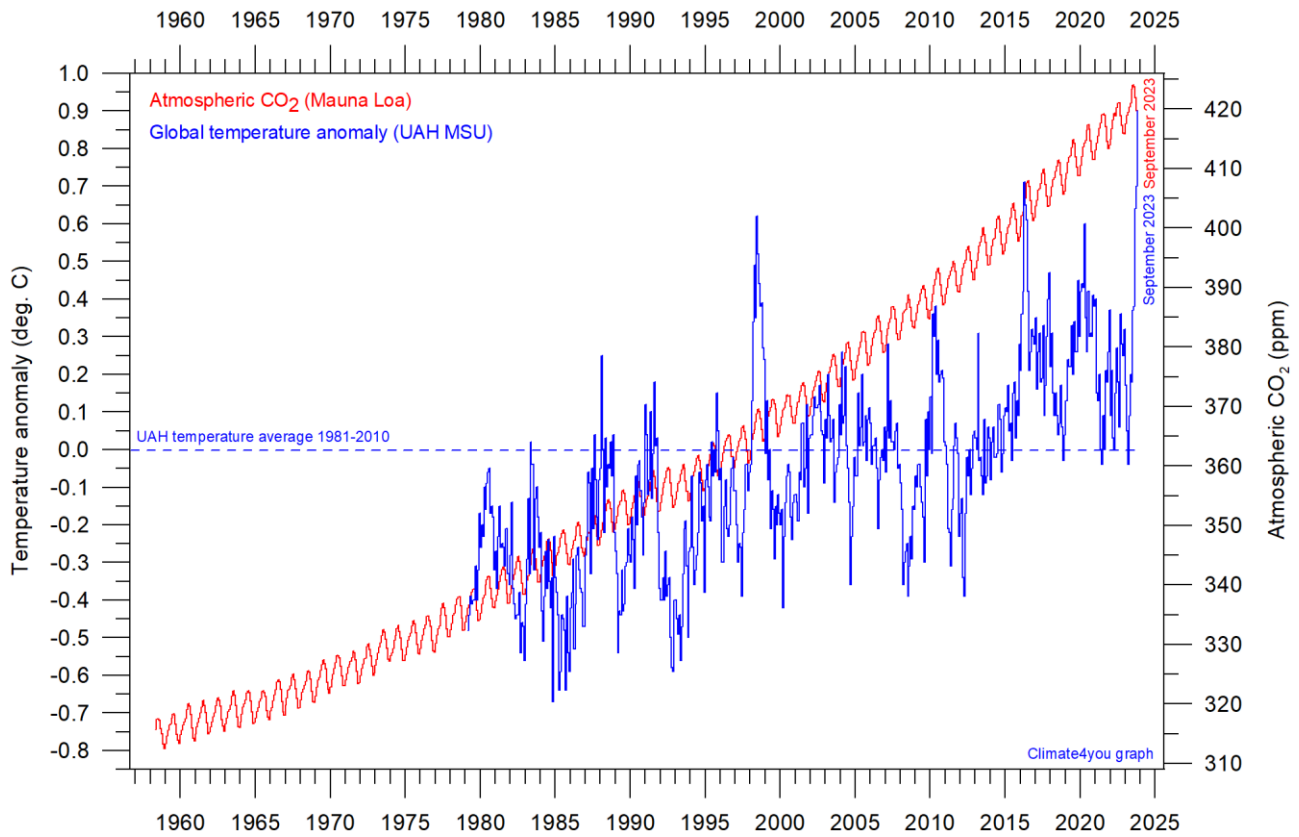
The typical sequence of events is seen to be that changes in the global atmospheric CO₂ follow changes in global surface air temperature, which again follow changes in global ocean surface temperatures. Thus, changes in global

atmospheric CO₂ usually are lagging 9.5–10 months behind changes in global air surface temperature, and 11–12 months behind changes in global sea surface temperature.

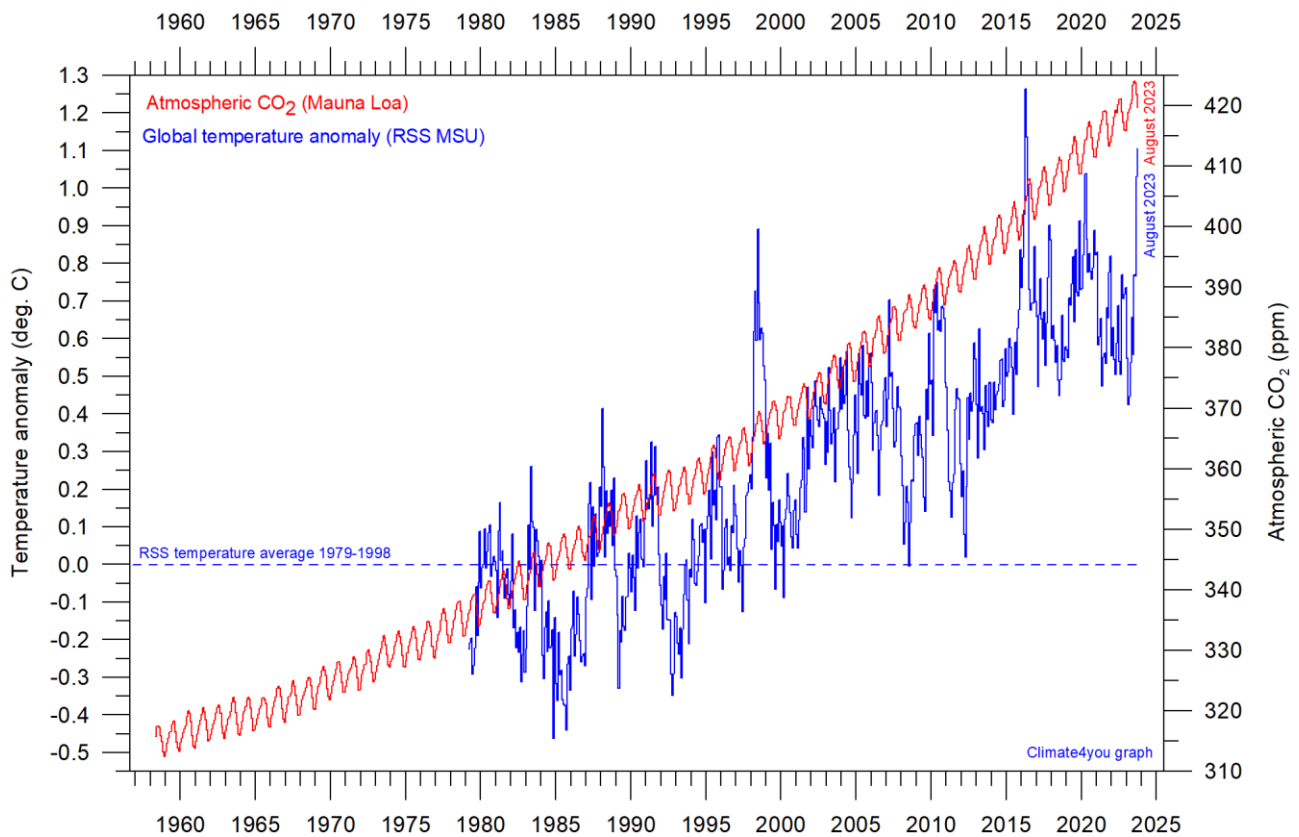
Reference: Humlum, O., Stordahl, K. and Solheim, J-E. 2012. The phase relation between atmospheric carbon dioxide and global temperature. *Global and Planetary Change*, August 30, 2012.

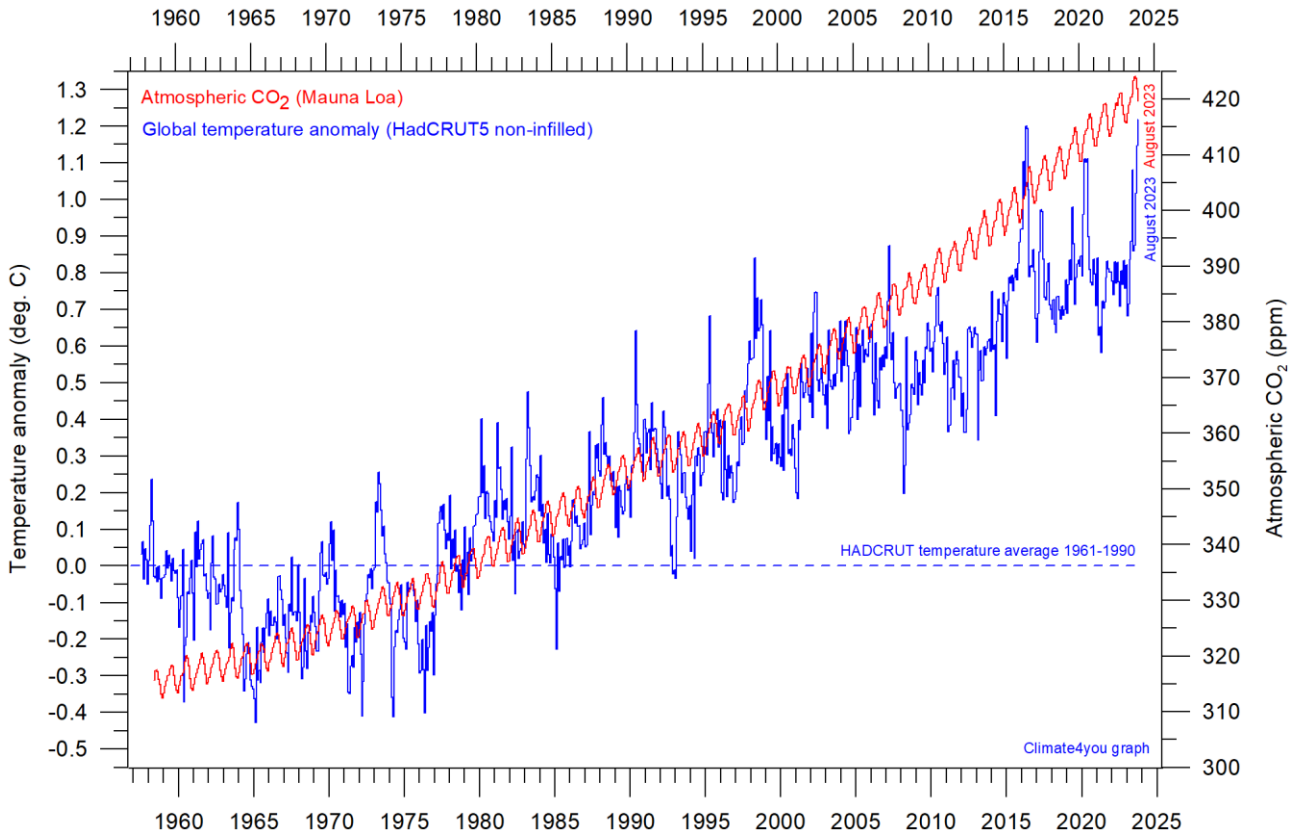
<http://www.sciencedirect.com/science/article/pii/S0921818112001658?v=s5>

Global air temperature and atmospheric CO₂, updated to September 2023

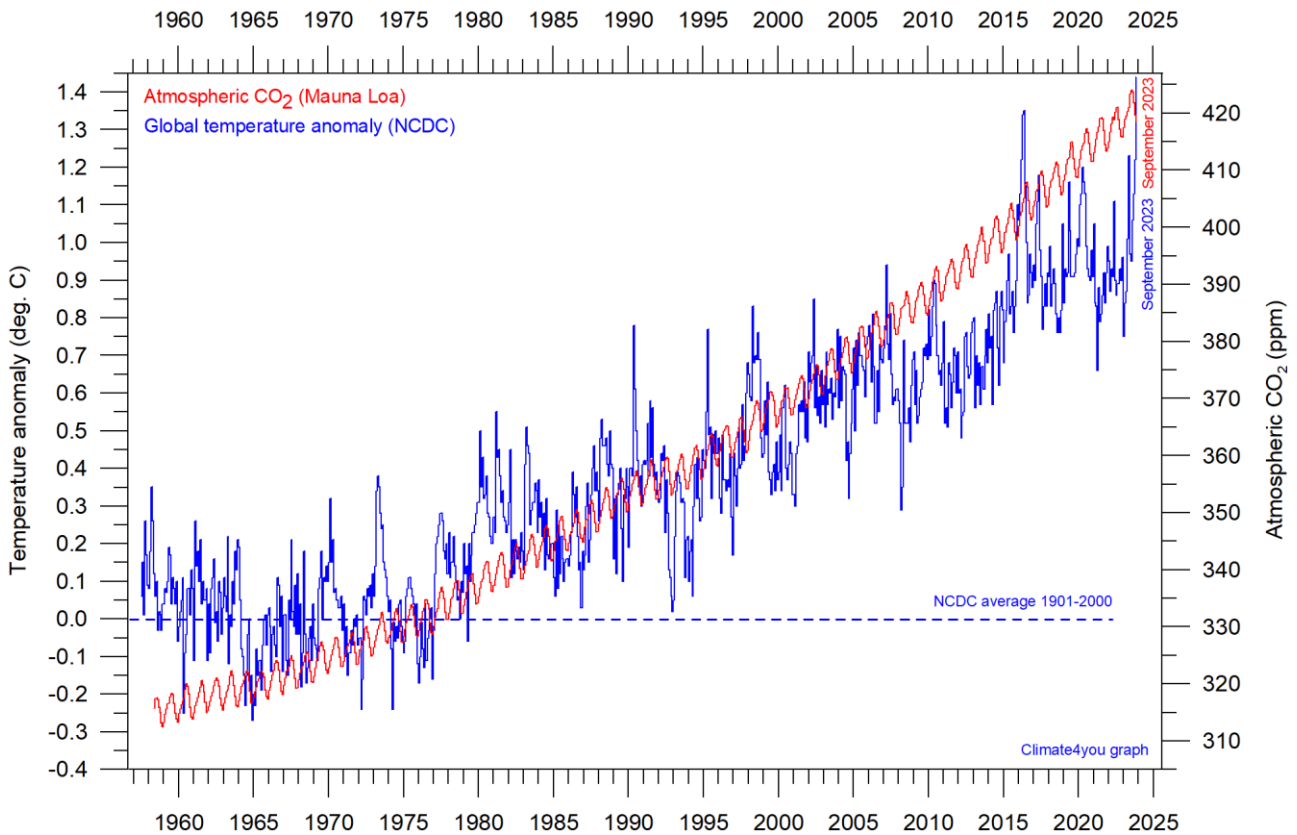


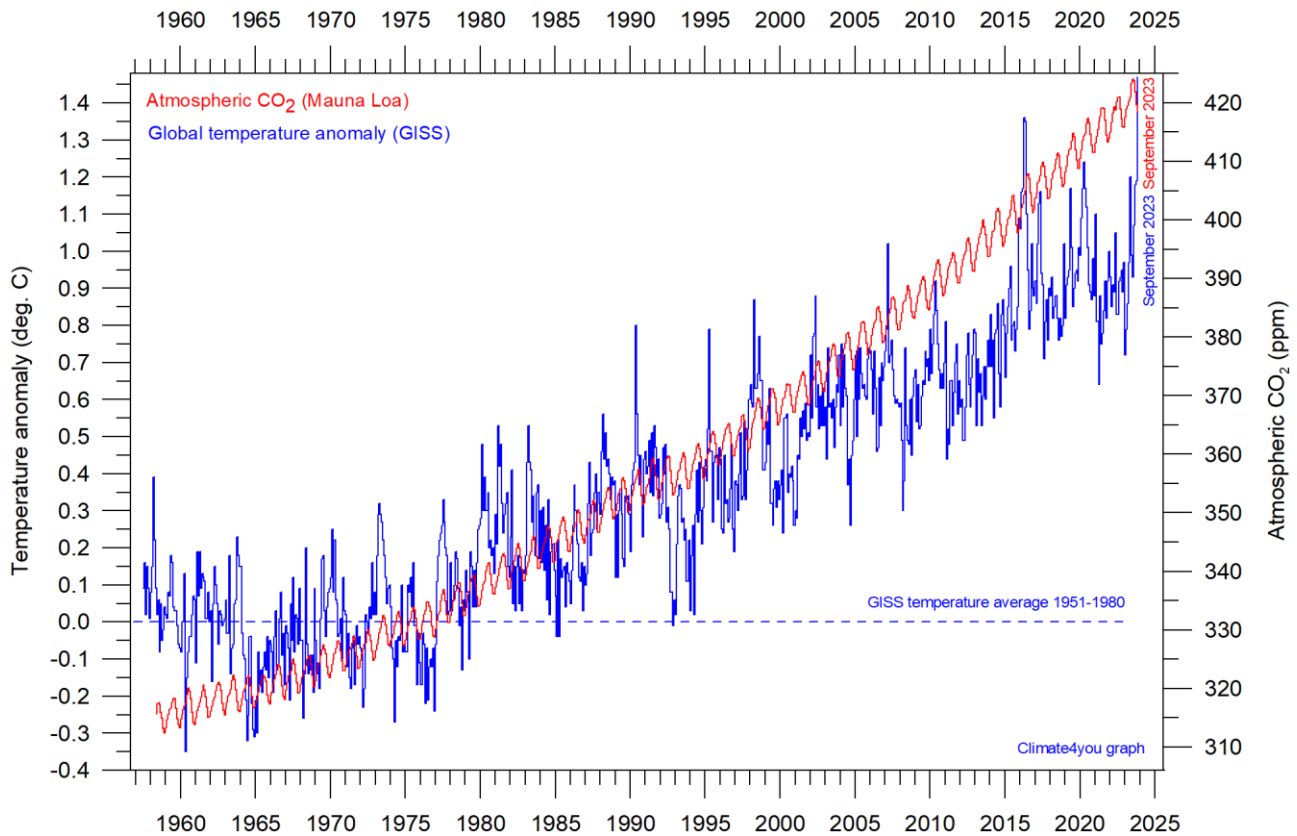
49





50





Diagrams showing UAH, RSS, HadCRUT5, NCDC and GISS monthly global air temperature estimates (blue) and the monthly atmospheric CO₂ content (red) according to the [Mauna Loa Observatory](#), Hawaii. The Mauna Loa data series begins in March 1958, and 1958 was therefore chosen as starting year for all diagrams above. Reconstructions of past atmospheric CO₂ concentrations (before 1958) are not incorporated in this diagram, as such past CO₂ values are derived by other means (ice cores, stomata, or older measurements using different methodology), and therefore are not directly comparable with direct atmospheric measurements.

Most climate models are programmed to give the greenhouse gas carbon dioxide CO₂ significant influence on the calculated global air temperature. It is therefore relevant to compare different air temperature records with measurements of atmospheric CO₂, as shown in the diagrams above.

Any comparison, however, should not be made on a monthly or annual basis, but for a longer time, as other effects (oceanographic, cloud cover, etc.) may override the potential influence of CO₂ on short time scales such as just a few years.

It is of cause equally inappropriate to present new meteorological record values, whether daily, monthly, or annual, as demonstrating the legitimacy of the hypothesis ascribing high importance of atmospheric CO₂ for global air temperatures. Any such meteorological record value may

well be the result of other phenomena. Unfortunately, many media repeatedly fall into this trap.

What exactly defines the critical length of a relevant period length to consider for evaluating the alleged importance of CO₂ remains elusive and still represents a theme for discussions.

Nonetheless, the length of the critical period must be inversely proportional to the temperature sensitivity of CO₂, including feedback effects. Thus, if the net temperature effect of atmospheric CO₂ is strong, the critical period will be short, and vice versa.

However, past climate research history provides some clues as to what has traditionally been considered the relevant length of period over which to compare temperature and atmospheric CO₂.

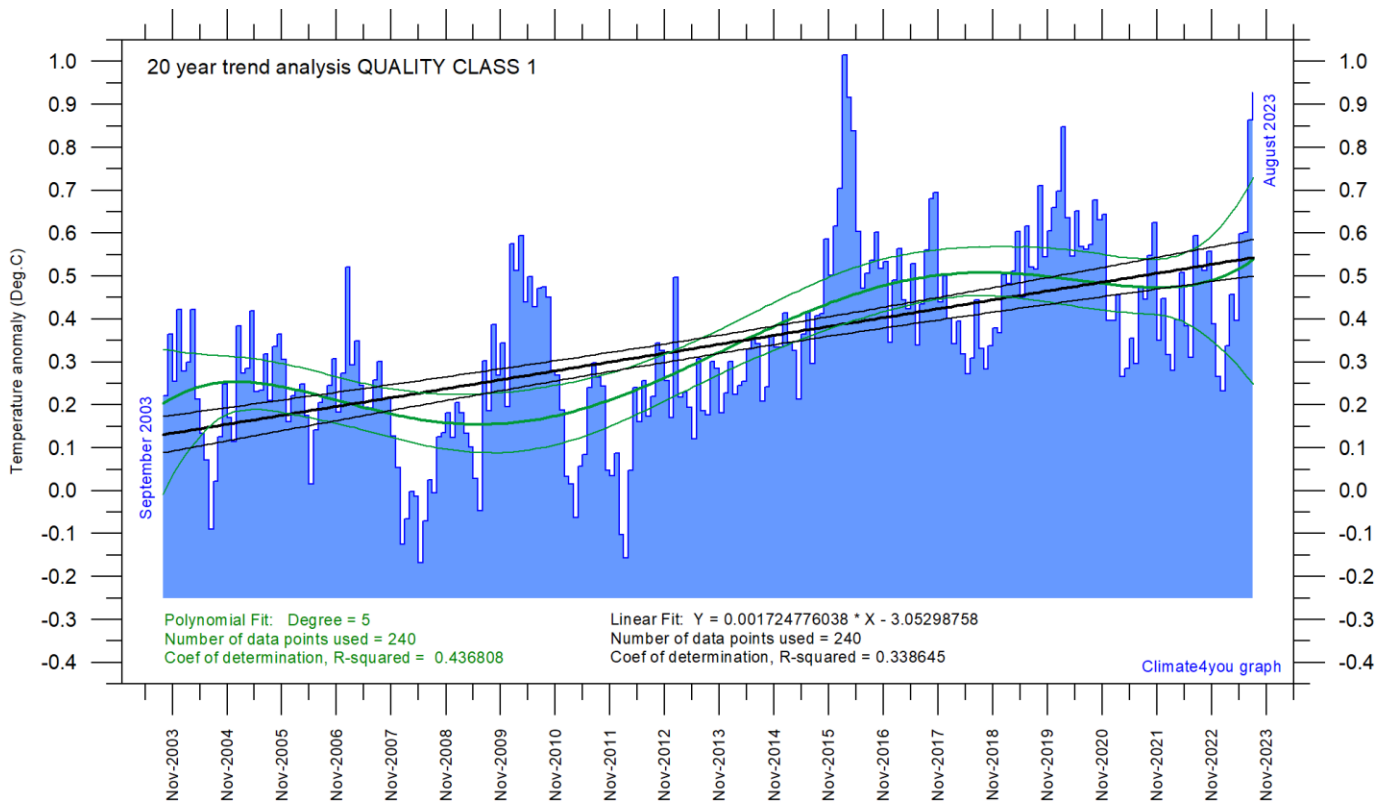
After about 10 years of concurrent global temperature- and CO₂-increase, IPCC was established in 1988. For obtaining public and political support for the CO₂-hypothesis the 10-year warming period leading up to 1988 most likely was considered important. Had the global temperature instead been decreasing at that time, political support for the hypothesis probably would have been difficult to obtain in 1988.

Based on the previous 10 years of concurrent temperature- and CO₂-increase, many climate scientists in 1988

presumably felt that their understanding of climate dynamics was sufficient to conclude about the importance of CO₂ for affecting observed global temperatures.

Thus, it may with confidence be concluded that 10 years in 1988 was considered a period long enough to demonstrate the effect of increasing atmospheric CO₂ on global temperatures. The 10-year period is also basis for the temperature anomaly diagrams shown on page 4.

Latest 20-year QC1 global monthly air temperature changes, updated to August 2023



53

Last 20 years' global monthly average air temperature according to Quality Class 1 (UAH and RSS; see p.6 and 9) global monthly temperature estimates. The thin blue line represents the monthly values. The thick black line is the linear fit, with 95% confidence intervals indicated by the two thin black lines. The thick green line represents a 5-degree polynomial fit, with 95% confidence intervals indicated by the two thin green lines. A few key statistics are given in the lower part of the diagram (please note that the linear trend is the monthly trend).

In the enduring scientific climate debate, the following question is often put forward: Is the surface air temperature still increasing or has it basically remained without significant changes during the last 15-16 years?

The diagram above may be useful in this context and demonstrates the differences between two often used statistical approaches to determine recent temperature trends. Please also note that such fits only attempt to describe the past, and usually have small, if any, predictive power.

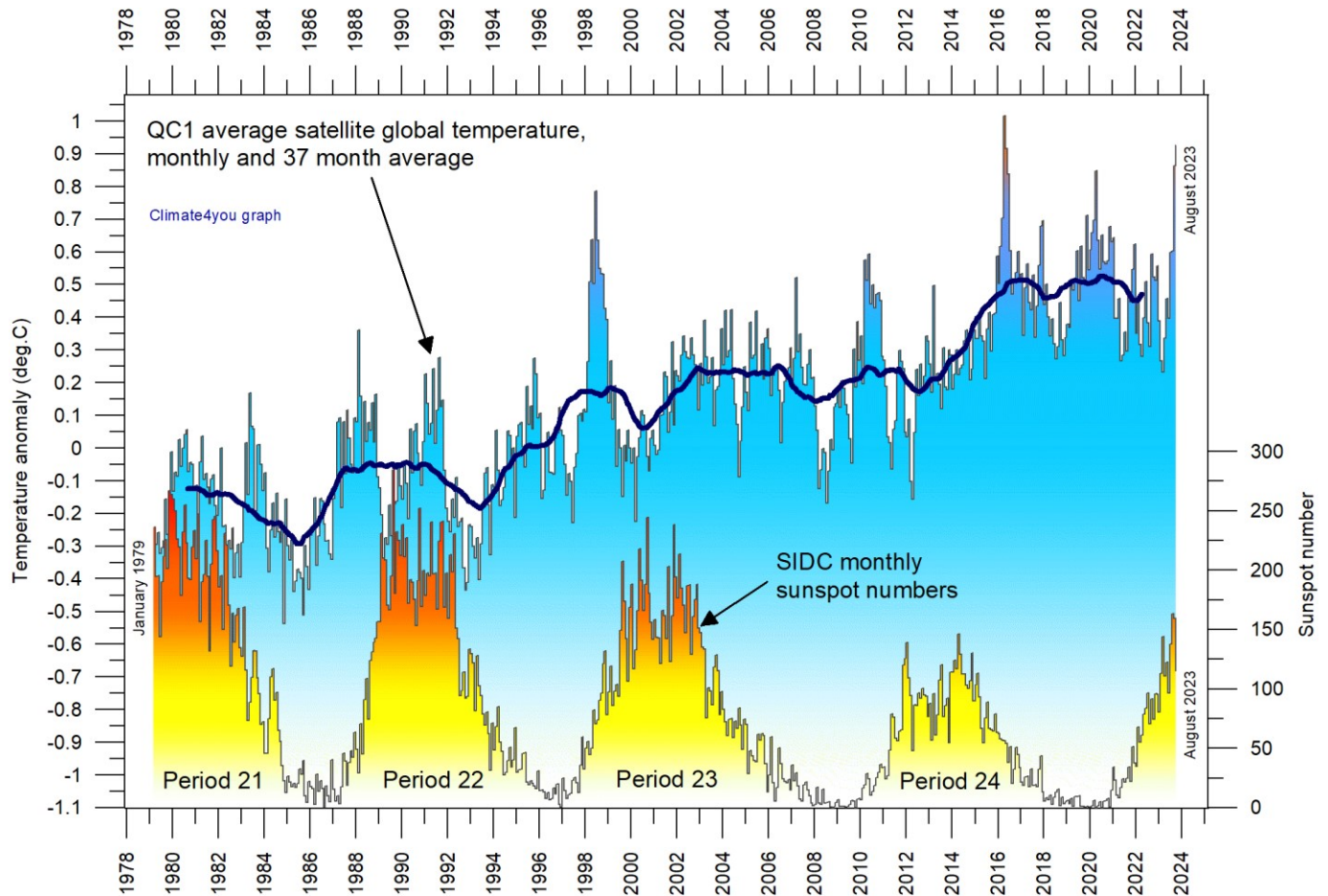
In addition, before using any linear trend (or other) analysis of time series a proper statistical model should be chosen, based on statistical justification.

For global temperature time series, there is no *a priori* physical reason why the long-term trend should be linear in time. In fact, climatic time series often have trends for which a straight line is not a good approximation, as is clearly demonstrated by several of the diagrams shown in the present report.

For an commendable description of problems often encountered by analyses of temperature time series analyses, please see [Keenan, D.J. 2014: Statistical Analyses of Surface Temperatures in the IPCC Fifth Assessment Report](#).

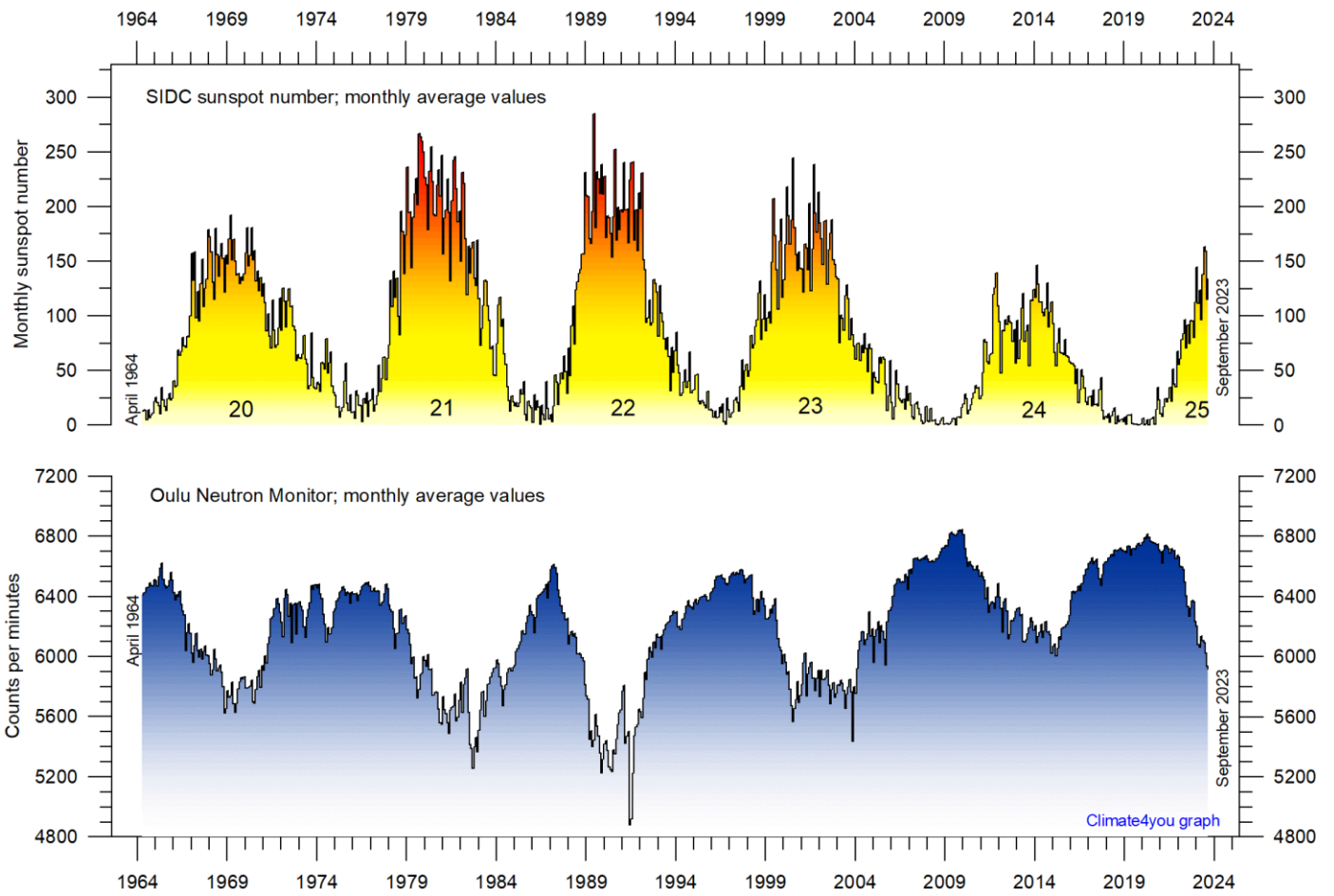
See also diagrams on page 12.

Sunspot activity (SIDC) and QC1 average satellite global air temperature, updated to August 2023



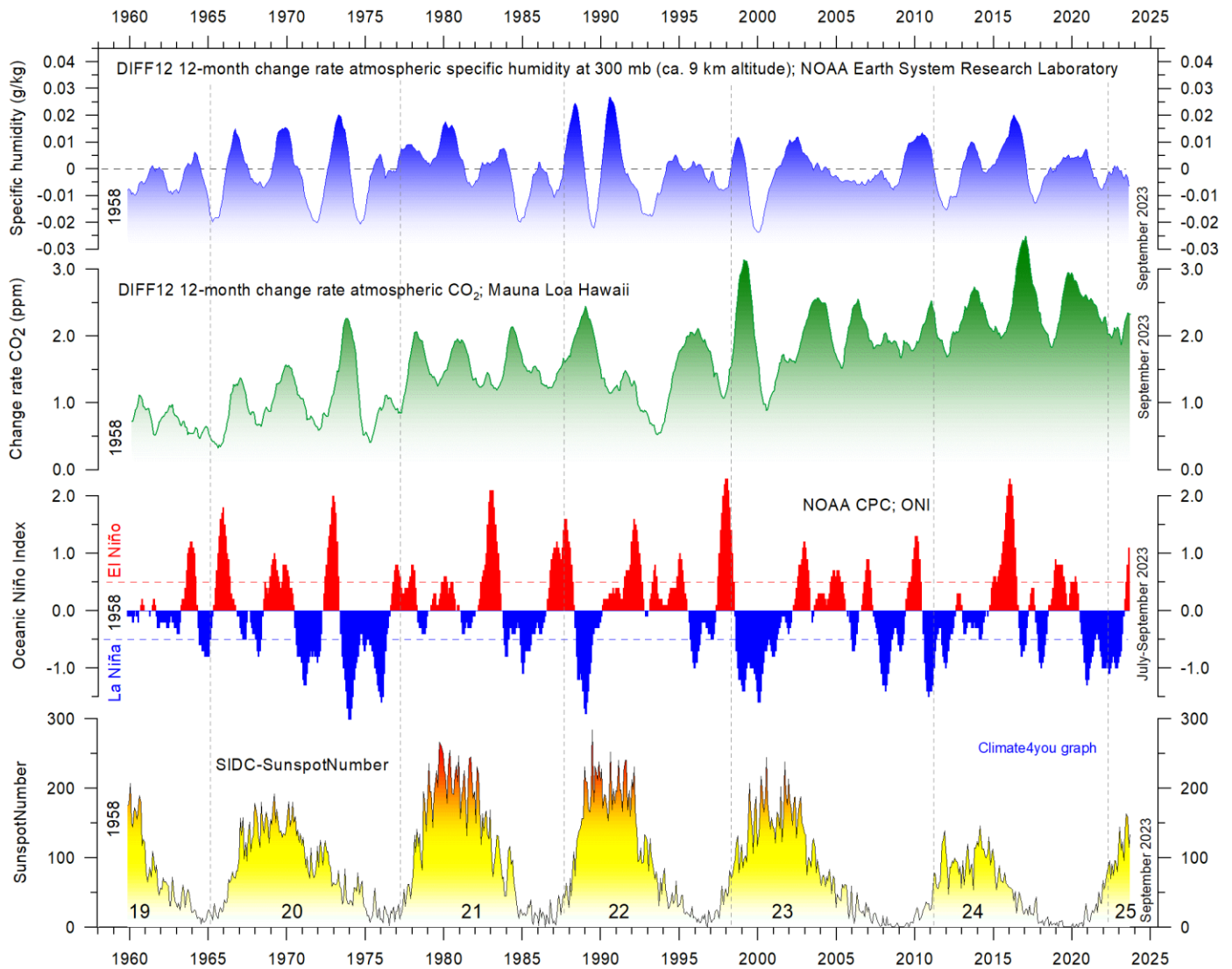
Variation of global monthly air temperature according to Quality Class 1 (UAH and RSS; see p.4) and observed sunspot number as provided by the Solar Influences Data Analysis Center (SIDC), since 1979. The thin lines represent the monthly values, while the thick line is the simple running 37-month average, nearly corresponding to a running 3-year average. The asymmetrical temperature 'bump' around 1998 is influenced by the oceanographic El Niño phenomenon in 1998, as is the case also for 2015-16. Temperatures in year 2019-20 was influenced by a moderate El Niño. In summer 2023 a new El Niño episode has begun.

Monthly sunspot activity (SIDC) and average neutron counts (Oulu, Finland), updated to September 2023



Observed monthly sunspot number (Solar Influences Data Analysis Center (SIDC) since April 1964, and (lower panel) monthly average counts of the Oulu (Finland) neutron monitor, adjusted for barometric pressure and efficiency.

Monthly sunspot activity (SIDC), Oceanic Niño Index (ONI), and change rates of atmospheric CO2 and specific humidity, updated to September 2023

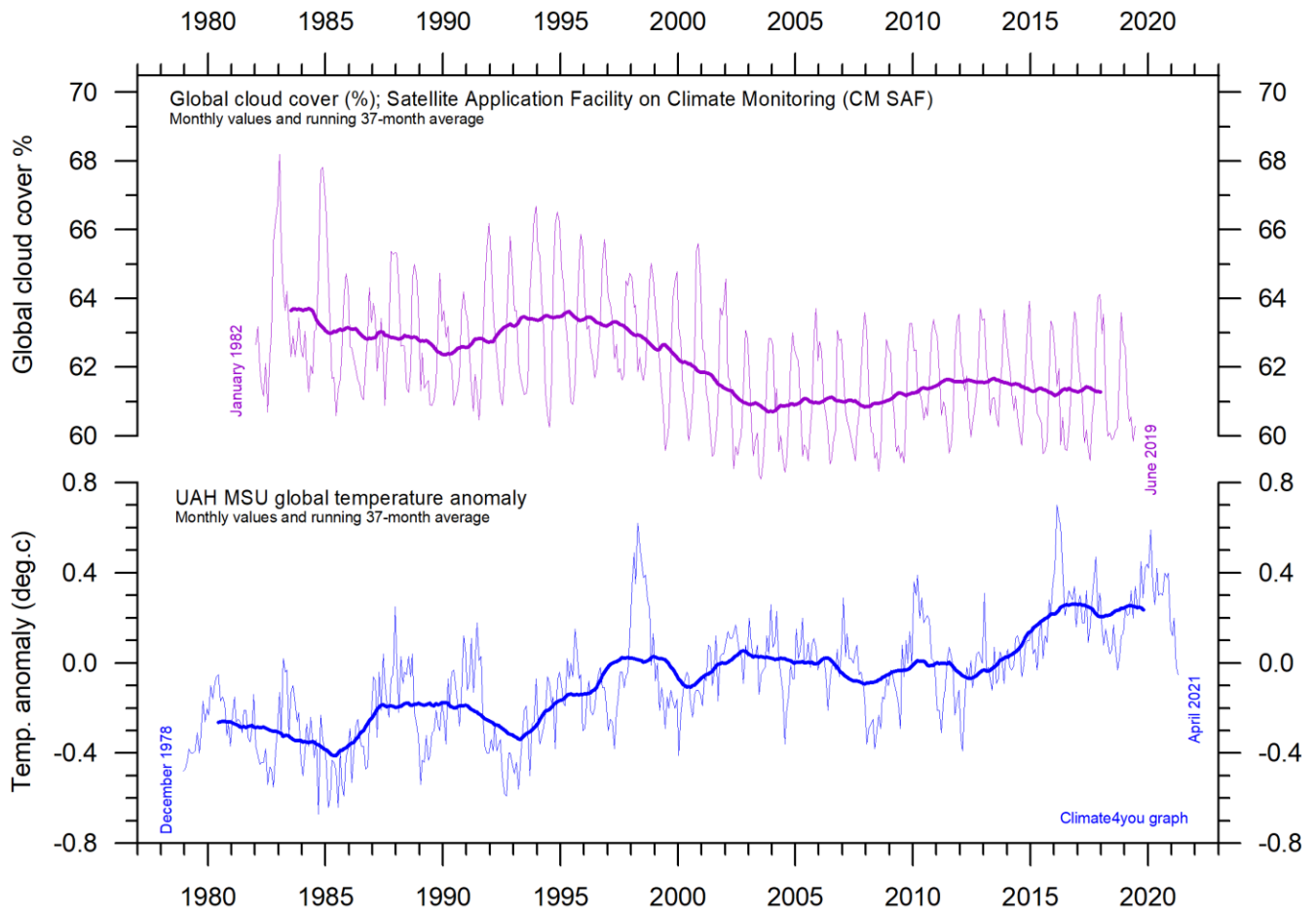


56

Visual association since 1958 between (from bottom to top) Sunspot Number, Oceanic Niño Index (ONI) and annual change rate of atmospheric CO₂ and specific humidity at 300 mb (ca. 9 km altitude). Upper two panels: Annual (12 month) change rate of atmospheric CO₂ and specific humidity at 300 mb since 1959, calculated as the average amount of atmospheric CO₂/humidity during the last 12 months, minus the average for the preceding 12 months (see also diagrams on page 43+44). Niño index panel: Warm (>+0.5°C) and cold (<-0.5°C) episodes for the Oceanic Niño Index (ONI), defined as 3 month running mean of ERSSTv4 SST anomalies in the Niño 3.4 region (5°N-5°S, 120°-170°W)]. For historical purposes cold and warm episodes are defined when the threshold is met for a minimum of 5 consecutive over-lapping seasons. Anomalies are centred on 30-yr base periods updated every 5 years. Thin vertical stippled lines indicate the visually estimated timing of sunspot minima. The typically sequence following a sunspot minimum appears to be a warm El Niño episode followed by a cold La Niña episode. Effects on change rates of atmospheric CO₂ and atmospheric specific humidity are visually apparent, with ONI variations being followed by changes in first humidity, and then (last) by CO₂.

The above diagram is inspired by the Leamon et al. 2021 publication: Robert J. Leamon, Scott W. McIntosh, Daniel R. Marsh. Termination of Solar Cycles and Correlated Tropospheric Variability. Earth and Space Science, 2021; 8 (4) DOI: [10.1029/2020EA001223](https://doi.org/10.1029/2020EA001223)

Monthly lower troposphere temperature (UAH) and global cloud cover, updated to April 2021



Lower tropospheric air temperature and global cloud cover. Upper panel: Global cloud cover according to Satellite Application Facility on Climate Monitoring. Lower panel: Global monthly average lower troposphere temperature (thin line) since 1979 according to [University of Alabama at Huntsville, USA](#). The thick lines represent the simple running 37-month average. Reference period for UAH is 1991-2020.

Cloud cover data citation: Karlsson, Karl-Göran; Anttila, Kati; Trentmann, Jörg; Stengel, Martin; Solodovnik, Irina; Meirink, Jan Fokke; Devasthale, Abhay; Kothe, Steffen; Jääskeläinen, Emmihenna; Sedlar, Joseph; Benas, Nikos; van Zadelhoff, Gerd-Jan; Stein, Diana; Finkensieper, Stephan; Håkansson, Nina; Hollmann, Rainer; Kaiser, Johannes; Werscheck, Martin (2020): CLARA-A2.1: CM SAF cCloud, Albedo and surface RAdiation dataset from AVHRR data - Edition 2.1, Satellite Application Facility on Climate Monitoring,

DOI:10.5676/EUM_SAF_CM/CLARA_AVHRR/V002_01, https://doi.org/10.5676/EUM_SAF_CM/CLARA_AVHRR/V002_01.

Climate and history; one example among many

1812: Napoleon's Russian 1812 campaign



The Battle at Borodino 6 September 1812 (oil painting by Hess), with Napoleon watching from the Shevardino Redoubt (oil painting by Vereschagin).

On 22 June 1812 Napoleon's Grande Armée invaded Russia, crossing the river Niemen. What officially was proclaimed as the Second Polish War had begun.

The Russian army had spent a year and a half deploying for an offensive, but instead began retreating the moment operations began. To add to the general confusion in the Russian headquarter, issues like command and strategy had not been decided because of chaos and intrigue. As nobody and nothing was prepared for a defensive warfare, the Russian army commanded by general Barclay therefore continued their retreat without major resistance, looking for a suitable position in which to make a stand. Apparently, such a position was not easily found, so the retreat continued for weeks. This development left people in Moscow and St. Petersburg bewildered about what was going on,

and Tsar Alexander found himself in a difficult position. Already on 28 June Napoleon entered Vilna, 170 km east of Niemen.

In western Russia the weather July 1806 turned out to be exceedingly warm with daytime temperatures reaching 36°C (Zamoyski 2005). Many French soldiers who had previously campaigned with Napoleon in Egypt claimed that they had never before marched in such a heat. Early July a heavy thunderstorm drifted across the area near Vilna, for a short time making all roads impassable. Worse, losses among the Grande Armée's horses were horrific. This left Napoleon's artillery in a difficult position, but the army's supply organisation was even harder affected. After the rainstorm, the warm weather continued. The remaining horses were having a terrible time. Unused to the kind of diet they were exposed to in Russia, they suffered from colic and diarrhoea

or constipation. The overall supply situation therefore rapidly deteriorated, and most soldiers had to find something to eat and to prepare it themselves. Not surprisingly, under these circumstances, many soldiers died of dehydration, malnutrition, and hunger, while others got dysentery. When the Grande Armée on 28 July reached Vitebsk 400 km into Russia, the whole army had already been reduced by a third, without fighting a single major battle. The summer weather was beginning to turn the whole campaign into a nightmare.

The Russian army was in no happier situation than the French, and its troops were in a state of misery as they retreated towards Smolensk, 380 km southwest of Moscow. Napoleon was convinced that the Russian army would have to fight in defence of the important city of Smolensk. The Russian forces and general Barclay were, however, in a state of tactical confusion, and no strong defence of the city was organised. Instead, Smolensk went up into flames and fell to Napoleon 17 August. The burnt-out city represented neither an effective bastion nor a hard-needed resource for his army. According to his secretary Baron Fain (Zamoyski 2005), Napoleon himself was now feeling disheartened and disgusted at the turn events had taken, and did not quite know what to do next.

The battle of Smolensk demonstrated an very unpleasant fact to Napoleon, that the individual Russian soldier did not lay down his arms even in extremely difficult situations. 129 years later Adolf Hitler would make the identical observation. Napoleon and his army were dismayed by all this. This was not how war was supposed to be. In addition, these discomforts were added to by the fact that the Russians had adopted a new tactic

now that the invaders were in the Russian homeland proper. They evacuated the entire population as they retreated, leaving towns and villages deserted and burnt down. It became increasingly difficult for the French army to find provisions.

Napoleon realised that he could not stop where he was, at Smolensk, and as he would not retreat for political reasons. Therefore, he could only advance further in the hope of eventually obtaining a decisive military victory over the Russians. If not before, the Russians would surely make a stand in defence of their old capital Moscow. Based on existing knowledge on climate in western Russia, Napoleon at that time expected at least two months of decent campaigning weather ahead, before winter would begin.

The mood at Russian headquarters was hardly any better, even though the general situation slowly was changing in their favour. The retreat was a good deal less orderly than before, and the Russian armies were now leaving behind them a trail of abandoned wagons and dead or dying men and horses. Like the French, the Russians were disturbed by the inhumane turn the campaign had taken. The ongoing retreat meant that discipline was breaking down, and everybody was on the lookout for traitors. All this was having a detrimental effect on the army and Barclay's authority.

In St. Petersburg Tsar Alexander found the general mood depressingly defeatist and decided that the Russian army needed a new commander instead of Barclay. He was hard pressed by the public opinion to choose Field Marshal Mikhail Ilarionovich Kutuzov as Barclay's successor. Alexander himself was not too happy about this,

as he considered Kutuzov both immoral and incompetent. His sister Catherine, however, urged him to bow to the inevitable, and Kutuzov was appointed 20 August 1812. Kutuzov declared that he was going to save Moscow and set off to find his headquarters.

After assessing the state of the Russian army Kutuzov suddenly felt that he could not face Napoleon, whose strength now was gauged at 165,000, down from the original 450,000. The Russian summer had taken its toll. Kutuzov therefore decided to continue the retreat initiated by Barclay two months earlier. Perhaps he also suspected Napoleon to be a superior general to himself. On 3 September Kutuzov inspected defensive positions found near the village of Borodino, about 100 km west of Moscow. Here he was going to make a stand.

60

Kutuzov took up entirely defensive positions without any tactical possibility of gaining the initiative. Luckily for him, Napoleon had just caught a cold with an associated attack of dysuria and was in anything approaching his usual form. In fact, Napoleon was going to deliver probably the worst performance of his entire military career. The invading French army was now down to 126,000, while Kutuzov had about 155,00 men under his command.

The first large battle during Napoleon's Russian campaign began in the morning of 6 September 1812. Before this battle, both armies had lost more than half their original strength exposed to eight weeks of Russian summer. The battle of Borodino was a hard-fought battle with several Russian counterattacks, but slowly the French was getting the upper hand due to its superiority on

the tactical level, and the Russian army had to retreat. The battle of Borodino was the greatest massacre in recorded history at that time, not to be surpassed until the first day of the battle at Somme in 1916. Recent estimates give a total of about 73,000 casualties, 45,000 Russian and 28,000 French, including allies.

Following Borodino, Kutuzov's army was in no condition to give battle at any positions, however strong. He therefore fell back to the village Fili west of Moscow, initially announcing that he would fight in front of Moscow to the last drop of blood. At the following war council of war in Fili, however, he took the decision to abandon Moscow to Napoleon, to preserve a Russian army in being, a scene memorably portrayed in Tolstoy's *War and Peace*. The Russian army therefore continued its retreat through the Moscow to the utmost consternation of the inhabitants. Kutuzov then turned south and later southwest, setting up a fortified camp for his army near Tarutino, about 120 km SW of Moscow.

The village Fili (now a suburb of Moscow) reappears later in history. Somewhat ironic, this was the location chosen by Trotsky in 1922 for cooperation with the German Junkers aircraft company for secret German-Russian production of aircrafts and engines, at a time where the German Reichwehr by the 1919 Versailles treaty was limited to 100,000 men and the development of military aircraft, tanks, battleships and other top-of-the-range military assets was limited (Bellamy 2007). In early December 1941, Fili also marks one of the foremost position reached by the German Wehrmacht on their trust towards Moscow during operation Barbarossa.

References cited:

Bellamy, C. 2007. *Absolute War. Soviet Russia in the Second World War*. Pan Books, Pan Macmillan Ltd., London, 814 pp.

Zamoyski, A. 2005. *1812 - Napoleon's Fatal March on Moscow*. Harper Perennial, London, 644 pp.

All diagrams in this report, along with any supplementary information, including links to data sources and previous issues of this newsletter, are freely available for download on www.climate4you.com

Yours sincerely,

Ole Humlum (Ole.Humlum@gmail.com)

Arctic Historical Evaluation and Research Organisation, Longyearbyen, Svalbard

21 October 2023.

Planned publication of next newsletter: around 25 November 2023.